INFORMATION TO USERS

This manuscript has been reproduced from the microfilm master. UMI films the text directly from the original or copy submitted. Thus, some thesis and dissertation copies are in typewriter face, while others may be from any type of computer printer.

The quality of this reproduction is dependent upon the quality of the copy submitted. Broken or indistinct print, colored or poor quality illustrations and photographs, print bleedthrough, substandard margins, and improper alignment can adversely affect reproduction.

In the unlikely event that the author did not send UMI a complete manuscript and there are missing pages, these will be noted. Also, if unauthorized copyright material had to be removed, a note will indicate the deletion.

Oversize materials (e.g., maps, drawings, charts) are reproduced by sectioning the original, beginning at the upper left-hand corner and continuing from left to right in equal sections with small overlaps. Each original is also photographed in one exposure and is included in reduced form at the back of the book.

Photographs included in the original manuscript have been reproduced xerographically in this copy. Higher quality 6" x 9" black and white photographic prints are available for any photographs or illustrations appearing in this copy for an additional charge. Contact UMI directly to order.

UMI

A Bell & Howell Information Company
300 North Zeeb Road, Ann Arbor MI 48106-1346 USA
313/761-4700 800/521-0600

Université d'Ottawa · University of Ottawa

METABOLIC CONTROL AND REGULATION OF MITOCHONDRIAL PROTON LEAK: EFFECTS OF UCP1 DEFICIENCY AND AGING IN MICE

Shadi Monemdjou

Thesis submitted to the Department of Biochemistry, Microbiology and Immunology
in partial fulfilment of the requirements for the Master of Science

University of Ottawa
Ottawa, Ontario, Canada
December 10,1998

ABSTRACT

The overall objective of this thesis was to examine various aspects of the metabolic significance and regulation of the mitochondrial proton leak. The research conducted specifically assesses the influence that leak has on age-associated changes in mitochondria, and the role that the leak plays in facultative energy expenditure of transgenic mice which lack uncoupling protein-1 (UCP1), a well known mediator of the proton leak. Proton leak in mitochondria has been studied for over ten years, but its exact mechanism has not yet been elucidated and only recently has it been realized that it might be mediated by uncoupling proteins (UCPs). UCPs may confer a mechanism for proton leakage and thus affect the efficiency of oxidative phosphorylation.

Age-related changes in mitochondria including decreased respiratory control ratios and altered mitochondrial inner membrane lipid composition led us to study oxidative phosphorylation in hepatocytes from old (30 mo.) and young (3 mo.) male mice. Top-down metabolic control analysis and its extension, elasticity analysis, were used to identify changes in the control and regulation, respectively, of three blocks of reactions constituting the oxidative phosphorylation system, namely, substrate oxidation, mitochondrial proton leak and ATP turnover reactions. Resting oxygen consumption of cells from old mice was found to be significantly lower than in young cells. This is explained entirely by a decrease in oxygen consumption supporting ATP turnover (phosphorylation) reactions. However, coincident with this decrease was an increase in the proportion of total oxygen consumption used to balance leak in old hepatocytes compared to young hepatocytes. Metabolic control

coefficients indicate a shift in control over respiration and phosphorylation away from substrate oxidation towards increased control by the leak and ATP turnover reactions. Control of the effective P/O ratio by the ATP turnover and leak reactions was shown to be greater in old than in young cells, showing that efficiency in older cells is more sensitive to changes in the activity of these two blocks of reactions.

Mice deficient in the gene for mitochondrial UCP1 (*Ucp1*-deficient mice) are cold-sensitive despite their abundant expression of genes for the isoforms (*Ucp2* and *Ucp3*), and do not become more obese than controls when fed a high fat diet (Enerback *et al.* 1997). The objective of our work was to analyse the metabolic control and characteristics of proton leak in mitochondria from brown adipose tissue (BAT) of *Ucp1*-deficient mice and of heterozygote controls in order to establish the role of the UCPs in facultative thermogenesis. We conducted the first top-down metabolic control analysis of oxidative phosphorylation in BAT mitochondria. Since purine nucleotides (*e.g.*, GDP) bind to and inhibit UCP1, and since UCP2 and $UCP3_L$ have putative purine nucleotide binding domains, we predicted that the proton leak in BAT mitochondria from *Ucp1*-deficient mice would be sensitive to GDP. On the contrary, flux control coefficients show that the control over mitochondrial oxygen consumption and proton leak reactions at *state 4* (maximal leak-dependent oxygen consumption) are strongly affected by the presence of GDP in control mitochondria, while in *Ucp1*-deficient mice there is no significant effect of GDP. The overall kinetics of the proton leak are virtually identical in mitochondria of deficient mice, in the presence and absence of GDP, and importantly, in control mitochondria in the presence of GDP. Thus,

the lean phenotype in the *Ucp1*-deficient mice is not due to an increased proton leak through other UCP isoforms in BAT.

The findings from our studies with BAT mitochondria from *Ucp1*-deficient mice show that there is no significant increase in the mitochondrial proton leak. Since the lean phenotype in the deficient mouse could not be attributed to increased proton leak in BAT, skeletal muscle (which expresses UCP2 and UCP3) was chosen as the next candidate tissue to study in relation to our hypothesis that the lean phenotype in the *Ucp1*-deficient mice is due to increased, or adapted, energy expenditure via the mitochondrial proton leak. The overall kinetics of the proton leak were altered and *state 4* respiration values were indeed significantly higher in skeletal muscle mitochondria from *Ucp1*-deficient mice compared to controls. This supports our hypothesis that skeletal muscle may be a potential site for an adaptative thermogenic mechanism favouring the lean phenotype observed in the *Ucp1*-deficient mouse, and also provides insight into the possible functions of UCP2 and UCP3.

Dedication

It was but yesterday I thought myself a fragment
quivering without rhythm in the sphere of life.
Now I know that I am the sphere, and all life in
rhythmic fragments moves within me.

Kahlil Gibran
Sand and Foam

For my best friend Richard who has taught me that having dreams and goals are only worth anything if you take the initiative to achieve them.

Acknowledgments

Over the past two years there have been several people who have contributed to the completion of this thesis. First and foremost, I would like to express my sincere gratitude to my supervisor, Dr. Mary-Ellen Harper. Dr. Harper has not only been my academic mentor, but has also been a friend and an inspiration.

I would like to thank Dr. Jon Ramsey and Dr. Richard Weindruch at the Wisconsin Primate Research Centre who collaborated with us and supplied us with the old and young mice for our aging study. Also, a sincere thanks to our collaborator Dr. Leslie Kozak at The Jackson Laboratory who made available to us the unique *Ucp1*-deficient mouse model, and for being a person I always looked forward to seeing at conferences.

My appreciation to everyone that I have worked with in Dr Harper's lab. I'd like to thank Manon Gagné, who not only has helped me with my research, but who also has been a friend and provider of comic relief. Thank you to Alex Zagorevski, Joey Bonacci, and Melissa Morrison for mastering Powerpoint and tirelessly finding journal articles. And finally, I extend my thanks to my partner in crime and co-hypochondriac, Shirin Lal. Shirin, thanks for always being there for me when I need you and giving me memories that will last a lifetime. I can no longer remember what it was like before you were in my life; I'm glad.

I would like to thank Dr. Jean Himms-Hagen for allowing me to occasionally use her laboratory for my experiments, serving on my advisory committee, and for being a symbol of knowledge and dedicated research. My appreciation to Linda Jui for her help with histology and electron microscopy. Thanks to Anna Melnyk for helping with Western Blotting, and for being a friend.

A special thanks to Julie, Joanne, and Crystal who have always helped me out in any way needed and also provided some much needed conversation on boring days.

Thanks to my two best friends who have been on the journey through life with me since childhood. Alia and Ladan, I couldn't be more proud and grateful than to have you two as my friends. Thanks for making my soul smile.

Finally, I would like to thank my family. Mom and Dad, thank you for giving me every opportunity to live my life to the fullest. You have given me the foundation to flourish in this world, and have never let me forget that there isn't anything I can't accomplish. I am who I am because of you. Roxana and Yasmin, I love you.

Table of Contents

List of Figures

List of Tables

List of Abbreviations

$\Delta\Psi_m$	mitochondrial membrane potential
$\Delta\Psi_P$	plasma membrane potential
Δp	mitochondrial protonmotive force
ΔpH	pH gradient
ϵ	elasticity
μCi	microcurie
μg	microgram
μl	microlitre
μM	micromole/litre
a_c	cytoplasmic and nuclear $TPMP^+$ activity coefficient
a_e	extracellular $TPMP^+$ activity coefficient
a_m	mitochondrial $TPMP^+$ activity coefficient
ADP	adenosine diphosphate
ATP	adenosine triphosphate
BAT	brown adipose tissue
BMR	basal metabolic rate
BSA	bovine serum albumin
C	control coefficient
$CaCl_2$	calcium chloride
CO_2	carbon dioxide
$CuSO_4 \cdot 5H_2O$	copper sulphate
ddH_2O	deionized distilled water
DNA	deoxyribonucleic acid
dpm	disintegrations/minute

EDTA	ethylene diamine tetraacetic acid
EGTA	ethylene glycol-bis (β-aminoethyl ether) tetraacetic acid
FCCP	carbonyl cyanide p-trifluoromethoxyphenylhydrazone
g	centrifugal force
g	gram
GDP	guanosine diphosphate
GTP	guanine triphosphate
H_20_2	hydrogen peroxide
HCl	hydrocholoric acid
HEPES	hydroxyethyl piperazine ethane sulphonic acid
J_L	rate of oxygen required to pump protons out of the mitochondrial matrix at a rate equal to the rate of their return through leak
J_P	rate of oxygen consumption required to pump protons out of the mitochondrial matrix at a rate equal to rate of return through ATPase
J_S	rate of mitochondrial or cellular oxygen consumption
KCl	potassium chloride
kDa	kilodalton
KH_2PO_4	potassium dihydrogen orthophosphate
KI	potassium iodide
KOH	potassium hydroxide
L	proton leak subsystem
LiCl	lithium chloride
LiOH	lithium hydroxide
M	moles/litre
mg	milligram
$MgSO_4 \cdot 7H_2O$	magnesium sulphate

MIM	mitochondrial inner membrane
min	minute
ml	millilitre
mo.	month
mM	millimole/litre
mRNA	messenger ribonucleic acid
mtDNA	mitochondrial deoxyribonucleic acid
mV	millivolt
MV	mitochondrial volume
Na_2HPO_4	di-sodium hydrogen orthophosphate
NaCl	sodium chloride
NAD	nicotinamide adenine dinucleotide
$NaHCO_3$	sodium carbonate
NaOH	sodium hydroxide
ng	nanogram
NIDDM	non-insulin dependent diabetes
nm	nanometres
nuDNA	nuclear deoxyribonucleic acid
$O_2^{-\cdot}$	superoxide
°C	degree Celsius
$OH^{-\cdot}$	hydroxyl radical
P	phosphorylation subsystem
Pi	inorganic phosphate
PUFA	polyunsaturated fatty acid
RbCl	rubidium chloride
RMR	resting metabolic rate

rpm	revolutions/minute
S	substrate oxidation subsystem
SEM	standard error of the mean
State 4	maximal non-phosphorylating (leak-dependent) respiration
State 3	maximal phosphorylating respiration
$TPMP^+$	methyltriphenylphosphonium cation
TPMP-Br	methyltriphenylphosphonium-bromide
Ucp	uncoupling protein gene
UCP	uncoupling protein
um	micrometre
v/v	volume/volume
V_c	cytoplasmic volume
V_m	mitochondrial matrix volume
w/v	weight/volume
WAT	white adipose tissue

I. INTRODUCTION

1. *Overview*

Obesity is a disorder of energy balance in which energy intake chronically exceeds its expenditure. Thus, regulation of body weight involves coordinating this intake and expenditure. The many health risks associated with obesity include cardiovascular disease, non-insulin-dependent diabetes mellitus (NIDDM), hyperlipidemia and hypertension. This has been a subject of numerous reviews (Kissebah *et al.* 1989; Pi-Sunyer 1993; Rosenbaum *et al.* 1997; Tung 1997).

Control of energy intake is complex and involves multiple neural circuits with specific neuropeptides, neurotransmitters and their cognate receptors. Although in recent years there have been significant advances in understanding the regulation of food intake, research is now being focussed on understanding the regulation and control of, and the molecular basis for, energy expenditure.

Overall energy expenditure is the sum of two categories, *obligatory* and *facultative*. Obligatory energy expenditure, or thermogenesis, includes the energy expenditure essential for cellular functions and physiological processes (*i.e.*, maintenance of ion gradients and protein synthesis, and cardiorespiratory activities; collectively termed as the ATP-consuming reactions) and energy expenditure for endothermy (Himms-Hagen 1990). Obligatory thermogenesis is primarily controlled by thyroid hormones (Himms-Hagen 1990). Whereas obligatory thermogenesis occurs in all organs of the body, facultative thermogenesis occurs principally in only two organs, skeletal muscle and brown adipose

tissue (BAT). Exercise-induced thermogenesis and cold-induced shivering thermogenesis takes place in skeletal muscle, while cold-induced non-shivering thermogenesis and diet-induced thermogenesis occur in BAT (Himms-Hagen 1990). Facultative thermogenesis is under the control of the nervous system, the motor nerves in skeletal muscle and the sympathetic nerves in the case of BAT (Himms-Hagen 1990). At a cellular level, processes of facultative thermogenesis include the the expression of proteins that control the rate of fuel oxidation and ATP synthesis in those mitochondria. Of particular interest to us are the mitochondrial uncoupling proteins (UCPs) and the mechanism by which they influence oxidative phosphorylation and contribute to overall energy expenditure.

Research done in the past decade has demonstrated that the overall rate of energy metabolism in an animal depends on various factors. Differences in mammalian body mass (Porter and Brand 1993), thyroid hormone levels (Hafner *et al.* 1988; Harper and Brand 1993), and phylogeny (Brand *et al.* 1991) have proven to be important determinants of the resting rate of energy expenditure.

2. *Mitochondrial Proton Leak*

Oxidative phosphorylation is the synthesis of adenosine triphosphate (ATP) from adenosine diphosphate (ADP) and inorganic phosphate (P_i) by mitochondria. It is driven by electron flow along a series of mitochondrial enzymes from a reduced substrate to oxygen. Electron transport results in the pumping of protons at three energy-transducing complexes in the respiratory chain (Complex I, III and IV) from the mitochondrial matrix into the intermembrane space. This forms an electrical potential gradient, and an electrochemical

potential, for protons across the mitochondrial inner membrane, known as the protonmotive force (Δp). Protonmotive force is composed of a pH gradient (ΔpH) and an electric membrane potential ($\Delta\Psi$). Δp drives protons back into the matrix through ATP synthase; the combined action of ATP synthase, the adenine nucleotide translocator and the phosphate carrier results in the formation of ATP. The coupling of oxidation to phosphorylation is not perfect, as suggested initially by Peter Mitchell (Mitchell and Moyle 1967), and described below. In the situation where the electron transport chain reactions result in protons being pumped out of the mitochondrial matrix, and returned exclusively through ATP synthase, oxidative phosphorylation is considered to be fully *coupled*. Research in the last decade has demonstrated conclusively that mitochondrial membranes passively leak protons such that a significant proportion leak back into the matrix without their entry being coupled to ATP synthesis or any other energy conserving reaction (Brown 1992; Brown and Brand 1986). Another phenomenon that may result in the uncoupling of oxidative phosphorylation is known as redox slip. Redox slip is electron flow without proton pumping to the intermembrane space (Pietrobon *et al.* 1981). Work done by Brand and colleagues (Brand *et al.* 1994b) has shown that at physiological temperatures, slip reactions are insignificant and need not be accounted for.

The first indications of proton leak were made by Mitchell and Moyle (Mitchell and Moyle 1967) by adding a small pulse of oxygen to anaerobic mitochondria or bacteria, which then pumped out a pulse of protons detected by a pH electrode. These early data were generally interpreted as artifacts of mitochondrial isolation. More recently, however, the proton leak rate has been measured directly at a high Δp by first inhibiting all known

proton transport processes and then inducing an artificial Δp with potassium gradients (Brown and Brand 1986; Krishnamoorthy and Hinkle 1984). The rate of leak was shown to be much greater at high Δp values and had an exponential dependence on Δp. The strong dependence on Δp explains the finding of Nicholls (Nicholls 1974) which showed that when mitochondria are respiring in the absence of ATP synthesis (*state 4*), respiration can be substantially reduced by titrating with respiratory chain inhibitors with only a small fall in Δp.

The quantitative importance of proton leak in energy expenditure is substantial. As studied in intact hepatocytes, thymocytes and in mitochondria from a variety of tissue types, mitochondrial proton leak has been shown to account for approximately 22-35% of total cellular oxygen consumption rate or 35-45% of mitochondrial respiration rate in isolated rat hepatocytes (Brand 1990a; Brand *et al.* 1994a; Brown *et al.* 1990b; Harper and Brand 1993; Nobes *et al.* 1990b). The contribution of mitochondrial proton leak to skeletal muscle respiration and to BMR was investigated by Rolfe and Brand (Rolfe and Brand 1996). They determined that mitochondrial proton leak accounts for up to 52% of oxygen consumption of resting perfused muscle and contributes approximately 16-31% (mean 25%) of the basal metabolic rate (BMR) of a rat. Since such a high proportion of oxygen consumption is used to drive the proton leak reactions, it has been suggested that the latter may have a significant influence over energy metabolism and heat production (Brand 1990a).

a) Hypothesized Functions of the Proton Leak

Several different functions have been suggested for proton leak. These include: *(i)* production of heat to maintain body temperature, *(ii)* increased potential for regulation of energy metabolism, and *(iii)* reduction of harmful free radicals.

(i) Proton Leak as a Means of Heat Production

It has been proposed that the mitochondrial proton leak in mammals is determined by the need to maintain constant body temperature, and thus the matching of heat production and heat loss.

The bulk of the heat produced is mainly by metabolically active organs (*e.g.*, liver, kidney, heart,...etc). Relative to body size, the mass of these organs is relatively larger in small animals. Larger animals have a smaller surface area to volume ratio, which has been correlated to a decrease in mass-specific metabolic rate (the metabolic rate per unit body mass) is observed with increased body size to allow heat dissipation to occur (Brand 1990a). In contrast, smaller animals tend to lose a large amount of heat since they have a larger surface area to volume ratio (Brand 1990a). This loss in heat is balanced by an increase in metabolic rate (Brand 1990a). Krebs (Krebs 1950) found that metabolic rate in individual organs was greater for small animals, for example, mouse liver slices consumed oxygen four times faster that horse liver slices. In 1985 Else and Hulbert (Else and Hulbert 1985) demonstrated that changes in the rate of oxygen consumption per unit mass of that tissue are parallelled by changes in the content of mitochondria and mitochondrial components. They found that in small mammals the mitochondria of liver and brain had

more surface area/volume of mitochondria and mitochondria of liver, kidney and heart occupied a greater proportion of the cell. It was not until 1993 that Porter and Brand (Porter and Brand 1993) discovered that the rate of mitochondrial proton leak is inversely related to body mass, as is metabolic rate. Their finding that liver mitochondria from mice are about 4-fold more leaky to protons than liver mitochondria from horses provided an explanation for Krebs' initial (Krebs 1950) finding that metabolic rate is increased in the tissues of small animals. Experiments with rats and poikilotherms (invertebrates, fish, amphibia and reptiles) have shown that hepatocytes isolated from rats consume oxygen 4-5 times faster than a poikilotherm of the same body mass. Brand and colleagues (Brand *et al.* 1991) found that isolated liver mitochondria of the bearded dragon (*Amphibolurus vitticeps*) has a lower mitochondrial proton leak activity than a rat of equivalent body size (Brand *et al.* 1991). This provides further evidence indicating that proton leak is involved in thermoregulation. However, the fact that the similarity between rat and lizard liver mitochondria with respect to proportion of energy consumed by the leak and other oxygen consuming processes implies that heat production is not the sole function of the leak.

(ii) Proton Leak increases Potential for Regulation of Energy Metabolism

Coupling and uncoupling processes in cellular metabolism allow for greater sensitivity to effectors, more sites at which control can be exerted and decreased transition time to new steady states (Rolfe and Brand 1997). Proton leak may increase sensitivity and decrease response time to changes in ATP utilization in the cell. For example, when ATP demand is high, the proton leak and coincident oxygen consumption could be minimized

in order to fulfill ATP requirements. Thus, proton leak can provide a mechanism for increasing sensitivity and responsiveness to effectors.

(iii) Proton Leak as a Means of Reducing Free Radical Production

The rate of generation of superoxide free radicals from oxygen is directly related to oxygen concentration within the cell (Halliwell and Gutteridge 1989) and the degree of reduction of electron donors. In its resting state, a cell consumes less oxygen, yielding a higher concentration of reduced electron transport chain components which could donate an electron to oxygen to form superoxide. This detrimental outcome could be minimized by a proton leak mechanism which would decrease oxygen levels as well as the increase the activity of the respiratory chain (Skulachev 1996).

b) Uncoupling Protein-Mediated Mitochondrial Proton Leak

The proton leak is a general property of mitochondrial membranes. It was initially postulated that proton leak was a non-enzymatic process of diffusion through the phospholipid bilayer which acts as an uncoupler of oxidative phosphorylation (Brand and Murphy 1987). However, Brookes and colleagues recently demonstrated that leak pathways through phospholipid bilayers account for only a small proportion (roughly 5%) of mitochondrial proton leak (Brookes *et al.* 1997). There exists another well known mechanism by which oxidative phosphorylation can be uncoupled. In 1977, Nicholls (Nicholls 1977) demonstrated that a 32 kDa uncoupling protein (UCP) resides in the mitochondrial inner membrane (MIM) of mature brown adipocytes and plays a role in

generating heat by creating a pathway that allows dissipation of protonmotive force across the mitochondrial inner membrane, without coupling to any other energy-conserving process (Nicholls andLocke 1984) (Figure 1). Acivation of UCP, therefore, causes increased oxidation of substrates and generation of heat.

It was not until nearly a decade after this proton leak in brown adipose tissue (BAT) was identified that Bouillaud and colleagues (Bouillaud *et al.* 1985) cloned this original UCP. UCP is a transmembrane protein with six transmembrane domains, and is a member of the mitochondrial carrier protein family which also includes the ATP/ADP translocator, and the phosphate translocator (Figure 2). In comparison to the ATP/ADP translocator, UCP was found to be more regulated and could be distinguished by its specific binding of purine nucleoside di- and triphosphates (*i.e.,* ADP, ATP, GDP and GTP) and their ability to inhibit mitochondrial proton leakage (Desautels *et al.* 1978; Heaton *et al.* 1978; Lin and Klingenberg 1982). Intracellular control of *BAT-specific* UCP can also be exerted by fatty acids, which modify the protein, most likely via a conformational change, in such a way as to lower the membrane potential at which proton conductance occurs (LaNoue *et al.* 1986; Locke *et al.* 1982; Rial and Nicholls 1983; Rial *et al.* 1983). Since the discovery of new UCP homologues, the original UCP, which is specific to BAT, is now termed uncoupling protein 1 (UCP1).

c) Uncoupling Protein Homologues

It has been well established that UCP1 plays an important role in energy balance and thermogenesis in small mammals (Nicholls and Locke 1984). However, UCP1-containing BAT is unlikely to be quantitatively important in adult humans since there is very little BAT

Figure 1: Proposed mechanisms for the mitochondrial proton leak. Activity of the redox pumps of the electron transport chain creates protonmotive force. Protonmotive force is used to drive the synthesis of ATP by ATP synthase. The mitochondrial proton leak, regardless of its mechanism, allows protons to bypass ATP synthase, and proton motive force is dissipated. Thus, additional oxygen is used by the electron transport chain to maintain protonmotive force.

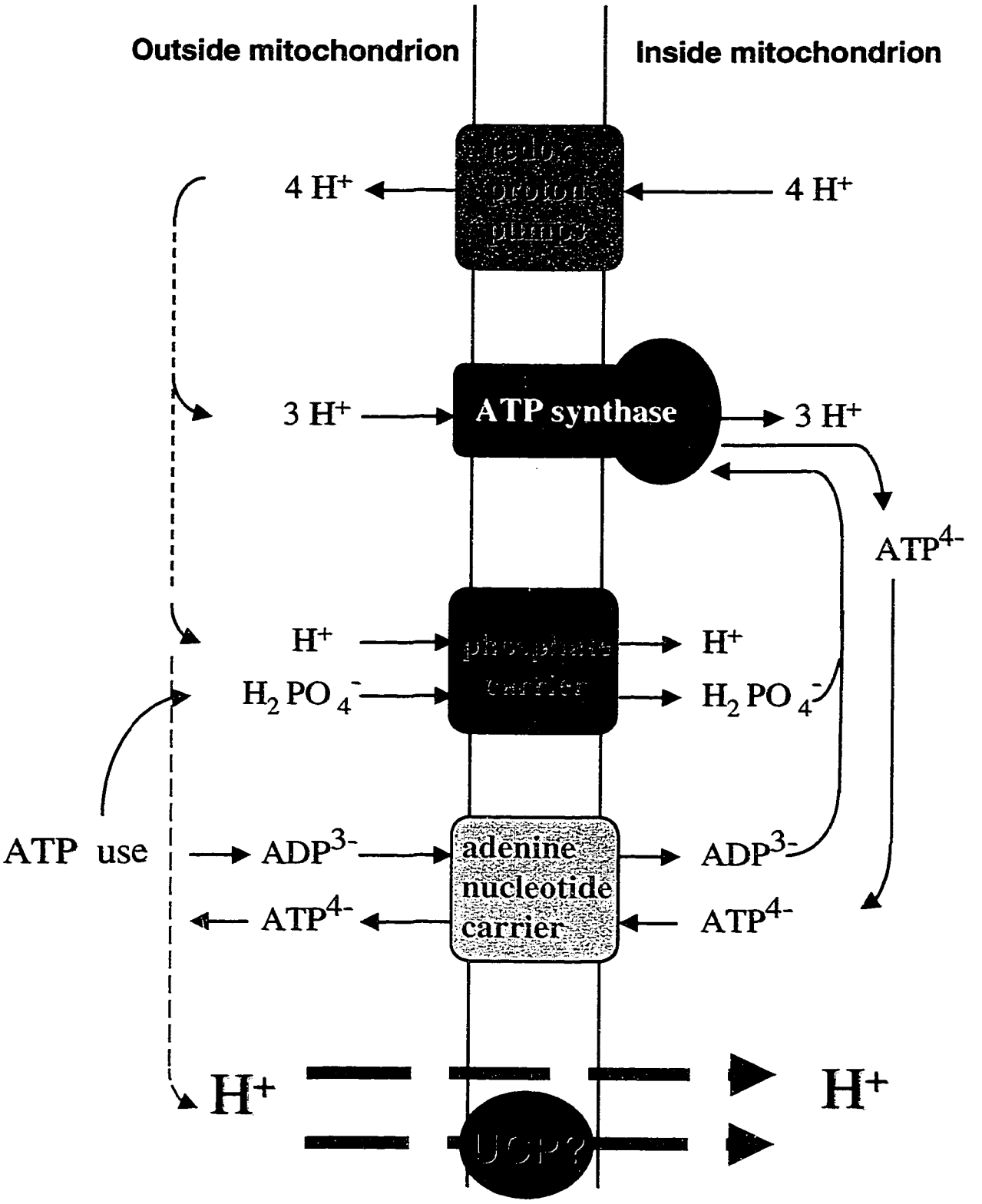
Outside mitochondrion
Inside mitochondrion
redox proton pumps
4 H+
4 H+
3 H+
ATP synthase
3 H+
ATP4-
H+
H2 PO 4-
phosphate carrier
H+
H2 PO 4-
ATP use
ADP3-
adenine nucleotide carrier
ADP3-
ATP4-
ATP4-
H+
UCP?
H+

Figure 2: Membrane-spanning model of uncoupling protein (UCP).

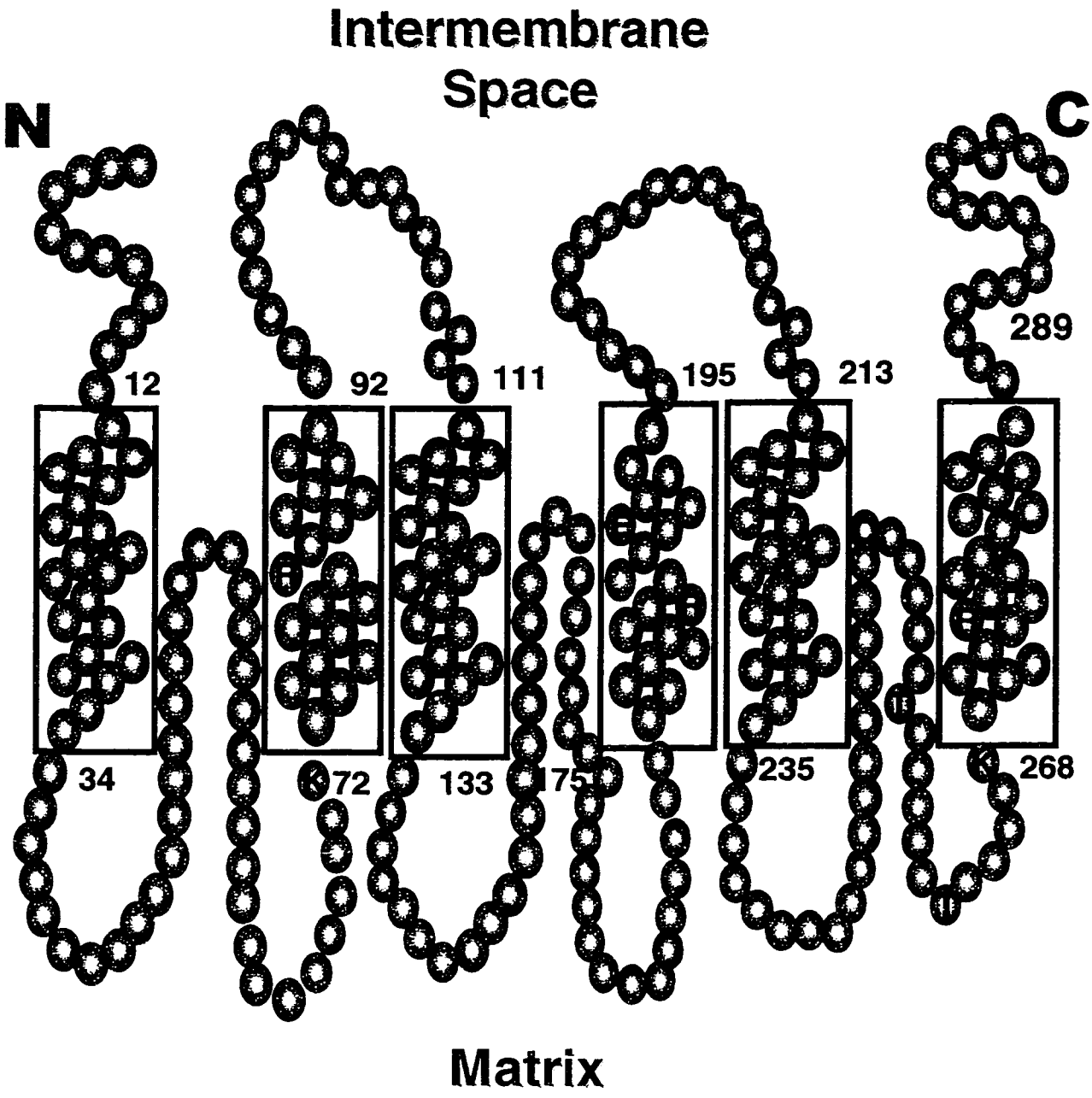
Intermembrane
Space
N
C
12
92
111
195
213
289
34
72
133
175
235
268
Matrix

present (Garruti and Ricquier 1992). This fact, and the evidence that proton leak significantly contributes to standard metabolic rate (Brand 1990a), led the search for identifying other members of UCPs in tissues other that BAT. In the past two years, two UCP homologues have been found that are expressed in many tissues, including BAT.

The first UCP1 isoform, UCP2, was cloned in early 1997 (Fleury *et al.* 1997; Gimeno *et al.* 1997). This protein has 59% amino acid identity to UCP1 and is also able to uncouple mitochondrial respiration, as assessed by flow cytometry with *Saccharomyces cerevisiae* (Fleury *et al.* 1997). Several protein motifs known to be important in UCP1 function are also conserved in UCP2, as are the putative purine nucleotide binding sequences. The amino acid sequence of mouse UCP2 is 95% identical to human UCP2 (Fleury *et al.* 1997). UCP2 is ubiquitously expressed in mouse tissues (Fleury *et al.* 1997; Gimeno *et al.* 1997), predominately in white adipose tissue (WAT) and BAT. It is also expressed in adult human tissues, including tissues rich in macrophages (Fleury *et al.* 1997). UCP2 is upregulated in WAT in response to a high-fat diet (Fleury *et al.* 1997); fasting does not affect the level of UCP2 in BAT, though it does cause a marked increase in levels in soleus muscle (slow-twitch oxidative muscle) (Boss *et al.* 1997a). In contrast to UCP1, mouse levels of Ucp2 mRNA in BAT and WAT have been reported to be unchanged by β_3 adrenergic stimulation with CL 316,243 (Fleury *et al.* 1997), to be unaffected by cold exposure (Fleury *et al.* 1997), or conversely to increase with cold exposure of rats in BAT, heart, and muscle (Boss *et al.* 1997a). Ucp2 mRNA was also found to be increased 5-fold in BAT of transgenic mice deficient in UCP1 (Enerbäck *et al.* 1997). One very interesting finding is that UCP2 maps to regions of mouse chromosome 7 and human chromosome 11

that have been linked to hyperinsulinemia and obesity (DeBry and Seldin 1996; Kleyn *et al.* 1996; Taylor and Phillips 1996).

Another isoform, UCP3, has also recently been cloned by two groups (Boss *et al.* 1997b; Vidal-Puig *et al.* 1997). At the amino acid level UCP3 is 73% identical to human UCP2 and 57% identical to human UCP1 (Vidal-Puig *et al.* 1997). UCP3 is exclusively expressed in skeletal muscle in humans, and BAT and skeletal muscle in rodents (Boss *et al.* 1997b; Vidal-Puig *et al.* 1997). Two isoforms of UCP3 have been identified; a long ($UCP3_L$) and a short form ($UCP3_S$) (Boss *et al.* 1997b). The $UCP3_S$ isoform lacks the sixth transmembrane domain and the potential purine nucleotide binding domain. The abundant and relatively selective expression of *Ucp3* in skeletal muscle suggests that it may be a mediator of facultative thermogenesis in humans.

The relative contributions of the activity of these three molecules to both facultative thermogenesis and basal metabolic rate are under active study. The current hypothesis is that these proteins may be conferring their role in energy balance by mediating the mitochondrial proton leak, although it appears that the mechanism of metabolic regulation are unique.

3. *Age-related changes in mitochondrial proton leak and oxidative phosphorylation.*

It has been postulated that mitochondrial dysfunction may be a principal underlying factor in aging (Shigenaga *et al.* 1994). Since mitochondria provide energy for basic metabolic processes, their decay with age impairs cellular metabolism and leads to decline of cellular functions. The concept that free radicals produced during aerobic respiration are involved in key processes resulting in aging was first proposed in the 1950s by Harman (Harman 1956). In recent years evidence has corroborated and extended Harman's original free radical theory of aging and together has been amalgamated into the now widely supported oxidative stress hypothesis of aging (Ames *et al.* 1993; Sohal and Weindruch 1996; Stadtman 1992). The latter implicates endogenous oxidants in age-related loss of cellular function. The underlying basis of the original free radical theory was that free radicals caused the progressive and irreversible damage and deterioration of cellular function. In contrast, the oxidative stress hypothesis of aging, does not limit the source of the damaging metabolites to oxygen-derived free radicals; however the scope has been expanded from oxidant-induced molecular damage to include oxidant modulation of gene expression, signal transduction and other normal processes (Shigenaga *et al.* 1994; Sohal and Weindruch 1996; Weindruch and Sohal 1997; Yu 1996).

Free radicals (oxidants) are highly reactive molecules that carry an unpaired electron on their surface. Oxidants are produced continuously at a high rate as a by-product of oxidative phosphorylation. These oxidants include superoxide ($O_2^{-}\cdot$), hydrogen peroxide (H_2O_2), hydroxyl radicals ($OH^{-}\cdot$). H_2O_2 is technically not a free radical, but can readily form

$OH^{\cdot}$. Mitochondria are the greatest source of oxidants on the basis that *(i)* the mitochondrial electron transport system consumes approximately 85% of the oxygen utilized by the cell and *(ii)* mitochondria are present in relatively high numbers in essentially all cells of the body. Once formed, free radicals can damage mitochondrial components, including DNA, protein, and lipids as reviewed in Shigenaga *et al.* (Shigenaga *et al.* 1994). Compared to nuclear DNA, the extent of oxidative damage to mitochondrial DNA (which encodes for several proteins of the electron transport chain) is much greater. Damage to mitochondrial DNA (mtDNA) from rat liver or human brain regions is approximately ten-fold higher than that in nuclear DNA (Mecocci *et al.* 1993; Richter *et al.* 1988). These higher levels of oxidative damage and mutation in mtDNA have been attributed to the proximity of the DNA to the electron transport chain in the mitochondrial inner membrane sites where oxidants are formed. Also, the lack of protective histones, and lack of DNA repair mechanisms, contribute to the vulnerability of mtDNA to oxidative damage. Over time, the damage to mtDNA results in the decrease in activities of protein it encodes such as complex I, II and IV of the electron transport chain (Boffoli *et al.* 1994; Bowling *et al.* 1993; Di Monte *et al.* 1993; Torii *et al.* 1992).

The accumulation of oxidatively damaged proteins increases with age (Stadtman 1992). The accumulation of oxidized dysfunctional proteins with reactive carbonyl groups can lead to inter- and intramolecular cross-links with protein amino groups and cause loss of biochemical and physiological function in mitochondria (Shigenaga *et al.* 1994). Thus, the age-related accrual of oxidized protein in mitochondria may also lead to loss of energy production and increased production of oxidants.

Effects of aging on MIM lipids include increased levels of long chain polyunsaturated fatty acids (PUFA) such as 22:4 and 22:5 and decrease in 18:2, 18:1 and 16:1. As a result, with increases in age there is an increased probability of membrane lipid peroxidation (Laganiere andYu 1993; Yu *et al.* 1992). Most of the decrease in 18:2 and increase in 22:4 and 22:5 occurs in the fatty acid composition of cardiolipin. Cardiolipin, a diphosphatidyl glycerol derivative, has been shown to play an important role in mitochondrial membrane structure and function (Hoch 1992). It interacts with various proteins of the MIM such as the ADP/ATP translocator, phosphate translocator, ATP synthase, and mitochondrial substrate transporters (Hoch 1988). In addition, it appears to be involved in the control of MIM permeability to small molecules as well as in establishing mitochondrial proton gradients (Shigenaga *et al.* 1994). Shigenaga *et al.* (Shigenaga *et al.* 1994) hypothesized that these decreases in inner membrane lipids containing 18:2 and altered cardiolipin-protein interactions may account for the decreased *state 3/state 4* ratio (also referred to as the respiratory control ratio) and contribute to the loss of efficiency in mitochondrial function.

Despite over forty years of research, there remains a lack of integrative data on the effects of oxidative stress on the metabolism of intact cells. Gerontologic investigations of mitochondrial function have been limited almost exclusively to isolated mitochondria. While these investigations have been useful, it must be taken into consideration that populations of mitochondria from tissues of old and young organisms can be differentially damaged by mitochondrial isolation procedures. Histological studies have shown that with increasing age, mitochondria tend to be larger, there is increased matrix vacuolization,

cristae are shorter and there is a decrease in dense granules (Wilson and Franks 1975). Importantly, it has been estimated that only about half of these enlarged mitochondria are retained in mitochondrial isolations from tissues of older animals (Wilson and Franks 1975). Thus, the quality of the mitochondrial preparations from old organisms may, in fact, be improved by the loss of unhealthy mitochondria during the isolation procedures (Wilson and Franks 1975), leading to potentially artifactual conclusions about changes in mitochondrial function with age. Moreover, oxidative damage occurs throughout the cell, emphasizing the importance of metabolic studies conducted using intact cells and tissues.

The objective of the work presented in this thesis was to focus on identifying the effects of aging on reactions that are central to oxidative phosphorylation in intact mouse hepatocytes. Analyses were conducted using top-down metabolic control analysis and its extension top-down elasticity analysis, both of which will be described in greater detail in Section 5 of the *Introduction* and in the *Methods and Materials* section.

4. *Mitochondrial Energetics in Ucp1-deficient Mice*

Mammalian BAT, because of its ability to uncouple mitochondrial respiration (Nicholls and Locke 1984), is an important site of facultative energy expenditure (Himms-Hagen 1990). The potential for energy expenditure depends on UCP1, which increases proton conductivity of the MIM and consequently heat production at the expense of ATP synthesis (Himms-Hagen 1992). Transgenic mice with ablation of brown adipocytes induced by brown adipocyte-specific expression of diphtheria toxin-A chain (DTA) driven by the UCP promoter (UCP-DTA mice) become obese and hyperphagic (Lowell *et al.* 1993). However, development of obesity and hyperphagia were eliminated in a thermoneutral environment (Melnyk *et al.* 1997), supporting the hypothesis that BAT thermogenesis plays a central role in energy expenditure and energy intake. The development of this murine model further supported the many earlier reports showing the critical role that BAT plays a critical role in the regulation of energy balance in mice, and that BAT dysfunction can cause obesity.

The extensive findings supporting the importance of BAT metabolism in the development of obesity in experimental animals, and the obese phenotype observed when BAT is ablated (Lowell *et al.* 1993), led a group directed by Dr. Leslie P. Kozak at the Jackson Laboratory in Bar Harbor (ME, USA) to create and study a transgenic mouse model in which UCP1 was completely absent (Enerback *et al.* 1997). It was expected that mice having gene-targeted inactivation of UCP1 would become obese and diabetic at a young age. It was surprising that *Ucp*1-deficient mice remained lean, and became no more obese on a high fat diet (58% of calories from fat) than did controls on the same diet (Enerback *et al.*

1997). *Ucp*1-deficient mice are, however, characterized by a moderately cold-sensitive phenotype. Work done in a our lab in collaboration with Enerbäck *et al.* (Enerbäck *et al.* 1997) demonstrated an abnormally low response in resting metabolic rate to acute treatments with the β_3 adrenergic agonist, CL 316,243. It was also shown that *Ucp2* mRNA is increased five-fold in BAT compared to message levels in BAT of control mice (Enerbäck *et al.* 1997). No significant changes in *Ucp2* expression were detected in any of the other tissues studied, including epididymal and inguinal white fat, liver and muscle (Enerback *et al.* 1997). Subsequent analyses showed that there were no significant changes in the levels of expression of *Ucp3* mRNA in any samples of BAT or skeletal muscle tissue studied (unpublished results, L.P. Kozak). It was thought that since *Ucp2* mRNA levels in BAT were increased in the absence of UCP1, and since it is functionally and structurally similar to UCP1, that UCP2 and UCP3 might provide a mechanism for maintaining body temperature (in the absence of UCP1) when mice were exposed to moderately cold temperatures. The fact that mice do not readily adapt to cold suggests that UCP2 and UCP3 cannot compensate for UCP1 with respect to the role of the latter in the regulation of body temperature upon exposure of to the cold.

The exact roles of UCP2 or UCP3 in the regulation of either body temperature or energy metabolism have yet to be elucidated. These, and perhaps other, yet to be cloned UCPs, have been proposed to mediate the mitochondrial proton leak (Boss *et al.* 1997b; Enerbäck *et al.* 1997; Fleury *et al.* 1997; Gimeno *et al.* 1997; Vidal-Puig *et al.* 1997). The purpose of my project was to investigate the characteristics of the proton leak in the context of oxidative phosphorylation in mitochondria isolated from BAT and skeletal muscle of

Ucp1-deficient and control mice. Specifically, in the presence and absence of guanosine diphosphate (GDP), to ascertain whether or not the residual uncoupling protein(s) in tissues of *Ucp*1-deficient mice were subjected to control by GDP at concentrations and conditions known to inhibit UCP1 activity. In addition, we wanted to determine whether the lean phenotype observed in the absence of any functional UCP1 could be attributed to increased proton leak mediated by the remaining UCPs in BAT.

To assess the metabolic significance and control of proton leak in BAT mitochondria from *Ucp1*-deficient mice and controls we have used top-down metabolic control analysis and its extension top-down elasticity analysis as our theoretical and experimental platforms (See Section 5 of the *Introduction* and in the *Methods and Materials* section).

Skeletal muscle mitochondrial energetics in UCP1-deficient mice

Brown adipose tissue, and therefore UCP1, may be of lesser importance in adult humans in whom the mass of BAT is limited. Instead, skeletal muscle is thought to be a major site of regulatory thermogenesis. It has been well established that skeletal muscle is a significant contributor to RMR in the rat (Field *et al.* 1939a; Field *et al.* 1939b). Rolfe and Brand (Rolfe and Brand 1996) have demonstrated that the mitochondrial proton leak accounts for 52% of the oxygen consumption rate of the resting respiration rate of perfused rat hind limb and 16-31% (mean 25%) of the BMR of a rat (Rolfe and Brand 1996). These findings support Brand's hypothesis that the mitochondrial proton leak plays an important role in resting energy expenditure (Brand 1990a).

The discovery that UCP2 and UCP3 are present in various tissues (Boss *et al.* 1997b; Fleury *et al.* 1997; Gimeno *et al.* 1997; Vidal-Puig *et al.* 1997), and the idea that proton leak contributes greatly to overall energy expenditure, led us to hypothesize that adaptative UCP-dependent thermogenesis may also occur in tissues other than BAT (*e.g.*, skeletal muscle) of the *Ucp*1-deficient mice, allowing them to maintain the observed normal RMR, feed efficiency, and a lean phenotype (Enerbäck *et al.* 1997). Mitochondria were isolated from hind limb and forelimb skeletal muscle tissue depots of *Ucp*1-deficient and control mice. Specifically, mitochondria of the muscles of the lower leg (gastrocnemius and soleus), thigh (vastus lateralis, rectus femoris, quadratus femoris, adductor brevis, semimembranosus, gluteus maximus, gluteus minimus, and gluteas medius), and shoulder (triceps longus and medius; biceps brevis and longus) were isolated for our investigation. These muscles comprise a wide range of fibre types (*i.e.*, fast-twitch glycolytic, fast-twitch oxidative-glycolytic and slow-twitch oxidative) and are reasonably representative of the entire skeletal muscle mass of a mouse.

As with our studies with BAT, we again used top-down metabolic control analysis and elasticity analysis to assess the metabolic significance and control of proton leak in skeletal muscle mitochondria from *Ucp*1-deficient mice and controls we used top-down metabolic control analysis (See below).

5. *Metabolic Control Analysis and the Top-down Elasticity Approach*

Metabolic control analysis was originally developed by Kacser and Burns (Kacser and Burns 1973), and Heinrich and Rapoport (Heinrich and Rapoport 1973), and has been reviewed extensively by others (Brand and Murphy 1987; Fell 1992; Kacser and Porteous 1987). It is an approach that is of both theoretical and practical use for determining quantitatively the control structure of a metabolic system. Metabolic control analyses provide quantitative information about the importance of reactions, or blocks of reactions, in the control of flux (rate) through a metabolic pathway and in the control of the concentration of metabolites within that pathway. This information is mathematically conveyed in the form of flux control and concentration control coefficients, respectively (Brown *et al.* 1990a; Hafner 1990). There are two approaches which can be taken when analysing a system using metabolic control analysis: the traditional approach, or the top-down approach. The aim of the former approach is to determine the flux control coefficients of *individual* enzymes of a metabolic pathway. By repeatedly applying this approach, the flux control coefficients of all the enzymes of each pathway of the system can be determined. The applicability of this approach is limited, however, since it is restricted to particular enzymes and systems because of the necessity for, and limited availability of, specific inhibitors for enzymes acting within the system being studied (Harper and Brand 1995).

In contrast to the traditional approach, the top-down approach provides flux control coefficients and concentration control coefficients for blocks of enzymatic reactions in a

metabolic pathway rather than for individual reactions. This approach involves dividing a metabolic pathway into two or three blocks of reactions around one of its intermediates. The intermediate chosen must be a component of the system which is produced by one or more pathway(s) and is consumed by subsequent pathway(s).

In both the traditional approach and the top-down approach, the sum of all flux control coefficients is one. The higher the value of the flux control coefficient, the more control that particular block of reactions has for the overall pathway. High and low values of concentration control coefficients indicate high and low amounts of control by blocks of reactions over the concentration of the common intermediate.

There are requirements which must be met before the top-down approach can be applied. First, the intermediate measured must be representative of the intermediate that the system actually uses. Thus, the intermediate cannot be channelled, compartmented, or diffusion limited. The second requirement is that the blocks of reactions affect each other solely through the concentration of the intermediate. In other words, there can be no 'cross talk' between the pathways within the system being studied.

While metabolic control analysis allows the identification and quantitative description of important sites of control within metabolic pathways, the top-down elasticity approach allows for the identification of the sites of regulation within metabolic pathways. Elasticity analysis can be valuable in identifying the sites of metabolic effects of the insertion of a transgene, of gene knockout, or of the treatment with hormones, or drugs. Top-down elasticity has been proven useful in elucidating the sites of action of glucagon (Brand *et al.* 1990), thyroid hormones (Hafner *et al.* 1990; Hafner *et al.* 1988; Harper and

Brand 1994), and of fatty acids in isolated hepatocytes of rats (Nobes *et al.* 1990b). Top-down elasticity analysis is an extension of metabolic control analysis and the data generated by this approach provides all of the information needed to complete a control analysis. Top-down elasticity analysis, thus allows for the determination of distribution of control between two or three distinct blocks of reactions comprising a system (Brown *et al.* 1990a; Hafner 1990).

At a practical level, to determine the distribution of control within the system being studied, the concentration of the intermediate is manipulated by titrating the blocks of reactions with various inhibitors or activators. Control coefficients can then be derived from the measurement of the dependence of flux on changes in the concentration of the intermediate. The fractional change in the flux through the block of reactions that is caused by an infinitesimal fractional change in the concentration of the intermediate is referred to as the *elasticity* (*i.e.*, overall kinetics) of that block of reactions (Harper and Brand 1995). The latter are described as elasticity coefficients (ϵ), and describe fundamentally the responsiveness of a branch of a metabolic pathway to changes in the amount of an intermediate in that pathway. The equations that are used to calculate control coefficients from the experimentally derived elasticities can be easily derived and are published (Hafner 1990) (also see *Appendix*). The metabolic system which is the focus of the work presented in this thesis is the oxidative phosphorylation system. Top-down elasticity has been used to determine how oxidative phosphorylation is regulated. For our investigations, we have defined the oxidative phosphorylation as the tripartite system shown in Figure 3. We then determined the overall elasticities to changes in Δp of the reactions that produce Δp (*i.e.*,

Figure 3: Schematic representation of the branched system of oxidative phosphorylation. The intermediate within the system, the mitochondrial protonmotive force (Δp), is produced by the substrate oxidation subsystem, which comprises of all of the reactions including and following the oxidation of glucose, lactate, pyruvate, and endogenous substrates. Δp is consumed by the proton leak and phosphorylating subsystems. The proton leak subsystem consists of the leak of protons and any cation cycles across the mitochondrial inner membrane. The phosphorylating subsystem includes Δp-dependent ATP synthesis and all cellular ATP-consuming reactions.

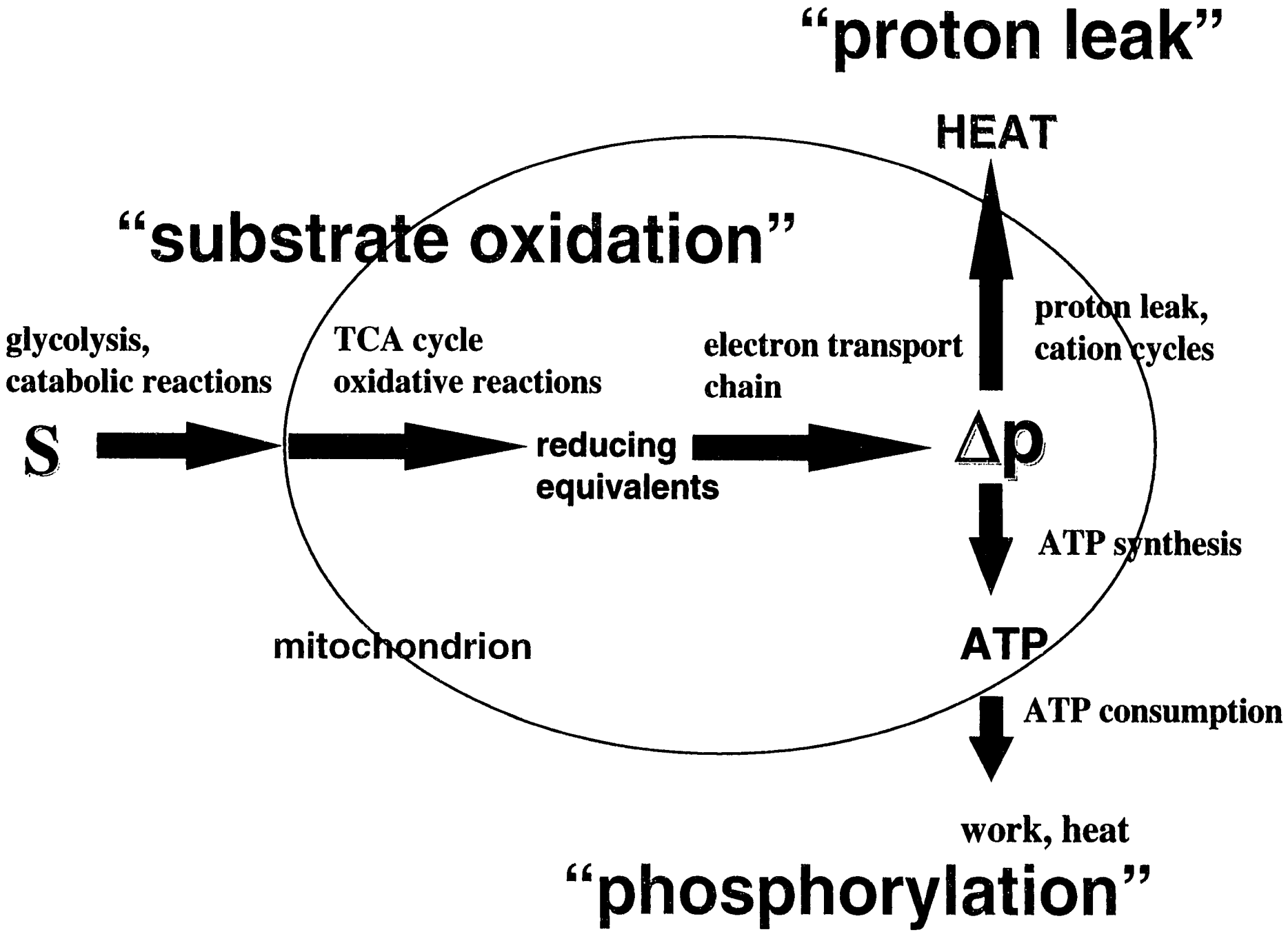
"proton leak"
HEAT
"substrate oxidation"
glycolysis,
catabolic reactions
TCA cycle
oxidative reactions
electron transport
chain
proton leak,
cation cycles
S
reducing
equivalents
Δp
ATP synthesis
mitochondrion
ATP
ATP consumption
work, heat
"phosphorylation"

substrate transport, the citric acid cycle and the electron transport chain- referred to as substrate oxidation reactions). As well we ascertained the overall kinetic response to changes in Δp of the two blocks of reactions that consume Δp (*i.e.*, ATP synthesis and consumption reactions, and the mitochondrial proton leak). We accomplished this by titrating with various inhibitors and activators of the blocks of reactions. For example, the kinetic response of the Δp-producers is measured by progressively inhibiting the consumers with oligomycin, an inhibitor of ATP synthase.

The top-down approach is widely applicable and can be applied to the study of metabolic systems in organelles, intact cells, and intact organs (Brown 1994). In this thesis the top-down approach is used as a tool assess the metabolic control and regulation of oxidative phosphorylation in intact hepatocytes, as well as isolated mitochondria from various tissues. Specifically, we want to ascertain the metabolic significance of the mitochondrial proton leak reactions.

II. METHODS and MATERIALS

1. *GENERAL*

a) Defatting of Bovine Serum Albumin (BSA)

BSA was defatted by method of Chen (Chen 1967). 50 g of BSA (fraction V, Sigma) was dissolved in 250 ml of ddH_2O. After approximately 1 h of magnetic stirring, 25 g of activated charcoal (acid washed, BDH), suspended in 100 ml of ddH_2O, was added. The suspension was then brought to a pH of 3.0 with 10 M HCl and stirred on ice for 1 h. Using a Beckman J2-21M centrifuge with a JA 14 rotor, the suspension was centrifuged at 11,300 rpm (20,000*g*) for 20 min at 4°C. The supernatant was carefully poured off into a 500 ml beaker, slowly brought to a pH of 7.0 with 10 M NaOH, and the centrifugation was repeated. The resulting supernatant was filtered through a vacuum filtration apparatus fitted with a 0.45 um filter membrane (Millipore HA type) and then through a 0.22 um filter membrane (Millipore GS type). Filtrate was dialysed against 153 mM NaCl and 10.8 mM KCl three times; twice for 1h and once overnight at 4°C. Prior to dialysis, the dialysis tubing was boiled in 75 mM ethylenediamine tetraacetic acid (Na_2EDTA; disodium salt) for 5 min and then in ddH_2O for an additional 5 min. Then 300 ml of the last dialysis medium was kept for dilutions. The concentration of defatted BSA was determined by the biuret method (Gornall *et al.* 1949), described below. The suspension was diluted in order to give a final stock concentration of 9% BSA (w/v) and then stored at -20°C in 10 ml aliquots for later additions to incubation media.

b) Biuret Determination of Protein Concentration

Protein concentration of the mitochondrial suspension was assayed by the biuret method (Gornall *et al.* 1949) using BSA as the reference standard. 25 ul of sample was added to 200ul of mitochondrial suspension medium[1] containing 25 ul sodium deoxycholate (0.1% w/v). The reference standard contained 225 ul of mitochondrial suspension medium and 0.1 % (w/v) sodium deoxycholate. 1.0 ml of biuret reagent (1.5g $CuSO_4 \cdot 5H_2O$, dissolved in 500 ml of ddH_2O, 6.0 g of potassium tartrate, 300 ml 10% NaOH, 1.0 g KI; diluted to 1.0 L) was added to both the reference standard and sample tubes, then incubated for 10 min at 37°C. Absorbances were read at 540 nm on a Beckman DU-50 spectrophotometer. The protein concentration was calculated using a six point calibration curve standardized with 0, 2, 4, 6, 8, and 10 mg BSA/ml.

[1] The suspension medium used in each assay was specific to that in which the mitochondria were originally suspended.

2. *AGE-RELEATED CHANGES IN OXIDATIVE PHOSPHORYLATION OF MOUSE HEPATOCYTES*

a) Treatment of Animals

Twenty-seven male 30 mo. old C57BL/6J mice were received from the Veterans Administration-Geriatric Research, Education and Clinical Centre at the University of Wisconsin, Madison, WI. These mice were part of a cohort purchased at one month of age from Charles River Laboratories (Wilmington, DE), group housed (3 mice/cage), and given free access to Purina 5001 chow diet and water. Twenty-seven young (3 mo.) control C57BL/6J mice were obtained from The Jackson Laboratory, Bar Harbor, ME.

Upon arrival, mice were housed individually in plastic cages at 23°C with light 07:00-19:00 and given free access to Purina 5001 chow diet and water. Mice used in this study were cared for in accordance with the principles and guidelines of the Canada Council on Animal Care, the Institute of Laboratory Animal Resources (National Research Council, USA), and with the "Guiding Principles for Research Involving Animals and Human and Human Beings".

b) Isolation and Incubation of Hepatocytes

Hepatocytes were isolated and incubated by a method adapted from Berry *et al.* (Berry *et al.* 1991). Non-fasted mice were anaesthetized with 1.0 mg sodium pentobarbital/100g body weight and killed between 07:30 and 11:00. The abdomen was opened by cutting centrally to the sternum, and anterior and posterior ends were then cut

outwards in order to expose the peritoneal contents. A loose tie was then placed around the inferior vena cava and around the portal vein. The portal vein was cannulated using a 22 gauge Angiocath® prefilled with Ca^{2+}-free pre-perfusion buffer (118 mM NaCl, 1.2 mM KH_2PO_4, 1.2 mM $MgSO_4 \cdot 7H_20$, 4.75 mM KCl, 25 mM $NaHCO_3$, 12 mM glucose). Once the vein was successfully cannulated, the tie was tightened to keep the cannula in place. After cutting through the inferior vena cava, the cannula was attached to an input line which delivered 4 ml/min of pre-perfusion medium maintained at 41°C and in an atmosphere of 5% CO_2 in air (pH 7.4). The pump flow rate was slowly increased to 8 ml/min. After 8-10 min, the pre-perfusion medium was switched over to a Ca^{2+}-containing perfusion media containing 0.02% (w/v) of Type IV collagenase (500 mM HEPES and 2.5 mM $CaCl_2 \cdot 2H_2O$), which was also maintained at 41°C[1] and equilibrated with 5% CO_2 in air. Flow rate was maintained at 8-10 ml/min for 10-15 min. Clearing of the liver occurred as the cells were mobilized, and once this was widespread the perfusion was stopped. The liver was then removed and placed in a 50 ml beaker containing 10 ml of collagenase-containing perfusion buffer. Gentle teasing apart of liver was done with scissors. The suspension was then decanted into 2 x 50 ml Erlenmeyer flasks, and placed in a 37°C shaking water bath (100 cycles/min) under 5% CO_2 in air for 10 min. The cells were then filtered through nylon mesh (250 um Nitex) into two 50 ml glass centrifuge tubes and spun at 50*g* for 3 min using a Damon/IEC centrifuge at room temperature. Most of the supernatant was then discarded and the cells resuspended with an inverted Pasteur pipette.

[1]Medium was kept at 41°C so that when it finally entered in the mouse it was at 37°C.

The decanted volume was replaced with isolation medium (148 mM NaCl, 5.0 mM KCl, 0.81 mM $MgSO_4 \cdot 7H_20$, 0.83 mM Na_2HPO_4, 0.14 mM KH_2PO_4, 1.0 mM $CaCl_2$, 25 mM $NaHCO_3$ and 15 mM glucose) and centrifuged again for 2 min at 50*g*.

Cells were resuspended once again and filtered through nylon mesh into a preweighed centrifuge tube and spun at 50*g* for 4 min. The resulting supernatant was then discarded and the weight of cells was determined.

We assumed that 1.0 g of wet cells weighed 1.0 ml and brought the volume of suspension to approximately 2.5 ml with isolation medium. Once the cells were well resuspended, hematocrit capillary tubes were used to draw out some cell suspension. The base of each tube was sealed with plasticine and centrifuged at 50*g* for 5 min. Hepatocrit was calculated as: 100 x (length of cell pellet/total length of cell pellet and supernatant). By dividing the hepatocrit by 6, the volume of isolation medium needed to obtain a cell suspension of approximately 7.5 x 10^6 cells/ml was obtained. The actual concentration of the cell suspension was determined by using a hemocytometer at 40x magnification. Then to estimate cell viability, four drops of isolation medium, two drops cells and five drops of 0.3% (w/v) Trypan blue were mixed in a minitube. Dead cells take up Trypan blue and appear as 'blue fried eggs' under the microscope. Using a Pasteur pipette, ~20 ul of cell suspension was carefully transferred to the hemocytometer slide by placing the tip of the pipette on the edge of the hemocytometer chamber and allowing the suspension to be drawn under the coverslip by capillarity. The number of cells which lay within the total area of the slide grid were counted.

The concentration of the sample was derived as follows:

$$c = n \cdot 10^4 \cdot \text{dilution factor}$$

where c = cell concentration (cells/ml), n = number of cells counted (Freshney 1987), and dilution factor = 5.5 . In instances where the concentration of the cell suspension was determined to be greater than 7.5 x 10^6 cells/ml, additional isolation medium was added and the suspension recounted. The total number of dead cells were subtracted from the total cell count and the percentage viability was determined as the number of viable cells divided by the total number of cells multiplied by 100. For all cell preparations the cell viability was greater than 92%.

For analysis of the overall kinetics of oxidative phosphorylation reactions, the cells were diluted approximately seven-fold in an incubation medium containing 106 mM NaCl, 5 mM KCl, 25 mM $NaHCO_3$, 0.41 mM $MgSO_4 \cdot 7H_20$, 10 mM Na_2HPO_4, 2.5 mM $CaCl_2$, 10 mM glucose, 10 mM lactate, 1.0 mM pyruvate and 2.25% (w/v) defatted BSA. Cell suspensions of 2.5 ml of 6-9 mg dry weight cells/ml (1.0 x 10^6 cell/ml) were incubated in 20 ml stoppered glass vials at 37°C in a shaking water bath (100 cycles/min). To allow equilibration of the medium to a pH of 7.4 the gas phase above each suspension during incubations was 5% CO_2 in 95% air. The cells were pre-incubated at 37°C in the shaking water bath for 10 min. to allow the hepatocytes to reestablish ion gradients after being stored on ice. Cells were then incubated for a further 20 min in the presence of inhibitors,

uncouplers and isotopes before aliquots were taken for the measurements of O_2 consumption and mitochondrial membrane potential ($\Delta\Psi_m$).

c) Measurement of Oxygen Consumption

The respiration rate of hepatocytes was measured using a Hansatech (Norfolk, UK) Clark-type oxygen electrode. The incubation chamber of the electrode was thermostatically maintained at 37°C and magnetically stirred. Each rate was assessed in duplicate using 1.0 ml of cell suspension. Oxygen consumption rates are reported here as that per 10^6 cells rather than per mg dry weight of cells as is more normal for rat hepatocyte preparations. The rationale behind this was that the yield of hepatocytes from a mouse is approximately one tenth of that from a rat and an inordinate amount of the final cell preparation would be needed to accurately assess dry cell weight. Respiration rates were determined approximately 3-5 min after the addition of cell suspension to the chambers (*i.e.*, once stable linear rates were determined). Resting respiration rates were defined as the oxygen consumption rate in the absence of inhibitors and uncouplers. To determine the rate of non-mitochondrial oxygen consumption, cells were incubated with maximal concentrations of oligomycin (1.0 μg/ml), antimycin (5.0 μM), valinomycin (0.1 μM) and carbonyl cyanide p-trifluoromethoxyphenylhydrazone (FCCP) (20 μM).

d) Measurement of Mitochondrial Membrane Potential ($\Delta\Psi_m$)

The $\Delta\Psi_m$ was measured simultaneously with oxygen consumption using the distribution of the lipophilic cation, triphenylmethylphosphonium ($TPMP^+$) and the Nernst

equation. Appropriate corrections were applied for cytoplasmic and mitochondrial binding of $TPMP^+$ and for other factors, as described by Nobes *et al.* (Nobes *et al.* 1990a) and are outlined below. The relationship between $\Delta\Psi_m$ (mV) and $TPMP^+$ distribution at 37°C is shown below:

$$\Delta\Psi_m = -61.5 \log \left| \frac{V_c \cdot a_m}{V_m \cdot a_c} \left[\frac{[Cl^-]_{tot}[TPMP]_{tot}\, a_c\, (V_c + V_m)}{[Cl^-]_e[TPMP]_e\, a_e\, V_c} - 1 \right] \right|$$

$\Delta\Psi_m$ can be calculated knowing the proportion of cytoplasmic volume that is occupied by the mitochondrial matrix (V_m/V_c), the apparent activity coefficient of $TPMP^+$ in each compartment (a_e, a_c, and a_m; where subscripts e, c and m represent extracellular, cytoplasmic plus nuclear, and mitochondrial), and the extent of the accumulation of $TPMP^+$ into the whole cell ($[TPMP^+]_{tot}/[TPMP^+]_e$) and into the cytoplasm in relation to the external medium ($[Cl^-]_e/[Cl^-]_{tot}$).

V_c and V_m values were determined using quantitative morphometric cytology as described by Weibel (Weibel 1969). Cells were sedimented for electron microscopy in isolation medium containing 2.5% (w/v) glutaraldehyde. The glutaraldehyde-fixed cells were then washed twice in 0.05% sodium cacodylate buffer. Electron micrographs of osmium-stained cells were prepared at a final magnification of 4950-fold. Mitochondrial matrix volume was determined from the number of intersections on a 1 cm grid that overlay the micrographs. The volume was then calculated as the total number of intersections in

mitochondria divided by the total number of intersections in cells (less the total number of intersections in lipid droplets). The cellular volume was corrected for the volume of lipid droplets as $TPMP^+$ is not taken up into fat (Davis *et al.* 1981). Mitochondrial matrix volume was calculated as 56.5% of total mitochondrial volume based on the work of Loud (Loud 1968) who calculated this weighted mean from the percentage matrix volume of midzonal, peripheral and central liver cells and the percentage of these cell types in the whole liver.

e) Determination of Apparent Activity Coefficients for $TPMP^+$ in the Cytoplasm (a_c)

Since $TPMP^+$ is a hydrophobic probe and is able to cross membranes, it is prone to non-specific binding. The proportion of $TPMP^+$ that is free (*i.e.*, not bound) in the cytoplasm (a_c) was determined as described by Nobes *et al.* (Nobes *et al.* 1990a). To determine a_c, we calculated the $TPMP^+$ accumulation ratio ($[TPMP^+]_{tot}/[TPMP^+]_e$) and the $^{86}Rb^+$ accumulation ratio ($[^{86}Rb^+]_{tot}/[^{86}Rb^+]_e$) in the presence of valinomycin (a K^+ ionophore), antimycin (an inhibitor of complex III of the electron transport chain) and oligomycin (an inhibitor of ATP synthase) at different external K^+ concentrations, with the assumption that $^{86}Rb^+$ does not bind to cytoplasmic components. Hepatocytes were incubated with variable concentrations of K^+ and Na^+ in a basic salts medium (25 mM $NaHCO_3$, 0.41 mM $MgSO_4$, 10 mM Na_2HPO_4, 10 mM glucose, 10 mM lactate, 0.1 mg/ml inulin, 1.0 mM pyruvate and 0.1 uM TPMP-Br; pH 7.2 with NaOH) at 37°C. Final $[K^+]$ concentrations used were : 0, 5.6, 45, 86, and 125 mM. For each concentration of K^+ two 20 ml glass incubation vials were setup with 0.375 ml of cells (1 x 10^6 cells/ml final concentration) to 2.125 ml of

medium (flushed with 5% CO_2 in 95% air) and sealed with a rubber stopper. After a 10 min incubation period at 37°C to allow equilibration of ions across membranes, 100 uM valinomycin, 5.0 μM antimycin, and 10 ug/ml of oligomycin were added. At this point, 0.1 μCi [^{3}H]TPMP$^+$/ml and 5.0 μCi ^{86}RbCl/ml were added to one vial, and 2.5 μCi ^3H_2O/ml and 0.5 μCi [^{14}C]methoxyinulin/ml to the other. After 20 min at 37°C, triplicate aliquots (0.70 ml) were removed from each vial and pipetted into 1.5 ml minitubes and immediately centrifuged in a Fisher minifuge for 2 min at 7000 rpm (12,000*g*). 200 μl aliquots of the supernatant were then removed and pipetted into 20 ml polyethylene scintillation vials and immediately mixed with 3.0 ml of scintillation cocktail (Amersham ACSII). The residual supernatant was aspirated; the sides and cap of each tube were wiped dry and 40 μl of 20% (v/v) Triton X-100 was added. Following the complete suspension of the pellet by vortex mixing, the bottom of the tube was cut off and placed into a scintillation vial and the pellet was resuspended in 3.0 ml of scintillant. The radioactivities of the supernatant and pellet were determined by dual-channel scintillation counting for ^{3}H and ^{14}C using the appropriate quench and cross-over corrections.

The apparent volume of pellet available to each isotope (its *space* in μl) was calculated as dpm in total pellet divided by dpm/ul of supernatant sample. The [^{3}H]TPMP$^+$ accumulation ratio ($[TPMP^+]_{tot}/[TPMP^+]_e$ was calculated as ([^{3}H]TPMP$^+$ space - [^{14}C]methoxyinulin space)/(^3H_2O space - [^{14}C]methoxyinulin space). The $^{86}Rb^+$ accumulation ratio $[^{86}Rb^+]_{tot}/[^{86}Rb^+]_e$ was calculated as ($^{86}Rb^+$ space - [^{14}C]methoxyinulin space)/(^3H_2O space - [^{14}C]methoxyinulin space). By plotting [^{3}H]TPMP$^+$ accumulation ratios against $^{86}Rb^+$ accumulation ratios a linear relationship is obtained. The inverse slope

of this line is defined as a_c. a_c values were determined to be 0.356 (± 0.019; n=2) and 0.322 (± 0.015; n=2) for hepatocytes from old and young mice, respectively, and indicate that roughly 65% of the $TPMP^+$ in our incubations is bound to cytoplasmic components.

f) Determination of Apparent Activity Coefficients for $TPMP^+$ in Mitochondria (a_m)

The non-specific binding of $TPMP^+$ in mitochondria is reflected in a_m. The latter indicates the proportion of the probe that is free. a_m was determined using a method similar to that described above which adjusts the $TPMP^+$ accumulation ratio, $([TPMP^+]_{tot}/[TPMP^+]_e)$ to the accumulation ratio for $^{86}Rb^+$ $([^{86}Rb^+]_{tot}/[^{86}Rb^+]_e)$, over a range of membrane potentials. $TPMP^+$ accumulation ratios and $^{86}Rb^+$ accumulation ratios in the presence of valinomycin were determined at four concentrations of KCl (0, 0.2, 1.0 or 5.0 mM). For each concentration of KCl, two sets of minitubes containing 40 µl of liver mitochondria (isolated using the procedure described briefly below), 1.0 ml of incubation medium (200 mM sucrose, 5.0 mM HEPES, 5.0 mM LiCl, 1.0 mM EGTA, 5.0 µM rotenone, 1.0 µM TPMP-Br), and 0.2 ug/ml valinomycin were prepared. To one set of triplicates 0.035 µCi ^{86}RbCl/ml and 0.15 µCi [^{3}H]TPMP/ml were added, and 1.5 µCi ^3H_2O/ ml and 0.15 µCi [^{14}C]sucrose/ml to the other. In each set, the concentration of KCl was assessed in triplicate. Succinate (5.0 mM; brought to pH 7.0 with LiOH) was added to all tubes and they were mixed by inversion. After 2 min at room temperature, the mitochondria were sedimented by centrifugation for 2 min at 7000 rpm (12,000*g*). 500 µl aliquots of the supernatant were transferred into scintillation vials containing 7.5 ml of scintillation cocktail. The residual supernatant was aspirated, the sides were wiped dry and 20 µl of Triton X-100 was added.

Following the complete suspension of the pellet by vortex mixing, the bottom of the tube was cut off into a scintillation vial and pellet was resuspended in 7.5 ml of scintillation cocktail. 150 µl of ddH_2O was also added to adjust for the aqueous volume added to supernatant-containing vials).

The apparent volume of pellet available to each isotope was calculated as dpm in total pellet divided by dpm/µl of supernatant sample. The [^{3}H]TPMP$^+$ accumulation ratio ($[TPMP^+]_{tot}/[TPMP^+]_e$ was calculated as ([^{3}H]TPMP$^+$ space - [^{14}C]sucrose space)/(^3H_2O space - [^{14}C]sucrose space). The $^{86}Rb^+$ accumulation ratio $[^{86}Rb^+]_{tot}/[^{86}Rb^+]_e$ was calculated as ($^{86}Rb^+$ space - [^{14}C]sucrose space)/(^3H_2O space - [^{14}C]sucrose space). By plotting [^{3}H]TPMP$^+$ accumulation ratios against $^{86}Rb^+$ accumulation ratios a linear relationship is obtained. The inverse slope of this line is defined as a_m. Values for a_m were determined to be 0.247 (±0.039; n=2) and 0.171 (±0.073; n=2) for liver mitochondria from old and young mice, respectively. Thus, roughly 80% of the TPMP$^+$ added is bound to mitochondrial components. These values are similar to previously published values (Porter and Brand 1993).

g) Isolation of Liver Mitochondria

Mice were killed by decapitation prior to removal of the liver. The abdomen was then cut just below the rib cage, and the liver was removed. The liver was placed in a beaker containing 25 ml of ice-cold isolation medium (250 mM sucrose, 5.0 mM Tris-HCl, 1mM EGTA; pH 7.1 with 10 M HCl) and then carefully chopped into 1 cm pieces with scissors. The suspension was then transferred into a glass/Teflon Potter-Elvehjem tissue

grinder (Wheaton Scientific, Millville, NJ) and carefully plunged approximately ten times. The homogenate was then poured into two 40 ml plastic centrifuge tubes and centrifuged at 3,000 rpm (1,500 *g*) for 3 min at 4°C using a Beckman RC2-B centrifuge (SS-34 rotor). The resulting supernatant was then removed and centrifuged again at 10,000 rpm (16,000*g*) for 10 min. The supernatant was discarded and the pellet resuspended with a glass rod (taking care not to disturb the blood spot). Both pellets were then transferred into one centrifuge tube and the tube was filled with isolation medium. The suspension was centrifuged again at 10,000 rpm for 10 min, then resuspended and centrifuged for a final 10 min at 10,000 rpm. The resulting pellet was resuspended and poured into a 10 ml plastic conical tube. Protein concentration was determined by the biuret method at 540 nm (See Section *1b.*) using BSA as a standard.

h) Determination of Cellular Volume

In order to assess cell volume, hepatocytes were incubated at 37°C in the presence of 2.5 μCi $^{3}H_2O$/ml and 1.0 μCi [^{14}C]methoxyinulin/ml. Incubations with $^{3}H_2O$ allowed the total pellet volume to be determined while [^{14}C]methoxyinulin allowed the calculation of extracellular volume in pellets; the cell volume was then calculated as the difference between the total pellet volume and the extracellular volume. The apparent volume of pellet available to each isotope was calculated as dpm in total pellet divided by dpm/μl of supernatant sample.

i) Determination of Plasma Membrane Potential ($\Delta\Psi_p$) and $^{36}Cl^-$ Distribution

$\Delta\Psi_p$ and $^{36}Cl^-$ Distribution ($[Cl^-]_e/[Cl^-]_{tot}$) were measured using the distribution of $^{36}Cl^-$ as described by Nobes and Brand (Nobes and Brand 1989). This method provides an

accurate quantitative measurement of plasma membrane potentials between -4 and 40 mV. 0.375 ml of hepatocytes (1 x 10^6 cells/ml, final concentration) were incubated in 20 ml stoppered glass vials containing 2.125 ml of incubation medium. Cells were incubated for 10 min at 37°C to allow the cells to reestablish ion gradients which are disturbed during cell storage on ice. Cells were then incubated for 20 min with 0.1 μCi/ml $^{36}Cl^-$ and 2.5 μCi/ml ^3H_2O. At the end of the incubations, three 0.7 ml samples were removed and pipetted into 1.5 ml minitubes and immediately centrifuged for 2 min at 7000 rpm (12,000*g*). 200 μl aliquots of the supernatant were removed, pipetted into scintillation vials and immediately mixed with 3.0 ml of scintillation cocktail. The residual supernatant was aspirated, the sides and cap of each tube were wiped dry and 40 μl of 20% (v/v) Triton X-100 was added. Following the complete suspension of the pellet by vortex mixing, the bottom of the tube was cut off into a scintillation vial and pellet was resuspended in 3.0 ml of scintillant. The radioactivities of the supernatant and pellet were determined by dual-channel scintiallation counting for ^3H and $^{36}Cl^-$ using the appropriate quench and cross-over corrections.

$[Cl^-]_e/[Cl^-]_{tot}$ was calculated as (^3H_2O space - [^{14}C]methoxyinulin space) - (^3H_2O space - $^{36}Cl^-$ space)/(^3H_2O space - [^{14}C]methoxyinulin space). Values for ^3H_2O space and [^{14}C]methoxyinulin space were obtained from cell volume determinations. $\Delta\Psi_p$ was calculated using the Nernst equation as:

$$\Delta\Psi_p = -61.5 \cdot \log [Cl^-]_e/[Cl^-]_{tot}$$

$\Delta\Psi_p$ was calculated to be 36.0 mV (± 6.2; n=3) and 39.3 mV (± 0.7; n=3) in hepatocytes from old and young mice, respectively. These values are similar to those previously determined (Harper and Brand 1993).

j) Application of Top-Down Elasticity Analysis and Top-Down Control Analysis

To quantitatively ascertain the important sites of effects of aging on oxidative phosphorylation processes we used the top-down elasticity analysis approach described in the Introduction and by Brand (Brand 1990b). We defined the oxidative phosphorylation system as the tripartite system shown in Figure 3 and then determined the overall elasticities to $\Delta\Psi_m$ of the reactions that produce $\Delta\Psi_m$ (cellular catabolic reactions, the citric acid cycle and the electron transport chain) and those that consume it (ATP synthesis and consumption, and the proton leak). The kinetic response (or 'elasticity') of the $\Delta\Psi_m$-producers to $\Delta\Psi_m$ was measured by titrating $\Delta\Psi_m$-consumption with oligomycin (0.01-0.05 μg/ml). Oligomycin inhibits ATP synthase and thus inhibits $\Delta\Psi_m$-consumption by this enzyme. The kinetic response of the leak to $\Delta\Psi_m$ was assessed by titrating with antimycin (0.05 μM- 0.25 μM), an inhibitor of complex III of the respiratory chain, in the presence of saturating amounts of oligomycin (1.0 μg/ml). The elasticity of the phosphorylating system to $\Delta\Psi_m$ was measured from titrations with antimycin alone (0.10-0.20 μM). However, since the latter titrations provide the kinetics of both $\Delta\Psi_m$-consuming subsystems (*i.e.*, the phosphorylating and leak subsystems) corrections were made for the amount of oxygen required to balance the rate of proton leak at each $\Delta\Psi_m$ measured. This was done using the proton leak titration curve; the oxygen used to support leak at each of the

determined membrane potentials was subtracted. The net effect is a line representing the kinetics of phosphorylation reactions alone.

To determine the distribution of control over respiration rate and over $\Delta\Psi_m$ in cells from old and young mice we used top-down control analysis and the published equations for elasticities, flux control coefficients and concentration control coefficients (Hafner 1990). (Refer to the *Appendix* for a list of equations used).

3. *BROWN ADIPOSE TISSUE (BAT) MITOCHONDRIA of Ucp1-DEFICIENT MICE*

a) Treatment of Animals

Male 6 month of age uncoupling protein 1-deficient (-/-) ($UCP1^{tm1}$) mice and male heterozygous controls (+/-) on a hybrid C57BL/6J and 129/SvPas genetic background (Enerback *et al.* 1997) were obtained from the research colonies of Dr. Leslie P. Kozak at The Jackson Laboratory (Bar Harbor, ME). The mice were group housed (3/cage), given free access to Charles River 5075 rodent chow (4.5% fat by weight) and water, and kept at 23°C with light 07:00-19:00. Mice used in this study were cared for in accordance with the principles and guidelines of the Canada Council on Animal Care and the Institute of Laboratory Animal Resources (National Research Council, USA).

b) Electron Microscopy of BAT

Mice were transcardially perfused with 0.01 M phosphate buffered saline (pH 7.4) followed by 2% (w/v) glutaraldehyde. Interscapular BAT was then fixed with 2% osmium tetroxide and 0.1 M imidazole in 0.01 M phosphate buffer, dehydrated and embedded as earlier described by Edwards *et al.* (Edwards *et al.* 1992).

c) Isolation of Mitochondria from BAT

Mitochondria were isolated from interscapular BAT depots of 12 UCP1-deficient and 12 control mice. Mice were killed by decapitation prior to removal of BAT. BAT was dissected free of other adhering tissues and homogenized in 3.5 ml of ice-cold buffer

containing 250 mM sucrose, 1.0 mM HEPES, and 0.2 mM EDTA (pH 7.2 with KOH) using a glass/Teflon Potter-Elvehjem tissue grinder. For all centrifugations, a Sorvall refrigerated centrifuge (RC2-B) was used with SS-34 rotor. Fractionation of the homogenate was carried out by centrifuging at 3,000 rpm (1,500*g*) for 10 min at 4°C. The supernatant was then poured through a 250 um filter (Nitex) and recentrifuged at 10,000 rpm (16,000*g*) for 14 min at 4°C to obtain a mitochondrial pellet. The pellet was resuspended (on ice) in 175 µl of a suspension medium containing 120 mM KCl, 20 mM sucrose, 3.0 mM HEPES, 2.0 mM $MgCl_2 \cdot H_2O$, 2.0 mM EGTA and 0.5% defatted BSA (pH 7.2 with KOH). Resuspension was carried out both in the presence and absence of 1.0 mM GDP. Protein concentration of the mitochondrial suspension corrected for BSA in the medium was assayed by the biuret method at 540nm (described in Section *1b*) using BSA as the reference standard.

d) Measurement of Oxygen Consumption

The respiration of BAT mitochondria was measured using a Hansatech Clark-type oxygen electrode whose incubation chamber was maintained at 37°C and magnetically stirred. Each rate was assessed by incubating enough mitochondria in 1.0 ml of suspension medium to give approximately 1.0 mg mitochondrial protein/ml in the electrode chamber. All respiration rates were determined simultaneously and in parallel with measurements of protonmotive force in the chamber. Titrations were done in the presence of 80 ng/ml nigericin in order to bring ΔpH close to zero and effectively convert it to millivolt units (Brand 1995). 5.0 µM of rotenone was added to prevent the oxidation of any endogenous

NAD-linked substrates. *State 3* respiration rate was defined as the oxygen consumption rate in the presence of 10 mM succinate, 0.75 units/ml hexokinase and 10 mM ADP. *State 4* oxygen consumption was determined in the presence of maximal amounts of the ATP synthase inhibitor, oligomycin (6 µg/mg mitochondrial protein). It was confirmed that ATP synthase was completely inhibited in each experimental condition by additional oligomycin which caused no further inhibition of oxygen consumption and no further increase in protonmotive force.

e) Measurement of Mitochondrial Protonmotive Force (Δp)

Δp was measured using a lipophilic organic ion probe, triphenylmethylphosphonium ($TPMP^+$). The accumulation of the probe was measured usin a $TPMP^+$-sensitive electrode (Kwik-Tip™) which was constructed by using the methods of Kamo (Kamo 1979). The outputs from the $TPMP^+$ electrode and the O_2 electrode were transferred to two voltmeters whose reference sockets were connected together; data were then fed into a data analysis software package (Duo 18™ data recording system) which allowed real-time monitoring and recording of data on a personal computer.

The calibration of the $TPMP^+$-sensitive electrode, determination of mitochondrial matrix volumes, measurement of non-specific binding in mitochondria (a_m), and calculation of Δp from $TPMP^+$ electrode data were carried out as outlined below. Δp was calculated using the Nernst equation as:

$$\Delta p = 61.5 \cdot \log (a_m \cdot TPMP^+_m / TPMP^+_e)$$

$TPMP^+_m/TPMP^+_e$ represents the ratio of the accumulation of the cation inside and external to the mitochondria (See Section *3g*.)

f) Calibration of $TPMP^+$-sensitive Electrodes

Prior to each titration the $TPMP^+$ electrode was calibrated. Mitochondria (1.0 mg protein/ml) were added to the electrode chamber which contained 1.0 ml of suspension medium, nigericin (80 ng/mg protein) and rotenone (5.0 μM). The $TPMP^+$ electrode was then inserted and the incubation chamber sealed; once the trace was steady, TPMP-Br (10μM) was added. When the trace reached a new steady state value (5-20sec) a second 10 μM aliquot of $TPMP^+$ was added and another new steady state achieved. These additions were repeated until the total final $TPMP^+$ concentration was 50 μM. Succinate (10 μM) was then added and mitochondria were allowed to accumulate the $TPMP^+$ for a minute or two until an equilibrium distribution was achieved and the extramitochondrial $TPMP^+$ concentration was stable. Subsequent additions of various inhibitors, ionophores, or other compounds were then made, with the new steady state values being obtained within approximately one minute of each addition.

g) Calculation of Δp from $TPMP^+$ Electrode Data

The deflection caused by each 10 μM $TPMP^+$ addition in chart units from the baseline recorded was measured and plotted against the logarithm of the final $TPMP^+$ concentration to produce a calibration graph. To measure the external $TPMP^+$

concentration, $TPMP^+_e$, for any given electrode signal, the deflection from the baseline (in chart units) to the new steady state was determined. $TPMP^+_e$ was then directly read off of the calibration graph. The concentration of $TPMP^+$ in the mitochondrial matrix ($TPMP^+_m$) was determined as follows:

$$TPMP^+_m = \frac{[TPMP]_{added} - [TPMP_e]}{(0.001 \cdot MV \cdot \text{mg protein/ml})}$$

where MV represents mitochondrial matrix volume (in ml). $TPMP^+_m$ and $TPMP^+_e$ were determined for each mitochondrial titration and used to calculate Δp.

h) Measurement of Mitochondrial Matrix Volume

When mitochondria are incubated with a radiolabelled probe such as ^3H_2O and then sedimented, the accessible volume of the pellet can be calculated from the specific activity of the probe in the supernatant and the total radioactivity in the pellet. The difference in accessible volume ('pellet space') for a permeant probes like H_2O and probes like [C^{14}]sucrose that do not cross the inner membrane reports the volume of the matrix. 40 µl of mitochondria (~2 mg protein) were incubated in 1.0 ml of suspension medium containing 5.0 µM rotenone, 1.0 µCi of ^3H_2O and 0.1 µCi of [^{14}C]sucrose, for 2 min in a 1.5 ml minitube maintained at 37°C in a water bath. Mitochondria were then sedimented by centrifugation at 7,000 rpm (12,000*g*) for 2 min in a Fisher minifuge. 500 µl supernatant was removed and added to 7.5 ml of scintillation cocktail. The remainder of the supernatant was decanted and the walls and cap of the tube carefully dried. Resuspension of pellet was

carried out with 40 µl of 20% (v/v) Triton X-100 and by vortex mixing. Once the pellet was completely resuspended, the tip of the tube containing the mitochondrial pellet was cut and placed in 7.5 ml of scintillation cocktail (Amersham ACSII). The radioactivity of the supernatant and pellet were determined by dual-channel scintillation counting for ^{3}H and ^{14}C using the appropriate quench and cross-over corrections. Mitochondrial matrix volume (MV) was calculated as:

$$MV = \frac{(^{3}H_2O \text{ space} - [^{14}C]\text{sucrose space})}{\text{mg protein}}$$

Average mitochondrial matrix volumes were 0.85 µl/mg protein (± 0.15; n=3) in *Ucp1*-deficient mice and 0.45 µl/mg protein (± 0.20; n=3) in controls. These values were based on triplicate determinations completed on BAT mitochondria isolated and pooled from 7 *Ucp1*-deficient and 7 control mice.

i) Measurement of Non-Specific Binding of TPMP^{+} (a_m)

a_m was determined as described by Nobes *et al.* (Nobes *et al.* 1990b). $TPMP^{+}$ accumulation ratios and $^{86}Rb^{+}$ accumulation ratios in the presence of valinomycin were determined at three concentrations of KCl (0.2, 1.0 or 5.0 mM). For each concentration of KCl, two sets of minitubes were prepared; each set contained 80 µl of mitochondria (~2 mg protein), 1.0 ml of incubation medium (200 mM sucrose, 5.0 mM HEPES, 5.0 mM LiCl, 1.0 mM EGTA, 5.0 µM rotenone, 1.0 µM TPMP-Br, and 0.2 µg/ml valinomycin. To one set 0.035 µCi $^{86}RbCl$/ml and 0.15 µCi [^{3}H]TPMP/ml was added, and to the other 1.5 µCi

^3H_2O/ml and 0.15 μCi [^{14}C]sucrose/ml was added. In each set, each concentration of KCl was assessed in duplicate. Succinate (5.0 mM; brought to pH 7.0 with LiOH) was added to all tubes and they were mixed by inversion. After 2 min at room temperature the mitochondria were sedimented by centrifugation for 2 min at 7000 rpm (12,000*g*). 500 μl aliquots of the supernatant were removed and pipetted into scintillation vials containing 7.5 ml of scintillation cocktail. The residual supernatant was aspirated; the sides and cap were wiped dry and 40 μl of Triton X-100 was added. Following the complete suspension of the pellet by vortex mixing, the bottom of the tube was cut off into a scintillation vial and pellet was resuspended in 7.5 ml of scintillation cocktail containing 150 μl of ddH_2O. The radioactivity of the supernatant and pellet were determined by dual-channel scintillation counting for ^{3}H, ^{14}C and ^{86}Rb using the appropriate quench and cross-over corrections.

The apparent volume of pellet available to each isotope (in μl) was calculated as dpm in total pellet divided by dpm/μl of supernatant sample. The [^{3}H]TPMP$^+$ accumulation ratio, $([TPMP^+]_{tot}/[TPMP^+]_e$, was calculated as ([^{3}H]TPMP$^+$ space - [^{14}C]sucrose space)/(^3H_2O space - [^{14}C]sucrose space). The $^{86}Rb^+$ accumulation ratio, $[^{86}Rb^+]_{tot}/[^{86}Rb^+]_e$, was calculated as ($^{86}Rb^+$ space - [^{14}C]sucrose space)/(^3H_2O space - [^{14}C]sucrose space). By plotting [^{3}H]TPMP$^+$ accumulation ratios against $^{86}Rb^+$ accumulation, a linear relationship is obtained. The inverse slope of this line is defined as a_m. Values for a_m were determined to be 0.25 and 0.20 respectively for UCP1-deficient mice and controls. These mean values were based on data from BAT mitochondria isolated and pooled from 12 UCP1-deficient and 12 control mice. It was necessary to pool the mitochondria within the two groups due

to relatively large concentrations of mitochondria required for accurate determination of a_m. As duplicate measurements were not made, no SEM values are given.

j) Application of Top-Down Elasticity Analysis and Top-down Control Analysis

To quantitatively determine the effects of knocking out UCP1 on oxidative phosphorylation processes in BAT mitochondria we used the top-down elasticity approach described by Brand (Brand 1990b; Brand 1998) and Harper and Brand (Harper and Brand 1995). We defined the oxidative phosphorylation system as the tripartite system shown in Figure 3. The overall elasticities to changes in Δp of the reactions that produce Δp (*i.e.*, substrate transport, the citric acid cycle and the electron transport chain - collectively termed the substrate oxidation reactions) and the two blocks of reactions that consume Δp (*i.e.*, ATP synthesis and consumption reactions, and the mitochondrial proton leak reactions), were then determined.

The kinetic response of the Δp-producers to Δp was measured by titrating the Δp-consumer, ATP-synthase, with oligomycin (1-6 μg/mg mitochondrial protein). The kinetic response of the leak to Δp was assessed by completely inhibiting proton return through ATP synthase using maximal amounts of oligomycin (6 μg/mg mitochondrial protein) and titrating with malonate (0.20-2.0 mM), a competitive inhibitor of complex II of the respiratory chain. The elasticity of the phosphorylating subsystem to Δp was measured by titrating Δp-producers with malonate (0.2-2.0 mM) in the presence of saturating hexokinase (0.75 units/ml) and ADP (100 μM). All titrations were performed in the presence and absence of 1 mM GDP.

4. *SKELETAL MUSCLE MITOCHONDRIA of Ucp1-DEFICIENT MICE*

a) Treatment of Animals

17 male (6 mo.) uncoupling protein 1-deficient (-/-) ($UCP1^{tm1}$) mice and 16 male (6 mo.) heterozygous controls (+/-) on a hybrid C57BL/6J and 129/SvPas genetic background (Enerbäck *et al.* 1997) were obtained from the research colonies of Leslie P. Kozak at The Jackson Laboratory (Bar Harbor, ME). The mice were group housed (3/cage), given free access to Charles River 5075 rodent chow (4.5% fat by weight) and water, and kept at 23°C with light 07:00-19:00. Mice used in this study were cared for in accordance with the principles and guidelines of the Canada Council on Animal Care and the Institute of Laboratory Animal Resources (National Research Council, USA).

b) Isolation of Mitochondria from Skeletal Muscle

Mitochondria were isolated from hind limb and forelimb skeletal muscles of *Ucp1*-deficient and control mice. Specifically, these muscles included the muscles of the lower leg (gastrocnemius), thigh (vastus lateralis, rectus femoris, quadratus femoris, adductor brevis, semimembranosus, gluteus maximus, gluteus minimus, and gluteus medius), and shoulder (triceps longus and medius; biceps brevis and longus).

Mice were killed by decapitation prior to removal of skeletal muscle. Tissue was then immediately placed in ice-cold isolation medium (100 mM sucrose, 10 mM EDTA, 100 mM Tris-HCl, and 46 mM KCl). The muscle was dissected free of any visible connective tissue and fat. Clean muscle depots were taken piece by piece and placed on a pre-chilled watchglass, carefully minced using safety razor blades and put back into

isolation medium. Prior to homogenization, the tissue was filtered through 250 um filter (Nitex) and placed in 25 ml of isolation medium containing 5.0 mg of Nagarse (type XXVII protease, Sigma) for 5 min at room temperature, with occasional stirring. Homogenization was performed using a cold glass/Teflon Potter-Elvehjem tissue grinder. Fractionation of the homogenate was carried out by centrifugation at 3,000 rpm (484*g*) for 10 min at 4°C in a Sorvall RC2-B centrifuge with a SS-34 rotor. The supernatant was then poured through a 250 um filter (Nitex) into a clean polyethylene centrifuge tube and recentrifuged at 10,000 rpm (16,000*g*) for 10 min. The resulting supernatant was discarded and the pellet was resuspended using 5.0 ml of isolation medium containing 0.5% defatted BSA and centrifuged again at 10,000 rpm for a final 10 min. The resulting pellet was resuspended in 250 µl of suspension medium (120 mM KCl, 20 mM sucrose, 20 mM glucose, 10 mM KH_2PO_4, 5.0 mM HEPES, 2.0 mM $MgCl_2$ and 1.0 mM EGTA; pH 7.2 with KOH). Protein concentration of the mitochondrial suspension (corrected for BSA in the medium) was assayed by the biuret method (described in Section *1b.*) using BSA as the reference standard.

c) Meausurement of Mitochondrial Oxygen Consumption

The respiration of skeletal muscle mitochondria was measured using a Hansatech Clark-type oxygen electrode whose incubation chamber was maintained at 37°C and magnetically stirred. Each rate was assessed by incubating enough mitochondria in 1.0 ml of suspension medium to give approximately 0.5 mg mitochondrial protein/ml in the electrode chamber. All respiration rates were determined simultaneously and in parallel

with measurements of protonmotive force. Titrations were done in the presence of 40 ng nigericin/ml in order to convert ΔpH to millivolt units, and in the presence of 5.0 μM of rotenone to prevent the oxidation of any endogenous NAD-linked substrates. *State 3* respiration rate was defined as the oxygen consumption rate in the presence of 10 mM succinate, 0.65 units/ml hexokinase, 100 μM ADP, and 100 μM ATP. *State 4* oxygen consumption was determined in the presence of maximal amounts of the ATP synthase inhibitor, oligomycin (8 μg/mg mitochondrial protein). It was confirmed that ATP synthase was completely inhibited in each experimental condition by additional oligomycin which caused no further inhibition of oxygen consumption and no further increase in proton motive force. Titrations were initially performed in the presence and absence of GDP in experiments with 3 *Ucp1*-deficient and 3 control mice. Once it was established that it had no effect, it was no longer used and the previous results were pooled.

d) Measurement of Mitochondrial Protonmotive Force (Δp) and Calibration of $TPMP^+$electrodes

Measurement of Δp and calibration of $TPMP^+$-sensitive electrodes was carried out as described earlier in sections (*3c,f and g.*).

e) Measurement of Mitochondrial Matrix Volume

80 μl of mitochondria (~2 mg protein) were incubated in 1.0 ml of suspension medium containing 5.0 μM rotenone and 1.0 μCi of ^3H_2O, and 0.1 μCi of [^{14}C]sucrose, for 2 min in a 1.5 ml minitube maintained at 37°C in a water bath. Mitochondria were then

sedimented by centrifugation at 7,000 rpm (12,000*g*) for 2 min in a Fisher minifuge. 500 µl supernatant was removed and added to 7.5 ml of scintillation cocktail. The remainder of the supernatant was decanted and the walls and cap carefully dried with a rolled-up tissue. Resuspension of pellet was carried out with 40 µl of 20%(v/v) Triton X-100 and by vortex mixing. Once the pellet was completely resuspended the tip of the tube was cut and placed in 7.5 ml of scintillant. The radioactivity of the supernatant and pellet were determined by dual-channel scintillation counting for ^{3}H and ^{14}C using the appropriate quench and cross-over corrections. Mitochondrial matrix volume (MV) was calculated as described in Section *3h.* Average mitochondrial matrix volumes were 0.52 µl/mg protein (± 0.16; n=2) in *Ucp1*-deficient mice and 0.48 µl/mg protein (± 0.18; n=2) in controls.

f) Measurement of Non-Specific Binding of TPMP^{+} (a_m)

[^{3}H]TPMP^{+} accumulation ratios and $^{86}Rb^{+}$ accumulation ratios in the presence of valinomycin were determined as described in Section *3i.* Values for a_m were determined to be 0.314 and 0.357 respectively for UCP1-deficient mice and controls. These mean values were based on data from skeletal muscle mitochondria isolated and pooled from 2 UCP1-deficient and 2 control mice. Since our results are based upon one experiment, no SEM values were obtained.

g) Application of Top-Down Elasticity Analysis and Top-down Control Analysis

To quantitatively determine the effects of knocking out UCP1 on oxidative phosphorylation processes in skeletal muscle mitochondria we used the top-down elasticity

approach described by Brand (Brand 1990b; Brand 1998) and Harper and Brand (Harper and Brand 1995). We defined the oxidative phosphorylation system as the tripartite system show in Figure 3 and then determined the overall elasticities to changes in Δp of the reactions that produce Δp (*i.e.*, substrate transport, the citric acid cycle and the electron transport chain - collectively termed the substrate oxidation reactions) and the two blocks of reactions that consume Δp (*i.e.*, ATP synthesis and consumption reactions, and the mitochondrial proton leak reactions).

The kinetic response of the Δp-producers to Δp was measured by using maximal amounts of oligomycin (8 μg/mg mitochondrial protein) to inhibit proton return through ATP synthase and then titrating with hexokinase (0.325 and 0.65 units/ml). The kinetic response of the leak to Δp was assessed by using maximal amounts of oligomycin and titrating with malonate (0.20-2.0 mM). The elasticity of the phosphorylating subsystem to Δp was measured by titrating Δp-producers with malonate (0.2-2.0 mM) in the presence of saturating amounts of hexokinase (0.65 units/ml).

5. MATERIALS

Oligomycin, antimycin, FCCP, malonate, BSA (fraction V), Nagarse (type XXVII), hexokinase (type III), succinic acid, and GDP were purchased from Sigma. $^{3}H_2O$, ^{14}C-sucrose, ^{14}C-methoxyinulin, $^{86}RbCl$, ^{36}Cl and ^{3}H-TPMP-Br were purchased from Mandel Scientific Ltd and Dupont-NEN.

6. STATISTICAL ANALYSIS

Data were analyzed using Student's t tests or ANOVA which was followed by Tukey's post hoc tests. Linear regression lines were compared by analysis of covariance using Prism 2 for Windows. A p value of less than 0.05 was considered statistically significant. Unless otherwise stated, results are presented as means and SEM.

III. RESULTS

1. Age-related changes in oxidative phosphorylation of mouse hepatocytes.

a) Resting respiration rates and mitochondrial membrane potentials in hepatocytes from old and young mice

The resting respiration rate of hepatocytes from old mice was significantly less than that of hepatocytes from young controls ($p<0.04$). Values were corrected for non-mitochondrial oxygen consumption, and were determined to be 70.9 ± 3.4 (n= 10) and 83.8 ± 5.1 (n= 7) nmol $O_2 \cdot min^{-1} \cdot 10^6$ $cells^{-1}$ for cells from old and young mice, respectively (Figure 5).

Resting state $\Delta\Psi_m$ was not significantly different between cells from old and young mice. Values were 149 mV ± 4.4 (n=8) and 147 mV ± 3.4 (n=7) in cells from old and young mice, respectively (Figure 5). *State 4* $\Delta\Psi_m$ values were 155 mV ±5.0 (n= 8) and 154 mV ± 3.0 (n=7), respectively (Figure 4). The finding that there were no significant effects of age on $\Delta\Psi_m$ results indicates that any age-induced changes in the $\Delta\Psi_m$-consumers (*i.e.*, leak and ATP turnover in the resting state, and leak alone in *state 4*) are matched by any changes in the $\Delta\Psi_m$-producers (*i.e.*, substrate oxidation reactions).

b) Comparison of the kinetic responses of the mitochondrial proton leak, substrate oxidation and phosphorylation subsystems to $\Delta\Psi_m$ in hepatocytes from old and young mice

The top-down elasticity analysis was used to assess the kinetic responses of the mitochondrial proton leak, substrate oxidation and phosphorylation subsystem of reactions

Figure 4: Relationship between mitochondrial membrane potential ($\Delta\Psi_m$) and non-phosphorylating respiration in isolated hepatocytes from old and young rats. The kinetic response of the proton leak subsystem to $\Delta\Psi_m$ was determined via inhibition of $\Delta\Psi_m$ producers (*i.e.*, substrate oxidation reactions) with increasing amounts of antimycin (0.05μM - 0.25μM) in the presence of saturating amounts of oligomycin (1.0 μg/ml). The two points on the top right represent *state 4* respiration. Each point is presented as the mean ±SEM of duplicate assays with cells from 8 old and 6 young mice.

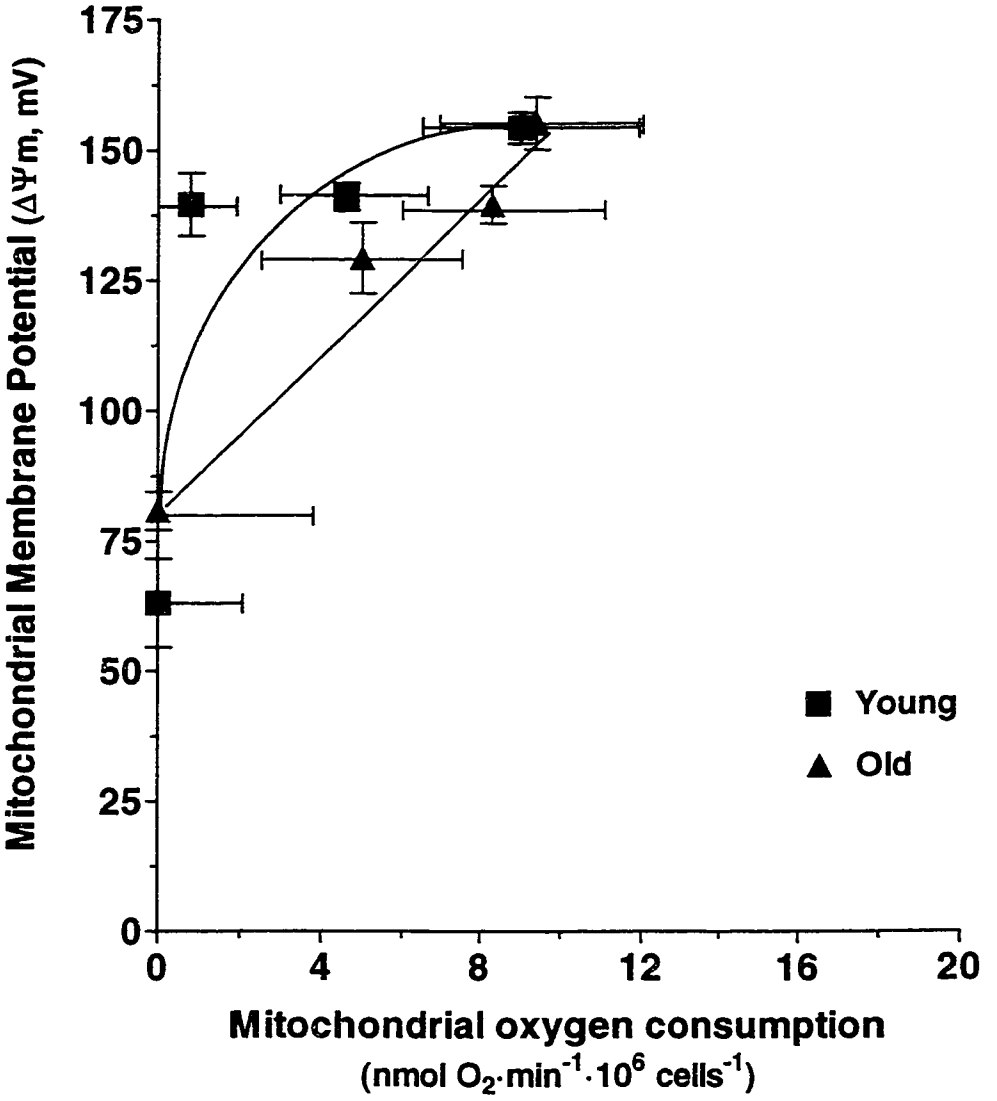
175
150
125
100
75
50
25
0
Mitochondrial Membrane Potential (ΔΨm, mV)
0
4
8
12
16
20
Mitochondrial oxygen consumption
(nmol O2·min-1·10^6 cells-1)
Young
Old

Figure 5: Relationship between mitochondrial membrane potential ($\Delta\Psi_m$) and respiration rate of substrate oxidation reactions in isolated hepatocytes from old and young mice. The kinetic response of the substrate oxidation subsystem was determined by titrating ATP-turnover reactions with oligomycin (0.01-0.05 μg/ml). The two furthermost points on the right represent the resting state $\Delta\Psi_m$ and respiration. Each point is presented as the mean ±SEM of duplicate assays with cells from 8 old and and 7 young mice. Oxygen consumption rates have been corrected for non-mitochondrial respiration rates.

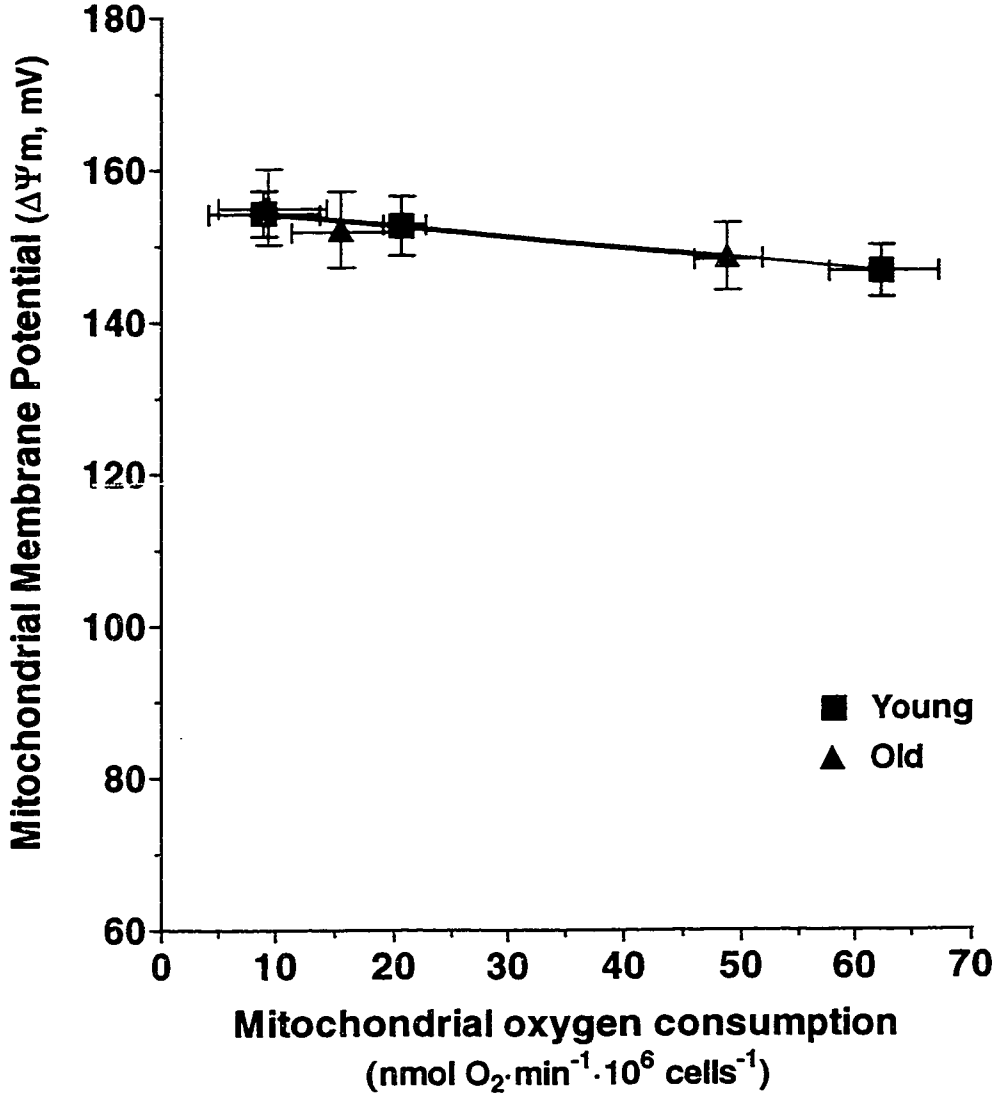
Mitochondrial Membrane Potential (ΔΨm, mV)
180
160
140
120
100
80
60
0
10
20
30
40
50
60
70
Young
Old
Mitochondrial oxygen consumption
(nmol O2·min-1·10^6 cells-1)

to $\Delta\Psi_m$ in hepatocytes and the results are shown in Figure 4-6. The oxygen consumption rates are corrected for non-mitochondrial oxygen consumption as described in the methods section. These results show that over a wide range of mitochondrial membrane potentials, the amount of oxygen used to support the mitochondrial proton leak is greater in cells from old mice. Because the kinetics of the proton leak subsystem are non-linear, an analysis of covariance could not be used to test for statistically significant differences. However, taken together, the results show that the overall kinetics of the mitochondrial proton leak are altered in hepatocytes from old mice in relation to the results from young mice.

The kinetic responses of the substrate oxidation subsystem to $\Delta\Psi_m$ in old and young hepatocytes are compared in Figure 5. The results indicate that at any value of $\Delta\Psi_m$, there is no difference in the rate of the $\Delta\Psi_m$-producing reactions between old and young hepatocytes. Thus there are no age-related differences in the overall responsiveness of the substrate oxidation reactions to $\Delta\Psi_m$ in cells from old and young mice.

A comparison of the kinetic responses of the phosphorylating subsystem to $\Delta\Psi_m$ in old and young hepatocytes revealed marked differences ($p<0.05$; analysis of covariance) (Figure 6). At the resting state, the rate of the phosphorylating subsystem was approximately 30% lower in the old cells than in the young cells at identical values of $\Delta\Psi_m$ (147 mV).

c) Quantitative analysis of the effects of the altered kinetics of the mitochondrial proton leak and phosphorylating subsystems to $\Delta\Psi_m$ on respiration rate in hepatocytes from old mice

The titrations of cellular respiration rate in old and young hepatocytes which were used to determine the kinetics of the subsystems described in Figures 4-6 can be used to quantify

Figure 6: Relationship between mitochondrial membrane potential ($\Delta\Psi_m$) and respiration rate of phosphorylation reactions in isolated hepatocytes from old and young mice. The kinetic response of the phosphorylating subsystem was obtained via titration of resting respiration (the furthermost data points on the right) with antimycin (0.10-0.20 μM). Each point represents the mean ±SEM of duplicate determinations of cells from 5 old and 5 young mice.

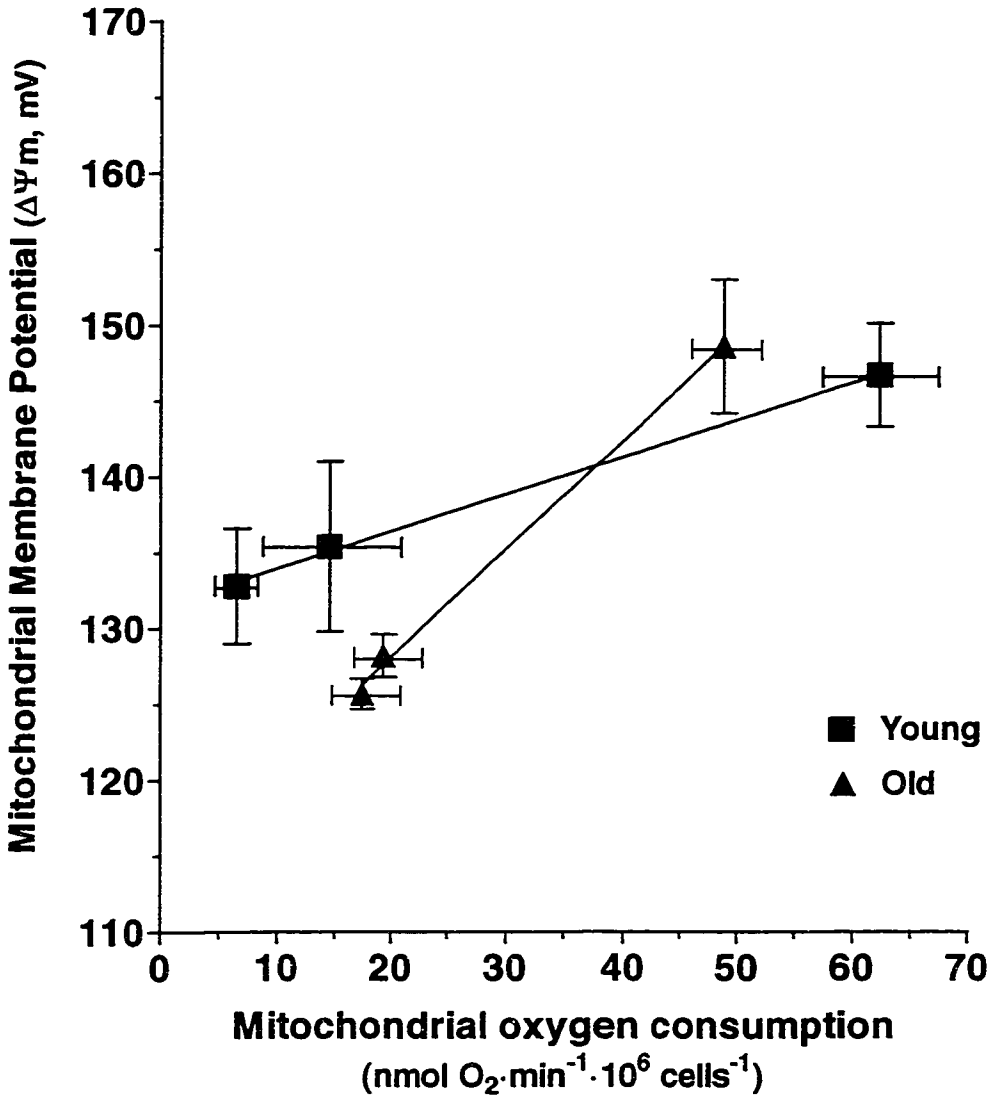
Mitochondrial Membrane Potential (ΔΨm, mV)
170
160
150
140
130
120
110
0
10
20
30
40
50
60
70
Mitochondrial oxygen consumption
(nmol O2·min-1·10^6 cells-1)
Young
Old

the proportions of oxygen consumption that sustains various blocks of energy dissipating reactions: non-mitochondrial oxygen consumption, proton leak reactions and ATP turnover reactions (Brand 1990b). The proportion of resting cellular oxygen consumption that is non-mitochondrial was identified as that which was insensitive to saturating amounts of antimycin (0.25 μM), oligomycin (1.0 μg/ml), valinomycin (0.1 μM) and FCCP (20 μM). There was no significant difference in the amounts of non-mitochondrial oxygen consumption; values for old and young cells were, 22.1 ±3.7 (n= 8) and 21.5 ±1.2 (n=7) nmol $O_2 \cdot min^{-1} \cdot 10^6$ $cells^{-1}$, respectively. The total mitochondrial oxygen consumption and the amounts used to balance the proton leak and ATP turnover reactions at the resting value of $\Delta\Psi_m$ are shown in Figure 7. Despite the fact that the proportion of resting mitochondrial respiration used to balance the mitochondrial proton leak is doubled in the cells from old mice compared to young there is a small but significant decrease in respiration ($p < 0.04$). This decrease can thus be accounted for entirely by a decrease ($p < 0.03$) in the rate of ATP synthesis and consumption.

d) Application of top-down control analysis

As well as being useful in the identification of the sites of action of an external effector, and in the quantitative determination of the importance of flux changes induced within the system by an external effector, top-down elasticity analyses provide all the data needed for a top-down control analysis of the system (Brown *et al.* 1990a; Hafner 1990a). Simply put, metabolic control analysis is a quantitative approach of both theoretical and practical use for determining the control structure of a metabolic system. A top-down

Figure 7: The proportions of resting mitochondrial oxygen consumption due to proton leak and ATP turnover reactions. Total oxygen consumption is the resting rate of mitochondrial oxygen consumption measured in the absence of any inhibitors or uncouplers, and represents the sum of the oxygen required to fuel the phosphorylation and leak pathways. Total oxygen consumption is significantly lower in the old than in the young hepatocytes ($p<0.05$). The oxygen used to balance the mitochondrial proton leak is determined by extrapolation from the titration curves shown in Figure 4; the oxygen consumption attributable to the leak at the resting mitochondrial membrane potential is subtracted from the total resting mitochondrial oxygen consumption. Statistical analyses show that the apparently greater leak in old cells does not reach the level of statistical significance. However, the oxygen consumed to support ATP production and turnover was significantly lower in the old compared to the young. Data were analyzed using ANOVA and Tukey's post hoc tests. SEM values are indicated; the ±SEM for the proton leak at resting $\Delta\Psi_m$ (mV) was estimated as the mean of the SEM for the two data points adjacent to it on the proton leak curve in Figure 4.

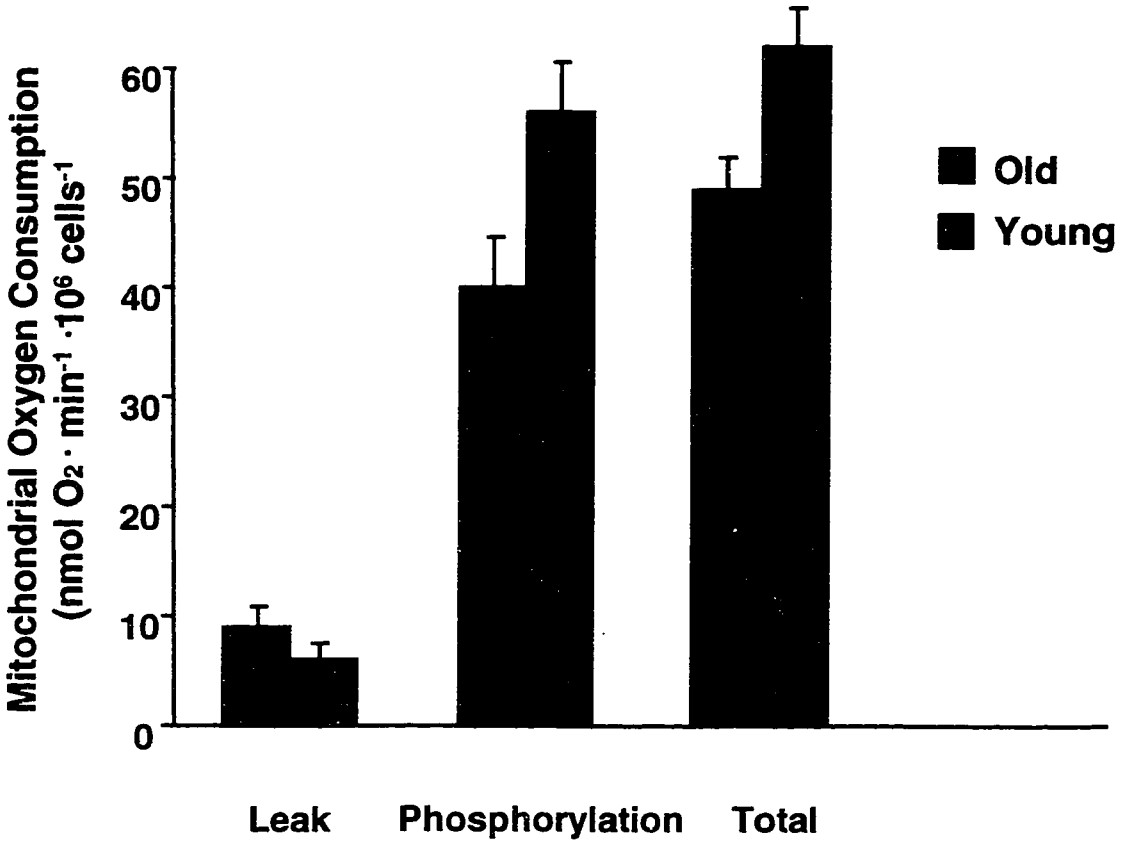
Mitochondrial Oxygen Consumption
(nmol O2 · min-1 ·10^6 cells-1
60
50
40
30
20
10
0
Old
Young
Leak
Phosphorylation
Total

control analysis was completed using the data from the elasticity analyses around $\Delta\Psi_m$ in old and young hepatocytes. All of the data needed for the calculation of elasticity and control coefficients can be obtained from mitochondrial membrane potential and oxygen consumption values in Figure 4-6. Values of each, and the inverse slopes of the respective elasticity lines, are then used in the published series of equations (Hafner 1990a) for the calculation of control coefficients (see *Appendix*). The results for cells in the resting state and in *state 4* are shown in Tables 1-3. The results were calculated using mitochondrial respiration rates; similar elasticities and control coefficients were obtained when calculations were based upon total cellular respiration rates. The elasticities to $\Delta\Psi_m$ of the substrate oxidation, phosphorylating and proton leak subsystems are given in Table 1.

The flux control coefficients of the three subsystems over the rate of each of the subsystems are shown in Table 2 A-C. The flux control coefficients describing the distribution of control over mitochondrial oxygen consumption (J_S) are shown in Table 2A. The results from the young control hepatocytes in the resting state indicate that the substrate oxidation reactions (0.51; *i.e.,* 51% of the control) and phosphorylation reactions (0.45) exert most of the control over J_S while the remainder of the control is through the proton leak (0.04). These results are similar to those obtained with hepatocytes from euthyroid rats (Harper and Brand 1993) (Harper and Brand 1994), - however, the amount of control exerted by the proton leak is smaller here than with the latter. This is most likely due to the respiration state in these cells under our resting incubation conditions; it is possible that these hepatocytes are respiring at a state closer to *state 3*. As mitochondrial respiration approaches their true *state 3* rates, the amount of control exerted by the leak over oxygen

Table 1

Overall elasticities to $\Delta\Psi_m$ for the substrate oxidation, phosphorylating and proton leak subsystems in hepatocytes from old and young control mice.

	Resting		State 4	
	Old	**Young**	**Old**	**Young**
$\epsilon^{S}_{\Delta\varphi m}$	-10.2	-13.2	-449.5	-243.3
$\epsilon^{P}_{\Delta\varphi m}$	5.2	10.3	---	---
$\epsilon^{L}_{\Delta\varphi m}$	3.3	8.3	20.4	14.5

§**Note:** Elasticity coefficients are defined as the fractional change in flux caused by an infinitesimal fractional change in the intermediate. Coefficients for each of the three branches of the overall system, substrate oxidation reactions, the phosphorylating reactions and the leak are shown here. Results were calculated from the resting and *state 4* values of $\Delta\Psi_m$ and hepatocyte mitochondrial oxygen consumption rates from the metabolic titrations described in Figure 4-6. Similar values of elasticities were obtained if total cellular oxygen consumption rates were used instead of mitochondrial oxygen consumption rates. As there is no ATP synthesis occurrin in *state 4*, there are no elasticity of control coefficients (Table 2) for this subsystem under *state 4* conditions.

§Note: Flux control coefficients of substrate oxidation, phosphorylating and proton leak subsystems over: **A)** substrate oxidation flux, **B)** phosphorylating system flux, **C)** proton leak flux. The concentration control coefficients over $\Delta\Psi_m$ by the substrate oxidation, phosphorylating and proton leak subsystems are shown in **D.** Results were calculated from the resting and *state 4* values of $\Delta\Psi_m$ and hepatocyte mitochondrial oxygen consumption rates from the metabolic titrations described in Figure 4-6. For the responses represented by straight lines (*i.e.*, phosphorylating and substrate oxidation subsystems) analyses of covariance showed that the lines representing the responses of the phosphorylating and substrate oxidation subsystems were and were not significantly different, respectively (p value of 0.05) between old and young cells. Similar values of control coefficients were obtained if total cellular oxygen consumption rates were used instead of mitochondrial oxygen consumption rates. The numbers of hepatocyte preparations used for these calculations are those described in the legends to Figure 4-6.

Table 2

Flux control coefficients over subsystem fluxes and concentration control coefficients over $\Delta\Psi_m$ in hepatocytes from old and young control mice.

	Resting		State 4	
	Old	**Young**	**Old**	**Young**
A				
C_s^{Js}	0.34	0.51	0.1	0.1
C_p^{Js}	0.54	0.45	---	---
C_L^{Js}	0.12	0.04	0.9	0.9
B				
C_s^{Jp}	0.36	0.53	---	---
C_p^{Jp}	0.7	0.51	---	---
C_L^{Jp}	-0.06	-0.04	---	---
C				
C_s^{JL}	0.22	0.31	0.04	0.1
C_p^{JL}	-0.18	-0.28	---	---
C_L^{JL}	0.96	0.97	0.96	0.9
D				
$C_s^{\Delta\varphi m}$	0.06	0.04	0.002	0.003
$C_p^{\Delta\varphi m}$	-0.05	-0.03	---	---
$C_L^{\Delta\varphi m}$	-0.01	-0.01	-0.002	-0.003

consumption approaches zero (Brown *et al.* 1990a). Moreover these metabolic control data are the first from cells of mice and these differences may reflect a species effect. Results from old mice, compared to those from young controls, show an interesting shift in control over J_S away from substrate oxidation reactions towards the phosphorylation and leak reactions. In old cells, 54% and 12% of the control over resting mitochondrial oxygen consumption are mediated through phosphorylation and leak reactions, respectively. The corresponding values in young control cells are 45% and 4%.

Results shown in Table 2B similarly show that in old cells compared to young there is a shift in control over the phosphorylation reactions away from substrate oxidation reactions towards phosphorylation reactions and leak reactions. Control by the substrate oxidation reactions and phosphorylation reactions over the flux through the mitochondrial proton leak reactions (Table 2C) in old cells compared to young show that there are decreases to roughly equal but opposite extents for these two blocks of reactions. Control over leak flux by the leak reactions themselves remains high in both old and young.

The concentration control coefficients of the three subsystems over the intermediate in the system, $\Delta\Psi_m$, are shown in Table 2D. Concentration control coefficients describe the distribution of control by blocks of reactions in a system over the amount of the intermediate in the system and, unlike flux control coefficients which sum to unity, concentration control coefficients sum to zero. The values are also similar to the values determined for hypothyroid cells (Harper and Brand 1993) and for euthyroid cells (Brown *et al.* 1990a; Harper and Brand 1993). The results for old and young cells are roughly similar and show that most of the control over the amount of the intermediate, $\Delta\Psi_m$, is

exerted by the substrate oxidation subsystem and the remainder of the control is through the activity of the $\Delta\Psi_m$- consumers: the proton leak and phosphorylating subsystems.

As described by Brand *et al* (Brand *et al.* 1993), it is possible to estimate the effective P/O ratio and the distribution of control (*i.e.*, control coefficients) over the effective P/O ratio using data such as those described above. Since phosphorylation flux is measured as the oxygen consumed to drive the phosphorylation reactions, the ratio of J_P divided by J_S provides the fraction of oxygen consumption that is used to support phosphorylation - irrespective of the true value of the maximum P/O ratio. The remaining fraction of the oxygen consumption (J_L/J_S) is used to support mitochondrial proton leak reactions. Thus the effective P/O ratio at any rate between *state 3* and *state 4* is this ratio multiplied by the maximum P/O ratio, P/O_{max}. The effective P/O ratios based on mitochondrial oxygen consumption data are shown in Table 3. In theory, the oxidation of glucose by cells produces a maximum of 31 molecules of ATP per molecule of glucose (Hinkle *et al.* 1991); this corresponds to a P/O_{max} of 2.58. The values shown in Table 3 for mitochondrial respiration are higher than the previously published values (Brand *et al.* 1993) and again support the postulate that cells are metabolically positioned close to *state 3* respiration.

Brand *et al* (Brand *et al.* 1993) describe the derivation of flux control coefficients which quantitatively describe the control by the three blocks of reactions over the effective P/O ratio:

$$C_S^{P/O} = C_S^{Jp} - C_S^{Js}$$

$$C_P^{P/O} = C_P^{Jp} - C_P^{Js}$$

$$C_L^{P/O} = C_L^{Jp} - C_L^{Js}$$

Table 3

Control coefficients over the effective P/O ratio in hepatocytes from old and young control mice.

	Resting	
	Old	**Young**
Effective P/O ratio (J_P/J_S) [§]	0.82	0.9
$C_s^{P/O}$	0.02	0.02
$C_p^{P/O}$	0.16	0.06
$C_L^{P/O}$	-0.18	-0.08

§Note: In intact hepatocytes there is a substantial rate of non-mitochondrial oxygen consumption, so the effective P/O ratio differs depending on whether this is subtracted or not. When total cellular oxygen consumption is used as Js, instead of mitochondrial oxygen consumption as above, the resulting effective P/O ratios are 0.56 and 0.67 for old and young, respectively.

These equations were used with the flux control coefficients shown in Table 2 using values from the resting respiration states; the resulting coefficients are shown in Table 3. Since these control coefficients describe control over the fraction of the oxygen flux that is used to drive ATP synthesis (*i.e.*, over the ratio Jp/Js) their values are independent of assumed or calculated values of P/O max.

Similar to the results for hepatocytes described earlier (Brand *et al.* 1993), the block of reactions with the least amount of control are the substrate oxidation reactions - showing that increases in substrate supply on their own, produce only very small changes in the effective P/O ratio. The control coefficients for the leak reactions over the effective P/O ratio are relatively large and negative - indicating that increases in mitochondrial proton leak reactions would cause substantial decreases in the effective P/O ratio. The coefficients from cells of old compared to those of young mice, differ in that the amounts of control by phosphorylation and leak reactions are more than double in each case. Control by substrate oxidation reactions remains low in old and young cells. These results indicate that in hepatocytes from old mice, the efficiency of oxidative phosphorylation is more sensitive to changes in the amount of mitochondrial proton leak and in the rate of ATP synthesis and turnover reactions.

2. Brown adipose tissue mitochondria of *Ucp1*-deficient mice.

a) Brown adipose tissue mitochondrial morphology in situ

The ultrastructure of interscapular BAT mitochondria from *Ucp1*-deficient mice is markedly different from that of controls. This is evident in the representative electron micrographs shown in Figure 8. In control mitochondria (Figure 8A), cristae are fairly tightly packed and often extend across the width of the mitochondrion, while in *Ucp1*-deficient mice (Figure 8B) there are fewer cristae; the intracristal space is contracted; the cristae often appear in semi circular systems, the matrix is expanded, and the size of the mitochondria is more variable than in controls. Interestingly, the unusual structure in *Ucp1*-deficient mice is somewhat similar to that of BAT mitochondria of the leptin deficient, *ob/ob* mouse in which BAT thermogenesis is abnormally low (Hogan andHimms-Hagen 1980).

b) Overall kinetics of the three blocks of reactions comprised by the oxidative phosphorylation system

As described in the Introduction, the approach that we have used to study metabolic differences in BAT mitochondria isolated from *Ucp1*-deficient and control mice is referred to as top-down elasticity analysis. In Figure 9 the overall responsiveness, or 'elasticity' to changes in Δp for the three blocks of reactions of the oxidative phosphorylation (as depicted in Figure 3) are shown. Figure 9 shows the overall kinetics of the leak, substrate oxidation reactions, and phosphorylation plus leak reactions from BAT mitochondria of *Ucp1*-deficient mice (Figure 9A) and control mice (Figure 9B). Mitochondria were incubated in

Figure 8: Electron microscopy of mitochondria in brown adipose tissue from control (A) and *Ucp1*-deficient (B) mice (60,000x magnification).

(Electron micrographs provided by Dr. L.P. Kozak)

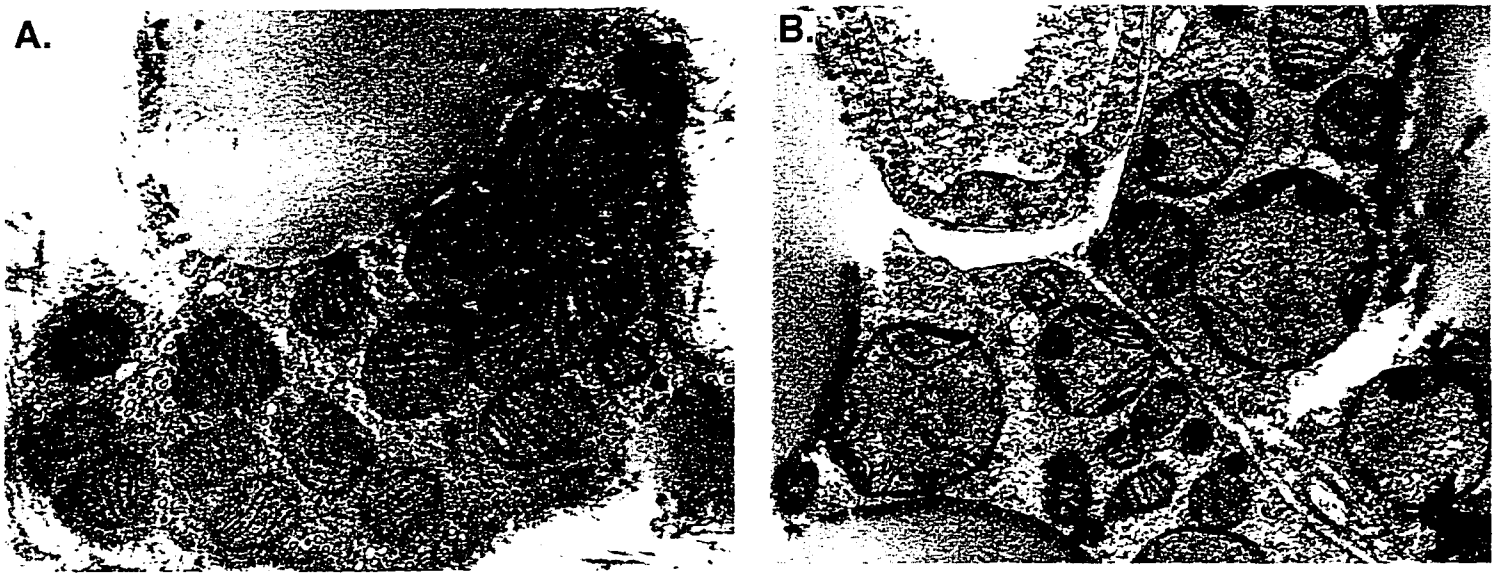
A.
B.

Figure 9: The overall kinetic responses of the substrate oxidation, proton leak, and phosphorylating subsystems to Δp in BAT mitochondria from *Ucp1*-deficient (A) and control (B) mice in the absence of 1 mM GDP, but presence of 0.5% defatted BSA. The kinetic response of the substrate oxidation subsystem (**circles**) to Δp is obtained by titration of *state 3* respiration (furthermost point on the right) with increasing amounts of oligomycin (1-6 μg/mg mitochondrial protein) to inhibit ATP synthase, a Δp consumer. The kinetic response of the proton leak pathway (**squares**) was determined via titration of *state 4* respiration (point with the highest Δp) with increasing amounts of malonate (0.2-2.0 mM) to inhibit the Δp producers; since ATP synthesis is completely inhibited with oligomycin, the only other route of proton return into mitochondria is via proton leak reactions. The kinetic reponse of the phosphorylation subsystem (**triangles**), was obtained by titration of *state 3* respiration with malonate (0.33, 0.66, 1.0, 2.0 and 3.0 mM) in the presence of saturating amounts of hexokinase (0.75 units/ml) and ADP (100 μM); since a small amount of leak remains at these Δp, the values plotted must be corrected for this to result in the kinetics of the phosphorylating system alone. These corrected values are plotted in Figure 12. The overall kinetics of the three blocks of reactions are further analysed in Figures 10-12.

A

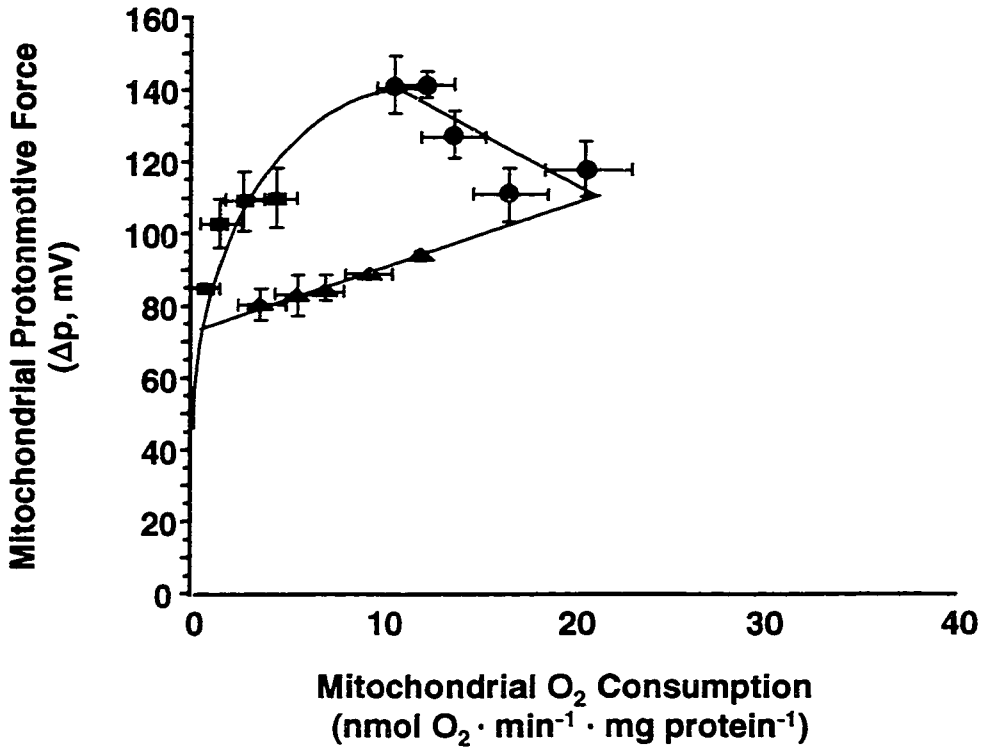
Mitochondrial Protonmotive Force
(Δp, mV)
160
140
120
100
80
60
40
20
0
0
10
20
30
40
Mitochondrial O2 Consumption
(nmol O2 · min-1 · mg protein-1)

B

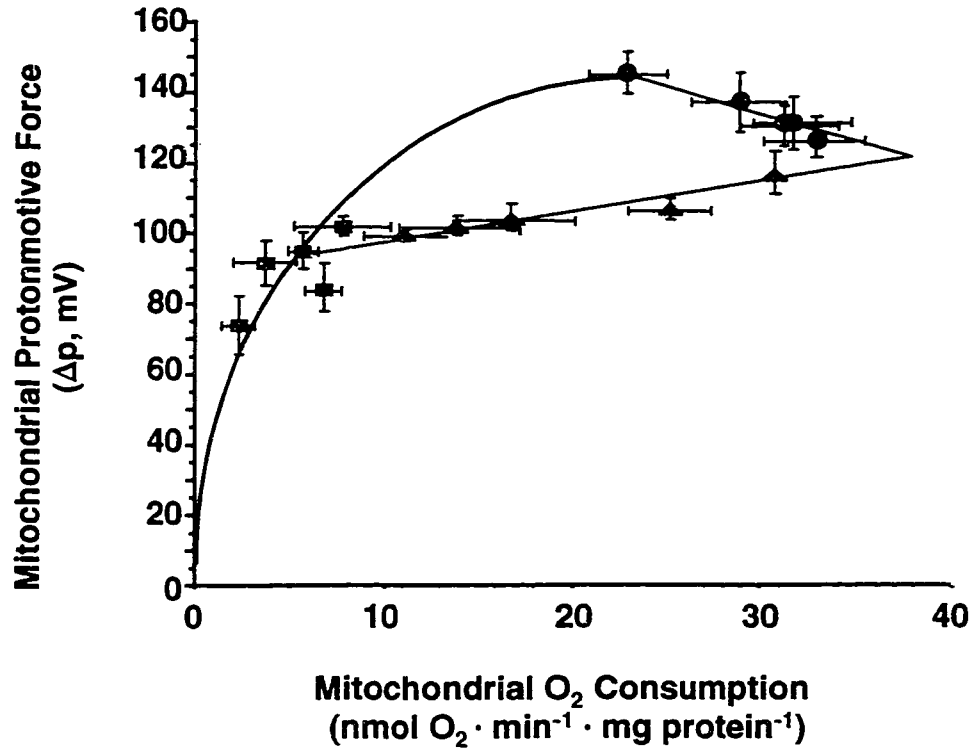
Mitochondrial Protonmotive Force
(Δp, mV)
160
140
120
100
80
60
40
20
0
0
10
20
30
40
Mitochondrial O2 Consumption
(nmol O2 · min-1 · mg protein-1)

the absence of GDP, but in the presence of 0.5% BSA to limit fatty acid activated uncoupling and extend the time over which the mitochondria respired. Fatty acids are known to activate uncoupling through UCP1 (Brown *et al.* 1990b; Desautels *et al.* 1978; Nicholls and Locke 1984). Whether or not fatty acids acutely activate other uncoupling proteins is not known. In Figure 9 A and B, the furthermost points on the right in each show the *state 3* respiration rates and Δp values. Comparison of values for *Ucp1*-deficient and control mitochondria shows that the presence of UCP1 in control mitochondria causes a ~70% increase in *state 3* respiration rate in the absence of GDP. It should be noted that in the absence of GDP the *state 3* respiration rate in control mitochondria is higher than that which is achieved in its presence. This results presumably from the situation where UCP1 is not inhibited by GDP, protons leak into the matrix through UCP1, and the chain responds by oxidizing substrates at a higher rate to sustain a Δp. *State 4* (*i.e.*, non-phosphorylating) respiration (highest Δp values and located at the top of the proton leak curves) is ~100% greater in mitochondria from control BAT than UCP1-deficient BAT - again this is due presumably to the activity of UCP1 in control mitochondria. The respiratory control ratios (*i.e.*, *state 3 / state 4* respiration rates) in the absence of GDP are 2.0 and 1.6, for control and *Ucp1*-deficient mitochondria, respectively.

c) Overall kinetics of the mitochondrial proton leak, and their sensitivity to the purine nucleotide, GDP

The data in Figure 10A clearly show that *state 4* respiration (maximal leak-dependent respiration) in BAT mitochondria from *Ucp1*-deficient mice is insensitive to GDP, while

Figure 10: The effect of 1 mM GDP on the kinetic response of the proton leak to Δp in BAT mitochondria from *Ucp1*-deficient (A) and control (B) mice. Results in (A) show that BAT mitochondria from *Ucp1*-deficient mice, the non-metabolizable purine nucleotide, GDP, does not affect the overall kinetics of proton leak reactions. In (B), results show that GDP inhibits proton leak reactions in BAT mitochondria from control mice. The kinetic response of the leak was determined via inhibition of Δp producers (*i.e.*, substrate oxidation reactions) with increasing amounts of malonate (0.33, 0.66, 1.0, 2.0 and 3.0 mM) in the presence of saturating amounts of oligomycin (6 μg/ mg mitochondrial protein) in order to obtain *state 4* respiration (two furthermost points on the right). Each point represents the mean ±SEM of duplicate experiments with 12 *Ucp1*-deficient and 13 control mice.

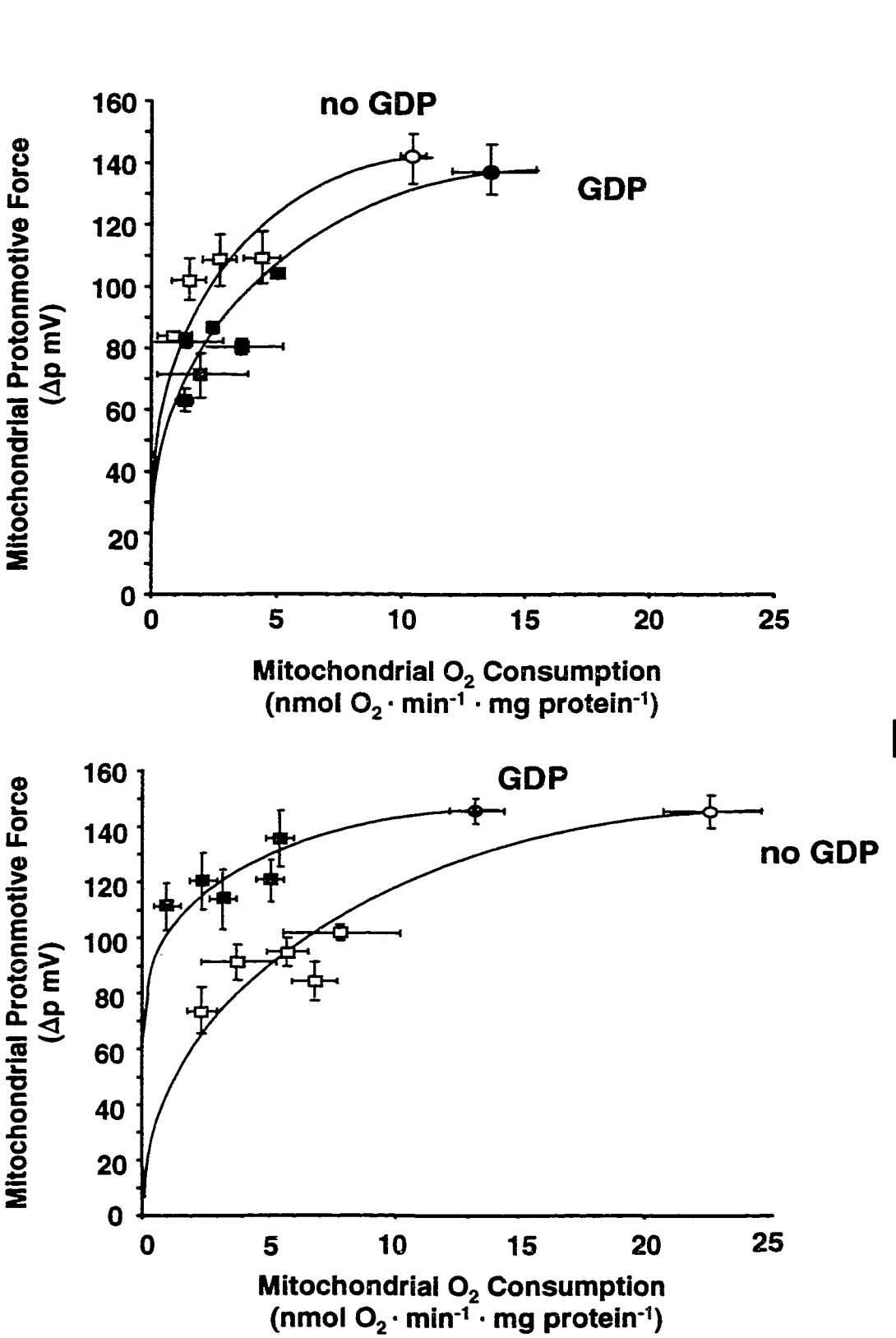
A
no GDP
GDP
Mitochondrial Protonmotive Force
(Δp mV)
160
140
120
100
80
60
40
20
0
0
5
10
15
20
25
Mitochondrial O2 Consumption
(nmol O2 · min-1 · mg protein-1)
B
GDP
no GDP
Mitochondrial Protonmotive Force
(Δp mV)
160
140
120
100
80
60
40
20
0
0
5
10
15
20
25
Mitochondrial O2 Consumption
(nmol O2 · min-1 · mg protein-1)

the leak in BAT mitochondria from control mice is inhibited by the presence of GDP (Figure 10B). Technical details are provided in the legend to the figure.

The results presented in Figure 10 also allow the comparison of the overall kinetics of the leak reactions over a range of mitochondrial membrane potentials between *Ucp1*-deficient and control BAT mitochondria. The overall kinetics of the leak in *Ucp1*-deficient mitochondria (Figure 10A) in the presence and absence of 1mM GDP are virtually identical. These data were unexpected; 1 mM GDP is well known to inhibit the activity of UCP1 in BAT mitochondria (Desautels *et al.* 1978). Because a 5 fold increase in mRNA for *Ucp2* in BAT was observed in *Ucp1*-deficient mice compared with heterozygous controls, it was hypothesized that an increased activity of UCP2 protein compensated to some degree for the loss of UCP1 and this, in turn, contributed to the lean phenotype. However, these results show that, over a wide range of Δp values, there is no increase in the oxygen used to balance the leak of protons back into the matrix. This is evident when the rate of leak is compared over a range of Δp values between controls in the presence of GDP (Figure 10B) and *Ucp1*-deficient mitochondria in the presence or absence of GDP (Figure 10A) - proton leak rate is roughly equal at any given Δp.

d) The overall kinetics of substrate oxidation and phosphorylation reactions in the presence and absence of GDP.

The results in Figures 11 and 12 show the overall kinetics of substrate oxidation and phosphorylation reactions, respectively. Some of the data points shown in Figure 11 and 12 are also included in Figure 10; the line representing the kinetics of substrate oxidation

Figure 11: The effect of 1 mM GDP on the kinetic response of the substrate oxidation subsystem of reactions to Δp in BAT mitochondria from *Ucp1*-deficient (A) and control (B) mice. The kinetics of the substrate oxidation reactions was obtained by titrating mitochondria with increasing amounts of oligomycin (1-6 μg/mg mitochondrial protein) in the presence of saturating amounts of hexokinase (0.75 units/ml). Lines were fitted by linear regression to the oligomycin titration points. The two furthermost points on the right represent *state 3*. Each point is presented as the mean ±SEM of duplicate experiments with 12 *Ucp1*-deficient and 13 control mice.

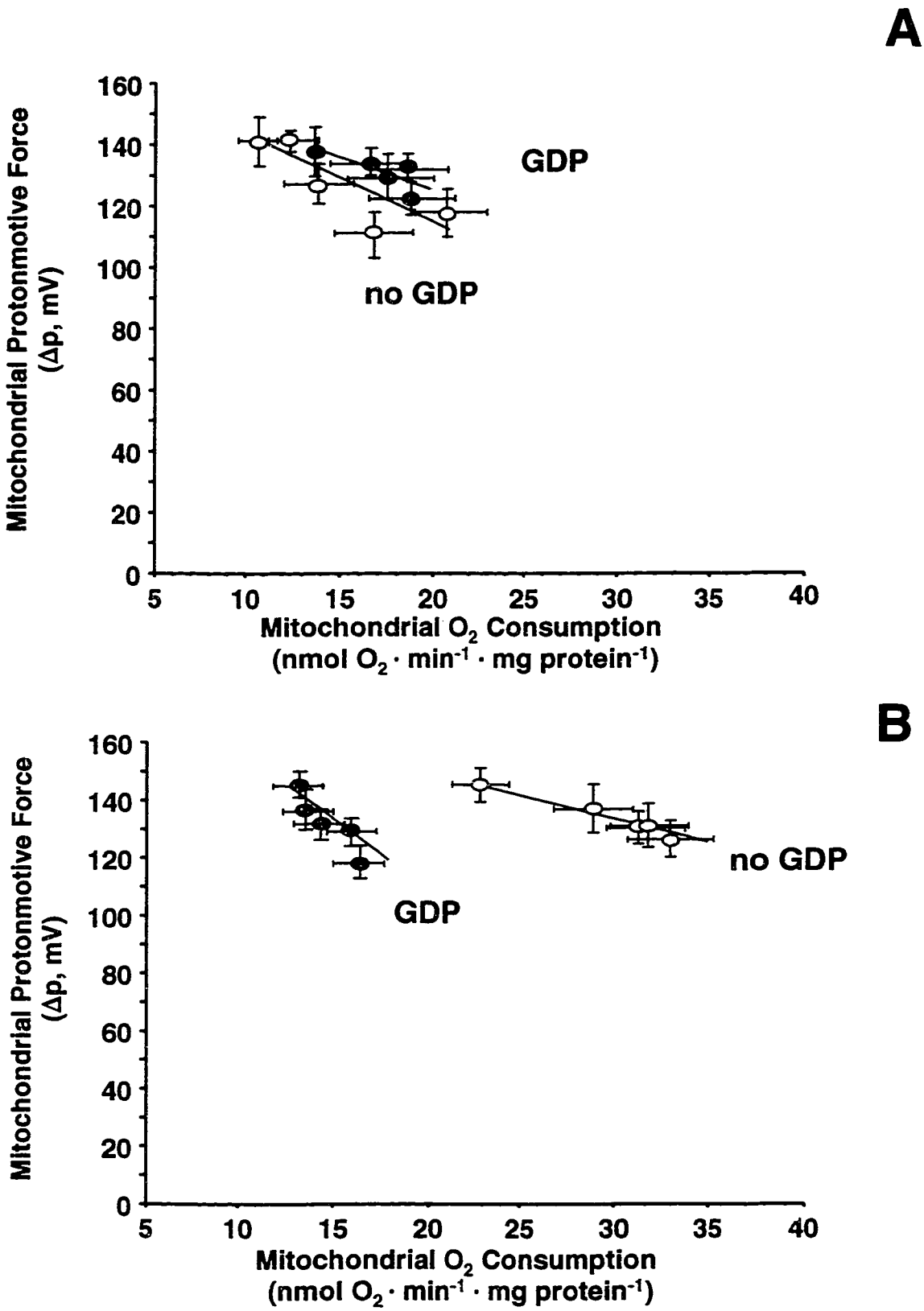
A
Mitochondrial Protonmotive Force
(Δp, mV)
160
140
120
100
80
60
40
20
0
GDP
no GDP
5
10
15
20
25
30
35
40
Mitochondrial O2 Consumption
(nmol O2 · min-1 · mg protein-1)
B
Mitochondrial Protonmotive Force
(Δp, mV)
160
140
120
100
80
60
40
20
0
no GDP
GDP
5
10
15
20
25
30
35
40
Mitochondrial O2 Consumption
(nmol O2 · min-1 · mg protein-1)

Figure 12: The effect of 1 mM GDP on the kinetic response of the phosphorylating subsystem to Δp in BAT mitochondria from *Ucp1*-deficient (A) and control (B) mice. The kinetic response of the phosphorylating reactions was obtained by titration of *state 3* respiration (furthermost points on the right) with increasing amounts of malonate (0.33, 0.66, 1.0, 2.0 and 3.0 mM)Lines were fitted by linear regression to the malonate titration points. Each point represents the mean ±SEM of duplicate experiments with 7 *Ucp1*-deficient and 8 control mice.

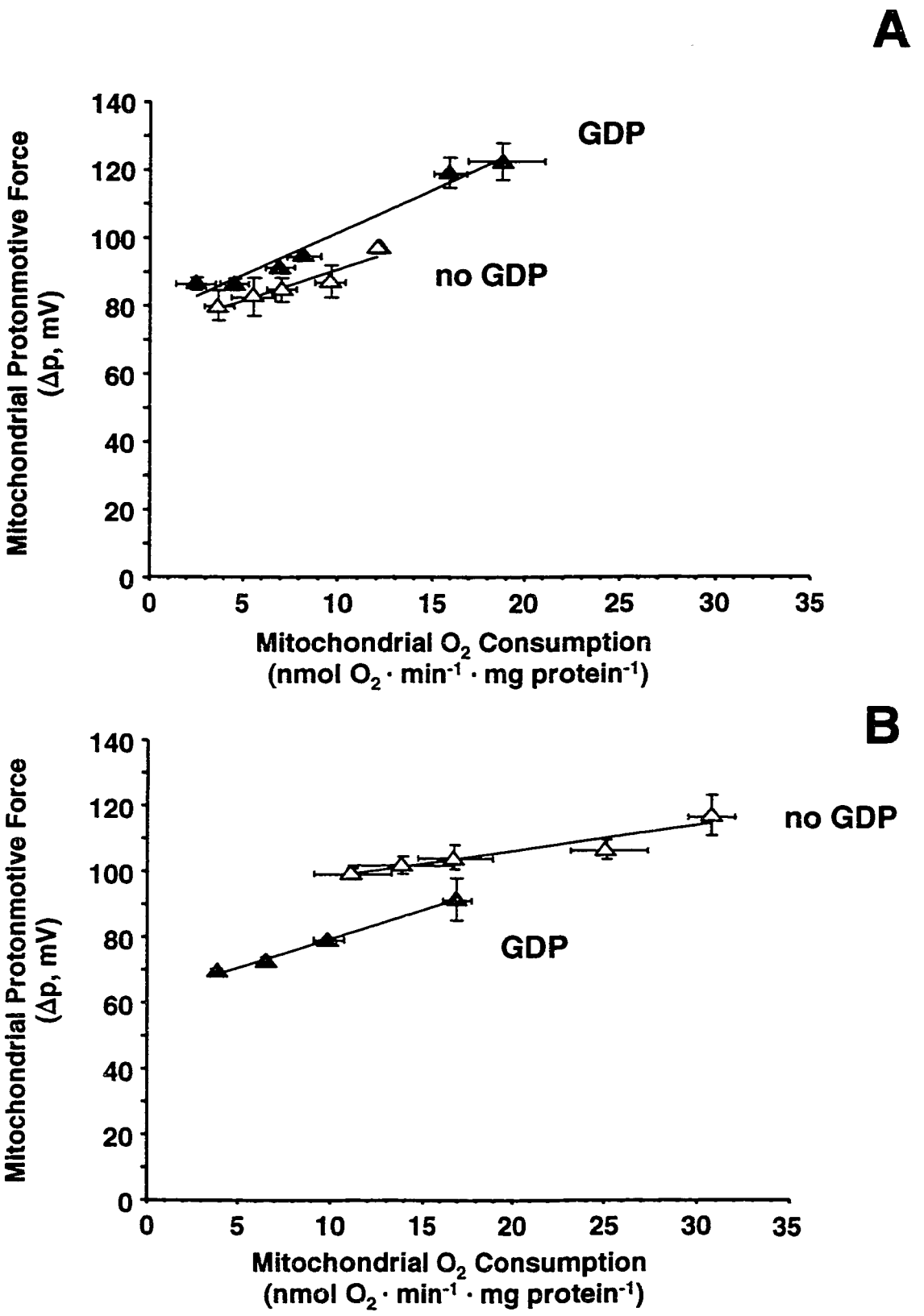
A
Mitochondrial Protonmotive Force
(Δp, mV)
140
120
100
80
60
40
20
0
GDP
no GDP
0
5
10
15
20
25
30
35
Mitochondrial O2 Consumption
(nmol O2 · min-1 · mg protein-1)
B
Mitochondrial Protonmotive Force
(Δp, mV)
140
120
100
80
60
40
20
0
no GDP
GDP
0
5
10
15
20
25
30
35
Mitochondrial O2 Consumption
(nmol O2 · min-1 · mg protein-1)

reactions in the absence of GDP are also shown as part of the latter figure. However, in Figure 11 and 12 the kinetics in the presence of GDP are also presented for comparison with the those in its absence. There is no difference between the kinetics of the substrate oxidation system of *Ucp1*-deficient mitochondria in the presence and absence of GDP (Figure 11A; $p > 0.05$ by analysis of covariance). These results show that, at any given value of Δp, the amount of oxygen used to balance the activity of the substrate oxidation reactions is not significantly affected by the presence of GDP. In mitochondria from control mice, however, the presence of GDP had a marked effect on the kinetics of substrate oxidation reactions (Figure 11B; $p < 0.002$ by analysis of covariance). These results show simply that when UCP1 is functional, the activity of the substrate oxidation reactions increases to fuel this leak and to maintain a relatively normal Δp value (*i.e.*, by increasing the activity of electron transport chain proton pumps).

The results Figure 12 depict the kinetics of the phosphorylation reactions. As indicated in the legend to Figure 9, and as described previously (Hafner 1990a), in order to obtain the kinetics of the phosphorylation reactions alone (*i.e.*, in the absence of proton leak reactions), the oxygen used to support leak reactions at each mean data point must be subtracted. The data from mitochondria of *Ucp1*-deficient mice shown in Figure 12A indicate that there is no significant effect of GDP on the kinetics of the phosphorylation reactions. At any given value of Δp, the amount of oxygen used to support ATP turnover reactions is not significantly different in the presence and absence of GDP. In control BAT mitochondria, there is however a significant difference between the kinetics of the phosphorylating system in the presence of GDP compared to in its absence. When GDP is

present the amount of oxygen used (at similar Δp values) to balance phosphorylation reactions is much greater than it is when GDP is absent (*e.g.*, compare rates at a Δp value of 100 mV). This is intuitive; when GDP is present and UCP1 is inhibited, the proton gradient is used to fuel the activity of ATP synthase; in its absence the gradient is rapidly dissipated through the UCP1- mediated leak

.

e) Application of top-down metabolic control analysis.

As described in the *Introduction* and *Methods* sections, top-down elasticity analysis provides all of the data needed for a top-down control analysis of the system (Brown *et al.* 1990a; Hafner 1990a). Metabolic control analysis provides extensive data describing the distribution of control by the blocks of reactions over the overall flux through the system (*e.g.*, mitochondrial oxygen consumption, as in the present study), and over each of the other blocks of reactions a system of pathways being studied. The elasticity coefficients, describing the responsiveness of the three blocks of reactions to Δp in *state 3* and *state 4* respiration are shown in Table 4.

Flux control coefficients and concentration control coefficients of the three blocks, or subsystems, of reactions over the rate of each of the subsystems are shown in Table 5 A-C. The concentration control coefficients of the three subsystems over the intermediate in the system, Δp, are given in Table 5D. The flux control coefficients in Table 5A show that the greatest proportion of control over *state 3* mitochondrial oxygen consumption (equivalent to flux through the substrate oxidation subsystem) is by the substrate oxidation reactions themselves, regardless of the presence or absence of 1 mM GDP. This is similar to the high

Table 4

Overall elasticities to Δp for the respiratory chain, phosphorylating, and proton leak subsystems in BAT mitochondria from *Ucp1*-deficient and control mice in the presence and absence of 1 mM GDP.

	STATE 3		STATE 4	
Ucp1-deficient	*with* GDP	*without* GDP	*with* GDP	*without* GDP
$\epsilon^{S}_{\Delta p}$	-3.65	-1.72	-6.1	-4.4
$\epsilon^{P}_{\Delta p}$	5.2	3.9	-----	-----
$\epsilon^{L}_{\Delta p}$	4	4.8	7.1	6.4
Control				
$\epsilon^{S}_{\Delta p}$	-0.68	-2.44	-1.42	-4.33
$\epsilon^{P}_{\Delta p}$	2.52	4.9	-----	-----
$\epsilon^{L}_{\Delta p}$	5.46	4.11	7.36	5.41

§**Note:** Elasticity coefficients are defined as the fractional change in flux caused by an infinitesimal change in the intermediate. Results were calculated from the mean values of Δp and mitochondrial oxygen consumption rates at *state 3* and *state 4* values from metabolic titrations described in Figure 9. As there is no ATP synthesis occurring in *state 4*, there are no elasticity or control coefficients (Table 5) for this subsystem under *state 4* conditions.

§**Note:** Flux control coefficients of substrate oxidation, phosphorylating and proton leak subsystems over the **A**, substrate oxidation subsystem flux; **B**, phosphorylating subsystem flux; **C**, the proton leak subsystem flux. **D**, concentration control coefficients over Δp by the substrate oxidation, phosphorylating, and proton leak subsystems. Results were calculated from the mean values of Δp and mitochondrial oxygen consumption rates at *state 3* and *state 4* conditions during the metabolic titrations described in Figure 9.

Table 5

Flux control coefficients over subsystem fluxes and concentration control coefficients over Δp in BAT mitochondria from *Ucp1-deficient* and control mice in the presence and absence of 1 mM GDP.

A

	STATE 3		STATE 4	
Ucp1-deficient	*with* GDP	*without* GDP	*with* GDP	*without* GDP
C_S^{JS}	0.56	0.7	0.54	0.59
C_P^{JS}	0.25	0.26	-----	-----
C_L^{JS}	0.19	0.04	0.46	0.41
Control				
C_S^{JS}	0.81	0.66	0.84	0.56
C_P^{JS}	0.17	0.23	-----	-----
C_L^{JS}	0.02	0.11	0.16	0.44

B

	STATE 3		STATE 4	
Ucp1-deficient	*with* GDP	*without* GDP	*with* GDP	*without* GDP
C_S^{JP}	0.63	0.68	-----	-----
C_P^{JP}	0.63	0.41	-----	-----
C_L^{JP}	-0.26	-0.09	-----	-----
Control				
C_S^{JP}	0.72	0.69	-----	-----
C_P^{JP}	0.36	0.54	-----	-----
C_L^{JP}	-0.08	-0.23	-----	-----

C

	STATE 3		STATE 4	
Ucp1-deficient	*with* GDP	*without* GDP	*with* GDP	*without* GDP
C_S^{JL}	0.48	0.84	0.54	0.59
C_P^{JL}	-0.28	-0.73	-----	-----
C_L^{JL}	0.8	0.89	0.46	0.41
Control				
C_S^{JL}	1.55	0.58	0.84	0.56
C_P^{JL}	-1.38	-0.38	-----	-----
C_L^{JL}	0.83	-0.8	0.16	0.44

D

	STATE 3		STATE 4	
Ucp1-deficient	*with* GDP	*without* GDP	*with* GDP	*without* GDP
$C_S^{\Delta p}$	0.12	0.18	0.11	0.1
$C_P^{\Delta p}$	-0.07	-0.16	-----	-----
$C_L^{\Delta p}$	-0.05	-0.02	-0.11	-0.1
Control				
$C_S^{\Delta p}$	0.28	0.14	0.11	0.1
$C_P^{\Delta p}$	-0.25	-0.09	-----	-----
$C_L^{\Delta p}$	-0.03	-0.05	-0.11	-0.1

degree of control over *state 3* respiration in liver mitochondria (*e.g.*, (Brown *et al.* 1990a)). However, the data in Table 5A show that presence of GDP in the incubation medium does have effects on the distribution of control over *state 3* respiration in both *Ucp1*-deficient and control BAT mitochondria. For example, in control mitochondria, there is an increase in the proportion of control by the substrate oxidation reactions, and slight decreases in the control by the phosphorylation and leak reactions. In *Ucp1*-deficient mitochondria, the effect of GDP is different - there is a decrease in the proportion of control by the substrate oxidation reactions, no change in control by the phosphorylation reactions and increased control by the leak. The data in Table 5B describe the distribution of control by the three blocks of reactions over the oxygen used to support the phosphorylating reactions in *state 3*. The control over phosphorylating reactions in *state 3* is held to a large extent by the substrate oxidation reactions; however the degree of control by the phosphorylating reactions is also relatively high. These results also show that the shifts in the control over phosphorylating reactions in the presence of GDP compared with its absence are similar to those described for the control over mitochondrial respiration (Table 5A). The flux control coefficients shown in Table 5C describe the distribution of control between the three blocks of reactions over the oxygen used to support the mitochondrial proton leak. In *state 3*, the control over the small rate of proton leak, is shared in most instances roughly equally between the three blocks of reactions. In control mitochondria in the presence of GDP, the control by substrate oxidation and phosphorylation reactions is greater than in the absence of GDP; the amount of control by leak remains approximately the same. In contrast, in *Ucp1*-deficient mitochondria in the presence of GDP, the control by substrate oxidation and

phosphorylation reactions is lower than in the absence of GDP; the amount of control by leak again remains approximately the same.

The distribution of control over the three subsystems during *state 4* respiration, both in the presence and absence of GDP, is also described in Table 5 A-C. As there is no synthesis of ATP during *state 4* respiration, there are no control coefficients for the phosphorylating subsystem. These data show clearly that there are differences in the control over *state 4* mitochondrial oxygen consumption in the presence and absence of GDP in control BAT mitochondria only. GDP does not alter the distribution of control in *Ucp1*-deficient BAT mitochondria.

In Table 5D the concentration control coefficients are presented. These values describe the distribution of control over Δp by the substrate oxidation, phosphorylating and leak reactions. At *state 3*, these results generally show that most of the control over Δp is exerted by the substrate oxidation subsystem, and the remainder of the control is through the Δp-consumers (*i.e.*, proton leak and the phosphorylating reactions). In *state 4*, control over Δp is shared equally between the producers and the consumers of Δp (*i.e.*, the substrate oxidation and proton leak subsystems). These results are thus similar to results from intact hepatocytes of hypothyroid, euthyroid and hyperthyroid rats (Harper and Brand 1993; Harper and Brand 1994).

3. Skeletal muscle mitochondria of *Ucp1*-deficient mice.

The observed insensitivity of the mitochondrial proton leak in BAT mitochondria from *Ucp1*-deficient mice to GDP, and the absence of a significant difference in the overall kinetics of the proton leak in the *Ucp1*-deficient mouse and controls led us to hypothesize that adaptative thermogenesis may be occurring in other tissues of the *Ucp1*-deficient mouse allowing them to maintain their normal RMR, feed efficiency, and adiposity. The tissue we decided to analyse in relation to this hypothesis was skeletal muscle.

a) Comparison of the kinetic responses of the mitochondrial proton leak, substrate oxidation and phosphorylation subsystems to Δp in mitochondria from Ucp1-deficient and control mice

Maximal leak-dependent oxygen consumption (*state 4*) rates were found to be significantly higher ($p < 0.02$) in the mitochondria of *Ucp1*-deficient mice than in controls Values were 146.3 nmol $O_2 \cdot min^{-1} \cdot mg\ protein^{-1}$ ±7.1 (n=9) and 121.9 nmol $O_2 \cdot min^{-1} \cdot mg\ protein^{-1}$ ±7.1 (n=8) in mitochondria of *Ucp1*-deficient control mice, respectively (Figure 13; furthermost points on the right). At *state 4*, Δp is significantly lower ($p < 0.002$) in *Ucp1*-deficient mice compared to controls. Values were 181.9 mV ±2.6 (n=9) and 168.4 mV ±3.2 (n=8) in *Ucp1*-deficient mice than in controls, respectively (Figure 13). No significant differences were detected in *state 3* respiration or *state 3* Δp values between the two groups (Figure 14 and 15; futhermost points on the right). Titrations were initially performed in the presence and absence of GDP in experiments with 3 *Ucp1*-deficient and 3 control mice. Once it was established that it had no effect, it was no longer used and the previous results were pooled.

Figure 13: Relationship between Δp and leak-dependent respiration in skeletal muscle mitochondria from *Ucp1*-deficient (▲) and control (■) mice. The kinetic response of the proton leak to Δp was determined via titration of *state 4* respiration (maximal non-phosphorylating respiration) with increasing amounts of malonate (0.33, 0.66, 1.0, 2.0, 3.0 and 5.0 mM) in the presence of saturating amounts of oligomycin (8 μg/mg mitochondrial protein). Each point represents the mean ±SEM of duplicate experiments with mitochondria from 9 *Ucp1*-deficient and 8 control mice.

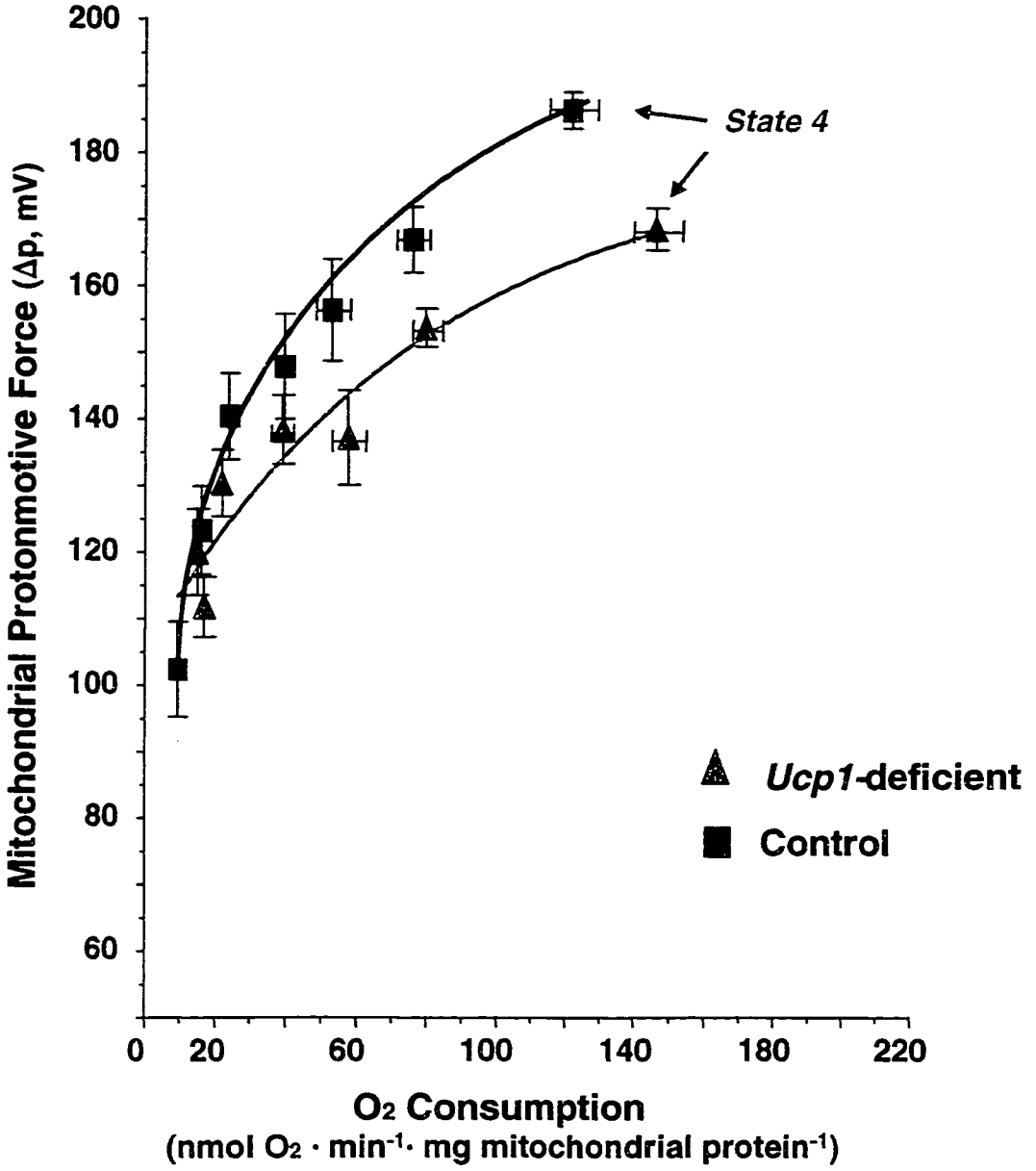
Mitochondrial Protonmotive Force (Δp, mV)
200
180
160
140
120
100
80
60
0
20
60
100
140
180
220
State 4
Ucp1-deficient
Control
O2 Consumption
(nmol O2 · min-1· mg mitochondrial protein-1)

Figure 14: Relationship between Δp and substrate oxidation rate in skeletal muscle mitochondria from *Ucp1*-deficient (▲) and control (■) mice. The kinetic response of the substrate oxidation subsystem was determined by titrating succinate fueled respiration with increasing amounts of hexokinase (0.65 and 1.2 units/mg mitochondrial protein). Each point represents the mean ±SEM of duplicate experiments with mitochondria from 7 *Ucp1*-deficient and 6 control mice.

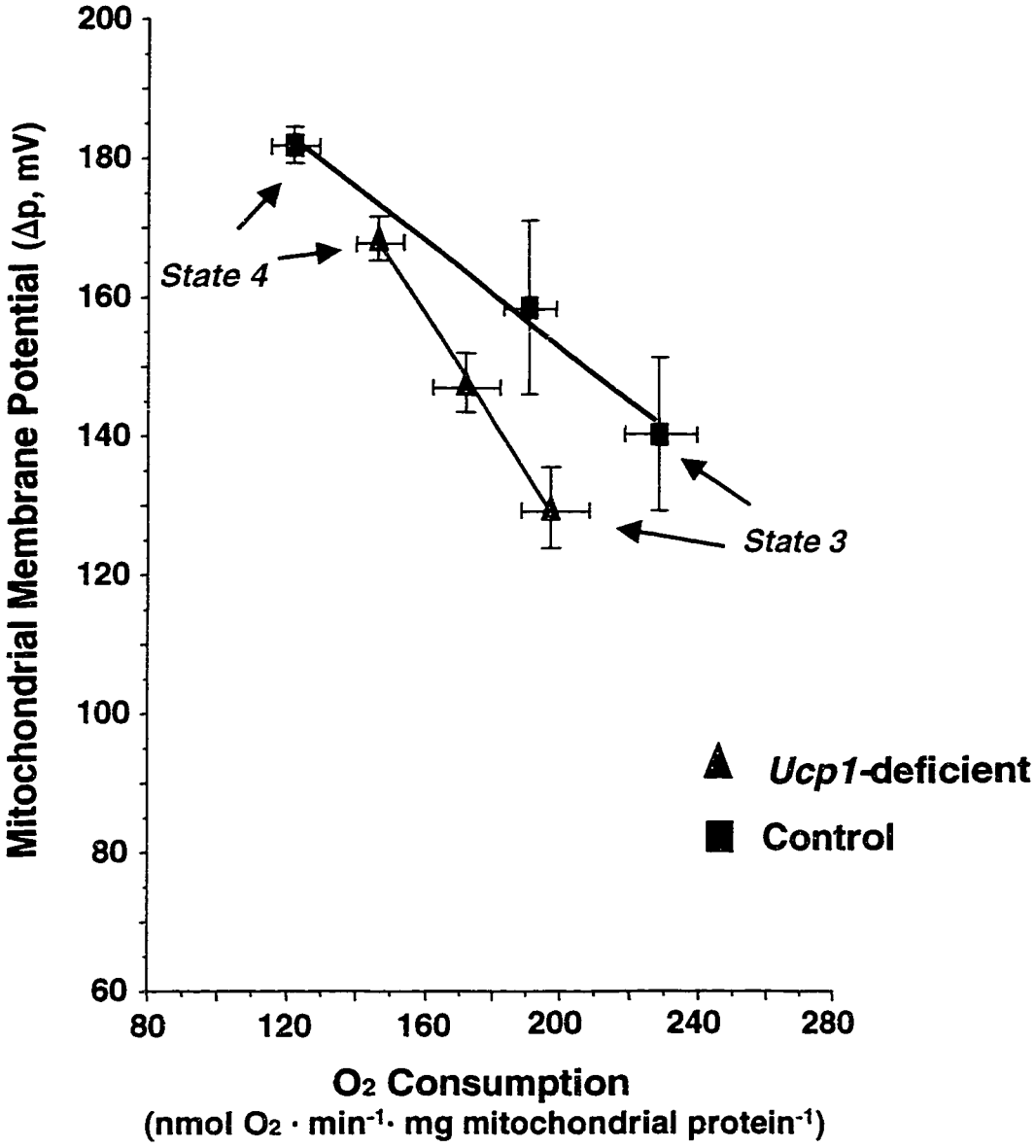
Mitochondrial Membrane Potential (Δp, mV)
200
180
160
140
120
100
80
60
80
120
160
200
240
280
O2 Consumption
(nmol O2 · min-1· mg mitochondrial protein-1)
State 4
State 3
Ucp1-deficient
Control

Figure 15: Relationship between Δp and rate of the phosphoryaltion subsystem in skeletal muscle mitochondria from *Ucp1*-deficient (▲) and control (■) mice. The kinetic response of the phosphorylation subsystem was obtained by titration of *state3* respiration (maximal phosphorylating respiration) with increasing amounts of malonate (0.33, 0.66, 1.0 and 2.0 mM) in the presence of maximal amounts of hexokinase (1.3units/mg mitochondrial protein). Each point represents the mean ±SEM of duplicate experiments with mitochondria from 5 *Ucp1*-deficient and 5 control mice.

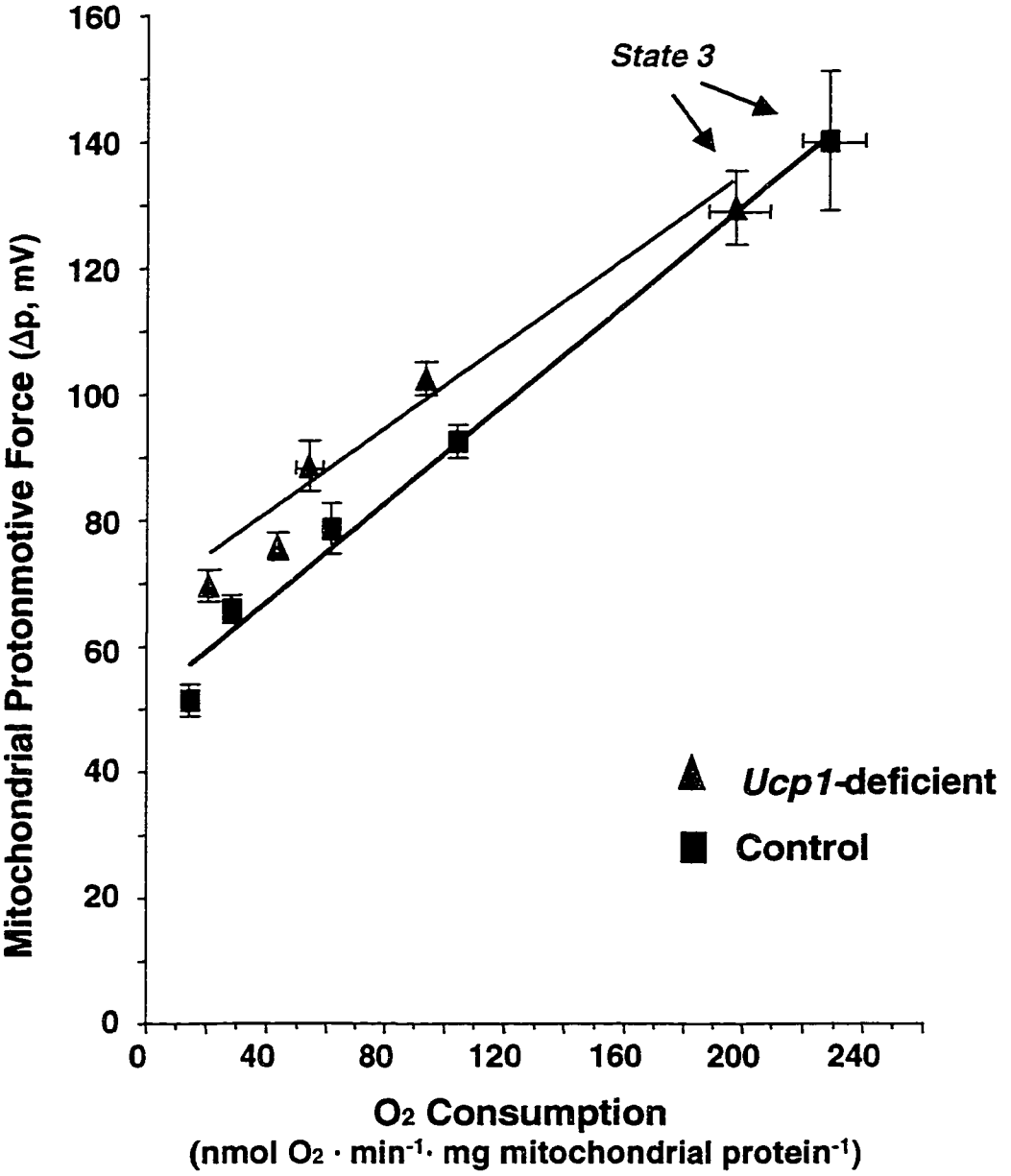
160
140
120
100
80
60
40
20
0
0
40
80
120
160
200
240
State 3
Mitochondrial Protonmotive Force (Δp, mV)
O2 Consumption
(nmol O2 · min-1· mg mitochondrial protein-1)
Ucp1-deficient
Control

The overall kinetics of the mitochondrial proton leak (Figure 13) show that oxygen consumption used to support the proton leak over a range of Δp values is *higher* in the mitochondria of *Ucp1*-deficient mice compared to controls. This is particularly clear at high Δp, for example at 160 mV, where oxygen consumption in mitochondria deficient in UCP1 is approximately double that of controls. The overall kinetics of the substrate oxidation subsystem (Figure 14) show that the respiratory chain activity is more sensitive to Δp in *Ucp1*-deficient mitochondria compared to controls. Furthermore, we found no differences in the overall kinetics of the phosphorylation reactions (Figure 15). As mentioned previously, in order to obtain the kinetics of the phosphorylation subsystem of reactions alone (*i.e.*, in the absence of proton leak reactions), the oxygen used to support the leak reactions at each mean data point was subtracted. Since the total oxygen consumption used to support the activity of the substrate oxidation reactions is the combined sum of that used to support the proton leak and the phosphorylation reactions, this suggests that the observed differences in substrate oxidation kinetics are due to the differences in mitochondrial proton leak.

IV. DISCUSSION

1. Age-related changes in oxidative phosphorylation of mouse hepatocytes.

Our initial hypothesis was that increases in the mitochondrial proton leak occur as a result of continuous oxidative damage to the lipids of the mitochondrial inner membrane. This damage affects the integrity of the lipid bilayer through altered lipid-lipid, or altered lipid-protein interactions. We expected the changes in the mitochondrial proton leak to be rather small, but it was anticipated that top-down elasticity analysis, an approach where the activities of blocks of reactions are assessed over a range of metabolic 'challenges', would identify and quantify any such changes.

The findings of our study show that the overall kinetics of the mitochondrial proton leak are indeed altered by age such that over a range of mitochondrial membrane potentials, there is an increased rate of oxygen consumed to balance the rate of leak (Figure 4). Changes in the overall kinetics of the proton leak are consistent with the recent report of Hagen *et al.* (Hagen *et al.* 1997) who studied mitochondrial membrane potential, cellular production of oxidants and levels of age-associated mitochondrial DNA deletions in rat hepatocytes. In these experiments, mitochondrial membrane potential was assessed using rhodamine 123 accumulation. Three distinct hepatocyte populations from old rats were collected by centrifugal elutriation and were found to have differing mitochondrial membrane potentials. One population of cells was collected from the young rats. In the largest population of old cells (~66% of cells in the preparation), membrane potential was about 40% lower that of the young cells. A smaller subset of hepatocytes from old rats

(~25% of the cells) had only slightly decreased fluorescence than from young rats. In the third subset of cells, membrane potential was equal or greater than that of the young cells. Their rhodamine 123 fluorescence results were corroborated by quantitative determinations of potentials by assessing mitochondrial uptake of radiolabeled TPP^+. They reported the resting membrane potential in young hepatocytes to be 154.3 mV ±20.4; this value is very similar to our value of 147 mV ±3.4. The resting mitochondrial membrane potential in the hepatocytes that we isolated from old mice was 149 mV ±4.4 (Figure 5), which is clearly not significantly different from our mean value in young cells (147 ± 3.4). Hagen *et al.* (Hagen *et al.* 1997) also examined resting oxygen consumption rates. While their absolute values appear high, their finding that oxygen consumption is 36% lower in the largest fraction of hepatocytes compared to young cells supports our findings (oxygen consumption is ~15% lower in old cells). Finally, in support of the oxidative stress theory, they found that both the largest and the smallest fractions of cells produced significantly more oxidants than cells from young rats.

The recent finding of Brookes and colleagues (Brookes *et al.* 1998) also supports our findings. They added three sequential additions of peroxynitrite (200 μM initial concentration), a cytotoxic agents proposed to be involved in lipid peroxidation, to rat brain mitochondria (0.2 mg protein/ml) and observed a significant stimulation of the mitochondrial proton leak. Cyclosporin A did not affect the stimulation, suggesting no involvement of the mitochondrial permeability transition pore. However, effects of peroxynitrite were reversed by the addition of Trolox, a vitamin E analogue, supporting the involvement the involvement of lipid peroxidation.

The mechanism of the mitochondrial proton leak in hepatocytes is still unclear. Within the past two years two new members of the uncoupling protein family, UCP2 and UCP3, have been identified (Boss *et al.* 1997b; Fleury *et al.* 1997; Gimeno *et al.* 1997; Vidal-Puig *et al.* 1997). The current hypothesis is that the UCPs mediate the proton leak that has been assessed in mitochondria from a variety of tissues. Thus far, none of the three currently known UCPs have been found in parenchymal cells of the liver (which constitute ~95-97% of the cells isolated using the techniques we have employed (Berry *et al.* 1991)). Fleury *et al.* (Fleury *et al.* 1997) have observed low levels of UCP2 mRNA in liver; however, recent findings have localized UCP2 to the Kupfer cells of the liver (Larrouy *et al.* 1997). Nevertheless, it is possible, and likely, that there is an, as yet unidentified, uncoupling protein in the parenchymal cells. Furthermore, it is possible that there are changes in the amount and/or activity of such an uncoupling protein in these cells. But, again, our underlying hypothesis, founded on a substantial supportive literature, implicates free radical damage to lipids, thus affecting the integrity of the bilayer at the lipid-lipid or lipid-protein interfaces.

It has been shown that the amounts and activities of a wide range of enzymes involved in substrate oxidation and specifically components of the electron transport chain (*e.g.*, complex I, II, IV) change with age (Boffoli *et al.* 1994; Hansford 1983; Torii *et al.* 1992). Based on this fact we expected that the overall kinetics of the substrate oxidation reactions would be altered as a result of aging. We hypothesized that one of two things could occur: *i)* the decreased activity and amount of electron transport chain enzymes would result in a decreased activity of the substrate oxidation block of reactions, or *ii)* as a result of the

mitochondrial proton leak, there may be a compensatory increase in the rate of substrate oxidation reactions in an effort to restore protonmotive force to normal values. The latter would then accelerate the productions of reactive oxygen species (*e.g.*, $O_2^{\cdot-}$, $OH^{\cdot-}$), which in turn would induce further damage to the mitochondria. Our data (Figure 5) clearly show that neither of these situations occurred. The overall kinetics of the substrate oxidation block of reactions were not significantly different between old and young hepatocytes. These findings do not necessarily imply that free radical damage has not occurred, but only shows that this group of reactions responds normally to changes in the rate of its activity, and may indicate that the functioning of this block of reactions is somewhat protected.

A comparison of our results from the kinetic responses of the phosphorylation subsystem to $\Delta\Psi_m$ in old and young hepatocytes showed significant differences (Figure 6). At the resting state, the rate of the phosphorylation system was approximately 30% lower in old cells than in young cells at the same membrane potential. The decreases in the proportion of resting oxygen consumption of hepatocytes and altered kinetics of the phosphorylation reactions were not anticipated. It is difficult to speculate about the specific mechanisms responsible for the decreased amount of oxygen used by cells to support these reactions. Despite extensive analyses of respiratory control ratios in the literature, little is known about the specific age-related changes in ATP synthesis and turnover reactions. As described in Figure 3, ATP synthesis and turnover mechanisms include ATP synthetic reactions such as the adenine nucleotide carrier and the phosphate transporter. This block of reactions also includes all cellular ATP-consuming reactions, such as those involved in maintaining ion gradients across membranes (*e.g.*, Ca^{++} ATPase, Na^+,K^+ ATPase), and in

protein, DNA and RNA synthetic reactions. Consistent with the oxidative stress theory, these findings may be related to known age-related increases in oxidative damage to mitochondrial proteins and DNA, and should be examined further.

This research provided the first metabolic control analysis of oxidative phosphorylation in relation to the metabolic effects of aging. The data provide quantitative information about the control over resting cellular oxygen consumption, over other blocks of reactions and over mitochondrial membrane potential. In old cells compared to young, we observed a shift in control over resting oxygen consumption away from the substrate oxidation reactions towards phosphorylation and leak reactions (Table 2A). Thus, oxygen consumption of old hepatocytes is more sensitive to changes in the rate of ATP turnover and in mitochondrial proton leak rate. Similarly, there is a shift in control over phosphorylation reactions away from substrate oxidation reactions towards phosphorylation reactions and leak in old cells (Table 2B). Control by the substrate oxidation and phosphorylation reactions over the flux through the proton leak reactions in old and young cells show that there are decreases to roughly equal but opposite extents for these two blocks of reactions (Table 2C). As anticipated, control over leak flux by the leak reactions themselves remained high in both young and old hepatocytes.

The control coefficients describing the control over the effective P/O ratio (Table 3) indicate that a greater amount of control is possessed by the ATP turnover reactions and the leak in old hepatocytes compared to young. In accordance with the results for hepatocytes described by Brand (Brand *et al.* 1993), the block of reactions with the least amount of control are the substrate oxidation reactions. These results suggests that in hepatocytes from

old mice, the efficiency of oxidative phosphorylation is more sensitive to changes in the rate of mitochondrial proton leak and in the rate of ATP synthesis and turnover reactions and they have a greater capability to affect changes in the efficiency of oxidative phosphorylation.

Overall our findings confer additional support for the oxidative stress theory of aging. They provide new quantitative data on the altered kinetics of the mitochondrial proton leak and of ATP turnover reactions and show shifts in metabolic control with aging.

2. Brown adipose tissue mitochondrial energetics in *Ucp*1-deficient mice

The overall aim of the studies with the *Ucp1*-deficient mouse model was to analyze the metabolic control and characteristics of the proton leak in mitochondria from brown adipose tissue (BAT) and skeletal muscle. It is well known that BAT is an important site of facultative energy expenditure, and that the potential for energy expenditure depends on UCP1(Himms-Hagen 1990). The role of BAT as a defense against obesity has been clearly illustrated through targeted toxigene-ablation of this tissue; 'BAT-less' mice develop a severe obesity with insulin resistance and other metabolic abnormalities typical of obesity (Lowell *et al.* 1993). Interestingly, mice lacking UCP1 (*Ucp1*-deficient mice) do not become more obese than controls when fed a high fat diet and maintain a normal feed efficiency and resting metabolic rate (RMR) (Enerbäck *et al.* 1997). We hypothesized that there may exist a compensatory (*i.e.,* increased proton leak via other members of the UCP family) mechanism in BAT whereby energy balance is maintained in the absence of UCP1, resulting in a lean phenotype. Presumably the leak that remains in these mitochondria is mediated by UCP2 and/or UCP3. Enerbäck and colleagues (Enerbäck *et al.* 1997) observed a 5 fold increase in UCP2 mRNA; however, UCP3 mRNA levels were not changed (Dr. Leslie Kozak, unpublished results). To date, the levels of the UCPs have not been quantified as antibodies which are unequivocally specific for UCP1, 2, or 3 are not available.

It has been well established that UCP1 possesses a binding site for purine nucleotide diphosphates or triphosphates and occupancy of this site in the absence of free fatty acids inhibits the proton conductance of the membrane (Heaton *et al.* 1978). UCP2 and the long

form of UCP3, $UCP3_L$, have been shown to possess a putative purine nucleotide binding domain (Boss *et al.* 1997b; Fleury *et al.* 1997). An important finding of this study is that the proton leak in the absence of UCP1 is insensitive to GDP at concentrations and incubation conditions that cause the inhibition of 50% of the leak in mitochondria from control mice. The flux control coefficients show that the control over mitochondrial oxygen consumption and proton leak reactions are strongly affected by the presence of 1 mM GDP in control mitochondria, while in UCP1-deficient mitochondria there is little effect of the purine nucleotide.

Analysis of *state 4* respiration (maximal leak-dependent respiration) and the overall kinetics of the mitochondrial proton leak clearly demonstrate that BAT mitochondria from *Ucp1*-deficient mice is insensitive to GDP, while the leak in BAT mitochondria from control mice is inhibited by it (Figure 10). In addition, we observed no effect of GDP on the overall kinetics of the leak in mitochondria from UCP1-deficient mice. Our hypothesis, based on the evidence that UCP2 is capable of uncoupling oxidative phosphorylation (Fleury *et al.* 1997) and the observation that UCP2 mRNA is increased 5 fold in *Ucp1*-deficient mice (Enerback *et al.* 1997), was that an increased activity of protein compensated to some degree for the loss of UCP1 and this, in turn, contributed to the lean phenotype. The fact that we did not observe any increase in leak dependent oxygen consumption (either in the presence or absence of GDP) in BAT mitochondria from *Ucp1*-deficient mice shows that the relative levels of UCP2 mRNA do not correspond to any differences in uncoupling.

The overall kinetics of the substrate oxidation reactions and the phosphorylation reactions (Figures 11 and 12, respectively) in the presence and absence of GDP also shed

new light on the metabolic control and regulation of oxidative phosphorylation in mitochondria of *Ucp1*-deficient mice. The kinetics of the substrate oxidation and phosphorylation reactions in UCP1-deficient mitochondria were found to be unaltered in the presence or absence of GDP in *Ucp1*-deficient mice. In the case of control mitochondria, both blocks of reactions were significantly affected by the presence of GDP. These results were not unexpected since it makes sense that in the absence of GDP the kinetics of the substrate oxidation reactions would increase in order to fuel UCP1-mediated leak and to maintain a normal protonmotive force by increasing the activity of electron transport chain proton pumps. As for the phosphorylation reactions, in the absence of GDP the proton gradient is rapidly dissipated through ATP synthase and UCP1, therefore, the kinetics of the phosphorylation reactions increase so as to balance this.

At this point it is not understood how the activities of UCP2 and UCP3 are controlled. UCP2 and $UCP3_L$ appear to have conserved nucleotide binding domains, however, after it was discovered almost twenty years ago that purine nucleotides bind and inhibit UCP1 (Desautels *et al.* 1978; Heaton *et al.* 1978), GDP binding was assessed in mitochondria from a variety of tissues and found to be low to negligible. As a result, nucleotide binding has been used as a key factor in identifying UCP1 activity. In addition, the loose coupling observed in skeletal muscle mitochondria has been shown to be insensitive to GTP, unlike that in BAT mitochondria (Desautels 1980) (Monemdjou *et al.* manuscript in preparation). Gimeno *et al.*(Gimeno *et al.* 1997) have put the idea forward that because a single amino acid mutation in the inhibitory nucleotide binding site of UCP1 (Phe268 to Tyr) creates a UCP that has higher uncoupling activity (Bouillaud *et al.* 1994) and because both mouse

and human UCP2 naturally contain Tyr at the equivalent position, UCP2 may be less susceptible to the inhibitory effects of purine nucleotides. This hypothesis complements our findings showing that the mitochondrial proton leak remaining in BAT mitochondria of *Ucp1*-deficient mice is insensitive to GDP. In addition, results from metabolic control analyses of oxidative phosphorylation show that proton leak in liver, kidney and skeletal muscle may be controlled independently of ATP turnover. Control over leak by phosphorylation reactions is very low (*i.e.*, less than 10%) (Brand *et al.* 1994a; Harper and Brand 1993). Therefore, from our results we can conclude that despite elevated levels of UCP2 mRNA in BAT mitochondria of *Ucp1*-deficient mice, any increase in uncoupling activity is negligible.

Our findings from these studies suggest that adaptative thermogenesis may be occurring in tissues other than BAT of the *Ucp1*-deficient mouse, allowing them to maintain a normal RMR, feed efficiency, and a normal lean phenotype (Enerbäck *et al.* 1997). It has been well established that proton leak accounts for a significant proportion of the oxygen consumption rate of resting perfused hind limb muscle and of the RMR of a rat (Rolfe and Brand 1996). Based on this evidence, and the facts that skeletal muscle is an important contributor to resting energy expenditure and that there are high levels of *Ucp3* expression in skeletal muscle (Boss *et al.* 1997b; Vidal-Puig *et al.* 1997), it was the obvious tissue to analyze next in the *Ucp1*-deficient mouse.

3. Skeletal muscle mitochondrial energetics of *Ucp1*-deficient mice

BAT plays a critical role in the regulation of energy balance in mice, however, BAT may be of lesser importance in adult humans in whom the mass of BAT is limited. The main objective of this study was to examine the characteristics of the proton leak in skeletal muscle mitochondria of *Ucp1*-deficient mice, and to verify whether our hypothesis that skeletal muscle may be a potential site for an adaptative thermogenic mechanism favouring the lean phenotype observed in this mouse was valid. The skeletal muscle of the *Ucp1*-deficient mouse was deemed as a suitable model for this investigation on the basis that it accounts for up to 52% of the oxygen consumption rate of resting perfused rat hind limb muscle and up to 25% of the RMR of a rat (Rolfe and Brand 1996). In addition, UCP2 and UCP3 are both expressed in skeletal muscle (Boss *et al.* 1997b; Fleury *et al.* 1997; Gimeno *et al.* 1997; Vidal-Puig *et al.* 1997), therefore, they may be important thermogenic mediators of this highly thermogenic tissue.

The finding of major interest from this study is that the overall kinetics of the mitochondrial proton leak show that oxygen consumption used to support the leak is higher in mitochondria of *Ucp1*-deficient compared to controls (*i.e.*, for any given value of mitochondrial protonmotive force (Δp), more oxygen is used to support the proton leak reactions in UCP1-deficient mitochondria compared to controls) (Figure 13). In addition, maximal leak-dependent oxygen consumption (*state 4* respiration) rates were found to be significantly higher ($p<0.02$) in the mitochondria of *Ucp1*-deficient mice than in controls, while the *state 4* mitochondrial Δp is significantly lower ($p<0.002$) in mitochondria from *Ucp1*-deficient compared to controls. The first five experiments with each strain of mouse

were performed in the presence and absence of GDP, but data was pooled since no significant differences were observed.

We found no significant differences in *state 3* respiration or *state 3* Δp values between the two groups, however, the overall kinetics of the respiratory chain show that respiratory chain activity is more sensitive to changes in Δp in UCP1-deficient mitochondria compared to controls (Figure 14). As the total oxygen consumption used to support the activity of the substrate oxidation reactions is the sum of that used to support proton leak and phosphorylation reactions (Figure 3), this suggests that the observed differences in substrate oxidation kinetics are due solely to differences in mitochondrial leak reactions. The overall kinetics of the phosphorylation reactions were found to be unaltered (Figure 15).

These results support our hypothesis that skeletal muscle may be a potential site for an adaptative thermogenic mechanism favouring the lean phenotype observed in the *Ucp1*-deficient mouse, and also provides some insight into the possible function of UCP2 and UCP3 in mitochondrial energetics.

V. CONCLUSION

The finding that the overall kinetics of the mitochondrial proton leak and ATP turnover reactions are altered by age provides evidence supporting the oxidative stress theory of aging. In addition, our finding show that there exists a shift in control over respiration and phosphorylation away from substrate oxidation towards increased control by the leak and ATP turnover reactions further demonstrates the influence that leak has on age-associated changes in mitochondria.

Unaltered kinetics of the proton leak in the presence and absence of GDP in BAT mitochondria from *Ucp1*-deficient mice indicates that UCP2 and $UCP3_L$ are possibly regulated differently from UCP1. The fact that no increase in leak was observed in the mitochondria which lack UCP1, as compared to control mitochondria, shows that the lean phenotype in the *Ucp1*-deficient cannot be attributed to and increase in the proton leak reactions in brown adipocytes. However, our experiments with skeletal muscle mitochondria showed significantly greater *state 4* respiration rates, significantly lower *state 4* Δp values, as well as overall differences in the kinetics of the mitochondrial proton leak. This supports the conclusion that increased leak-dependent oxygen consumption may be a potential thermogenic mechanism favouring the lean phenotype in the absence of UCP1.

VI. FUTURE PROSPECTS

In the future I plan on continuing my studies on the *Ucp1*-deficient mouse. Many questions still remain to be addressed in relations to the *Ucp1*-deficient mouse.

***(i)* Do levels of message for UCP2 and UCP3 in BAT mitochondria correlate to levels of protein?**

We need to assess whether the levels of message for UCP2 and UCP3 in BAT mitochondria correlate to levels of protein. Dr. Kozak gave us probes for RNA of UCPs 1-3, and we now are beginning our own Northern blots. There is a 5 fold increased expression of UCP2 mRNA in BAT of *Ucp1*-deficient mice, and Dr. Kozak has recently found normal expression of UCP3 mRNA in BAT (unpublished). To assess the relative amounts of protein we will use Western blotting and will use commercial and donated antibodies, and purified proteins. Based on the facts that GDP-insensitive leak is the same between mice deficient in UCP1 and controls, and that message for UCP1 poorly correlate to levels of protein (Kopecky), we suspect that levels of UCP proteins are similar between *Ucp1*-deficient and control mice.

***(ii)* Are the levels of message and protein for UCP2 and UCP3 increased in skeletal muscle of *Ucp1*-deficient mice?**

It will also be necessary to determine whether the levels of message and protein for UCP2 and UCP3 are increased in skeletal muscle mitochondria of *Ucp1*-deficient mice. We will do this via Northern and Western blotting of isolated skeletal muscle mitochondria (from gastrocnemius, soleus and quadriceps). Since we observed an increase in the proton

leak in skeletal muscle mitochondria of these mice, it would be useful to know if there is a correlation between the amount of protein and the rate of proton leak.

(iii) Is the proton leak in skeletal muscle mitochondria altered after acclimation to different environmental temperatures?

We want to assess whether the proton leak in skeletal muscle mitochondria is altered after acclimation to different temperatures. We will gradually cold acclimate 12 *Ucp1*-deficient and 12 control to 12°C. Body weight, food intake and resting metabolic rate (via indirect calorimetry) before and during cold acclimation will be measured, and then, at day 8, we will assess leaks in mitochondria from BAT and skeletal muscle. Relevant factors in sera (*i.e.*, thyroid hormones and free fatty acids) before and after cold acclimation must also be ascertained. We will also have to flash freeze tissues for Northerns, save mitochondria for Westerns, and fix tissue (BAT, WAT, muscle, liver) samples for histology (light and electron microscopy). After this is project is completed, we will repeat the above after acclimation to thermoneutrality (34°C). We hypothesize that there will be an inverse relationship between leak and environmental temperature. UCP message and protein levels may also be altered.

(iv) How is BAT mitochondrial structure altered by the absence of UCP1?

Our electron micrographs of BAT mitochondria from *Ucp1*-deficient mice show that their structure is dramatically different from controls and they have fewer cristae, and an expanded matrix. We will analyze tissues of room temperature, cold- acclimated, and

thermoneutrality acclimated mice and examine the structure and numbers of inner- outer membrane contact points and assess activities of several mitochondrial marker proteins (*e.g.*, cytochrome oxidase).

VII. APPENDIX

(a) Elasticity Coefficients (Brown *et al.* 1990a)

$$*\varepsilon^{S}_{\Delta p} = \frac{dJ_S}{d\Delta p} \cdot \frac{\Delta p}{J_S}$$

$$*\varepsilon^{L}_{\Delta p} = \frac{dJ_L}{d\Delta p} \cdot \frac{\Delta p}{J_L}$$

$$*\varepsilon^{P}_{\Delta p} = \frac{d(J_S - J_L)}{d\Delta p} \cdot \frac{\Delta p}{J_S - J_L}$$

(b) Flux control Coefficients (Brown *et al.* 1990a)

$$*C^{Js}_{S} = \frac{(J_P \bullet *\varepsilon^{P}_{\Delta p} + J_L \bullet *\varepsilon^{L}_{\Delta p})}{(J_P \bullet *\varepsilon^{P}_{\Delta p} + J_L \bullet *\varepsilon^{L}_{\Delta p} - J_S \bullet *\varepsilon^{S}_{\Delta p})}$$

$$*C^{Js}_{P} = \frac{J_P \bullet (1 - *C^{Js}_{S})}{J_S}$$

$$*C^{Js}_{L} = \frac{J_L \bullet (1 - *C^{Js}_{S})}{J_s}$$

$$*C^{Jp}_{S} = \frac{J_S \bullet *\varepsilon^{P}_{\Delta p}}{(J_P \bullet *\varepsilon^{P}_{\Delta p} + J_L \bullet *\varepsilon^{L}_{\Delta p} - J_S \bullet *\varepsilon^{S}_{\Delta p})}$$

$$*C^{Jp}_{P} = (1 - J_P) \bullet \frac{*C^{Jp}_{S}}{J_S}$$

$$*C^{J_P}_{\ L} = -J_L \bullet \frac{*C^{J_P}_{\ S}}{J_S}$$

$$*C^{J_L}_{\ S} = \frac{J_S \bullet *\varepsilon^{L}_{\Delta p}}{(J_P \bullet *\varepsilon^{P}_{\Delta p} + J_L \bullet *\varepsilon^{L}_{\Delta p} - J_S \bullet *\varepsilon^{S}_{\Delta p})}$$

$$*C^{J_L}_{\ P} = -J_P \bullet \frac{*C^{J_L}_{\ S}}{J_S}$$

$$*C^{J_L}_{\ L} = (1 - J_L) \bullet \frac{*C^{J_L}_{\ S}}{J_S}$$

(c) Concentration Control Coefficients (Brown *et al.* 1990a)

$$*C^{\Delta p}_{\ S} = \frac{J_S}{(J_P \bullet *\varepsilon^{P}_{\Delta p} + J_L \bullet *\varepsilon^{L}_{\Delta p} - J_S \bullet *\varepsilon^{S}_{\Delta p})}$$

$$*C^{\Delta p}_{\ P} = -J_P \bullet \frac{*C^{\Delta p}_{\ S}}{J_S}$$

$$*C^{\Delta p}_{\ L} = -J_L \bullet \frac{*C^{\Delta p}_{\ S}}{J_S}$$

Ames, B.N., Shigenaga, M.K. andHagen, T.M. (1993) Oxidants, antioxidants and the degenerative diseases of aging. *Proceedings of the National Academy of Science* **90**: 7915-7922.

Berry, M.N., Edwards, A.M. andBarritt, G.J. (1991) *Isolated Hepatocytes - Preparation, Properties and Applications.* Laboratory Techniques in Biochemistry and Molecular Biology. Amsterdam: Elsevier.

Boffoli, D., Scacco, S.C., Vergari, R., Solarino, G., Santacroce, G. andPapa, S. (1994) Decline with age of the respiratory chain activity in human skeletal muscle. *Biochimica et Biophysica Acta* **1226**: 73-82.

Boss, O., Samec, S., Dulloo, A., Seydoux, J., Muzzin, P. and Paoloni-Giacobino, J.P. (1997a) Tissue-Dependent Upregulation Of Rat Uncoupling Protein-2 In Response to Fasting or Cold. *FEBS Letters* **412**: 111-114.

Boss, O., Samec, S., Paolonigiacobino, A., Rossier, C., Dulloo, A., Seydoux, J., Muzzin, P. and Giacobino, J.P. (1997b) Uncoupling Protein-3 - a New Member Of the Mitochondrial Family With Tissue-Specific Expression. *FEBS Letters* **408**: 39-42

Bouillaud, F., Arechaga, I., Petit, P.X., Raimbault, S., Levi-Meyrueis, C., Casteilla, L., Laurent, M., Rial, E. and Ricquier, D. (1994) A sequence related to a DNA recognition element is essential for the inhibition by nucleotides of proton transport through the mitochondrial uncoupling protein. *EMBO Journal* **13**: 1990-1997.

Bouillaud, F., Ricquier, D., Thibault, J. and Weissenbach, J. (1985) Molecular approach to thermogenesis in brown adipose tissue: cDNA cloning of the mitochondrial uncoupling protein. *Proceedings of the National Academy of Sciences* **82**: 445-448.

Bowling, A.C., Mutisya, E.M., Walker, L.C., Price, D.L., Cork, L.C. and Beal, M.F. (1993) Age-dependent impairment of mitochondrial function in primate brain. *Journal of Neurochemistry* **60**: 1964-1967.

Brand, M.D. (1990a) The contribution of the leak of protons across the mitochondrial inner membrane to standard metabolic rate. *Journal of Theoretical Biology* **145**: 267-286.

Brand, M.D. (1990b) The proton leak across the mitochondrial inner membrane. *Biochimica et Biophysica Acta* **1018**: 128-133.

Brand, M.D. 1995 Measurement of Protonmotive Force. In *Bioenergetics: A Practical Approach*, vol. 154 (ed. G. C. Brown & C. E. Cooper), pp. 39-62. Oxford: IRL Press.

Brand, M.D. (1998) Top-down elasticity analysis and its application to energy metabolism in isolated mitochondria and intact cells. *Molecular and Cellular Biochemistry* **184**: 13-20.

Brand, M.D., Chien, L.-F., Ainscow, E.K., Rolfe, D.F.S. and Porter, R.K. (1994a) The causes and functions of mitochondrial proton leak. *Biochimica et Biophysica Acta* **1187**: 132-139.

Brand, M.D., Chien, L.-F. and Diolez, P. (1994b) Experimental discrimination between proton leak and redox slip during mitochondrial electron transport. *Biochemical Journal* **297**: 27-29.

Brand, M.D., Couture, P., Else, P.L., Withers, K.W. and Hulbert, A.J. (1991) Evolution of energy metabolism: Proton permeability of the inner membrane of liver mitochondria is greater in a mammal than in a turtle. *Biochemical Journal* **275**: 81-86.

Brand, M.D., D'Alessandri, L., Reis, H. and Hafner, R.P. (1990) Stimulation of the electron transport chain in mitochondria isolated from rats treated with mannoheptulose or glucagon. *Archives of Biochemistry & Biophysics* **283**: 278-284.

Brand, M.D., Harper, M.-E. and Taylor, H.C. (1993) Control of the effective P/O ratio of oxidative phosphorylation in liver mitochondria and hepatocytes. *Biochemical Journal* **291**: 739-748.

Brand, M.D. and Murphy, M.P. (1987) Control of electron flux through the respiratory chain in mitochondria and cells. *Biological Reviews of the Cambridge Philosophical Society* **62**: 141-193.

Brookes, P.S., Land, J.M., Clark, J.B. and Heales, S.J.R. (1998) Peroxynitrite and Brain Mitochondria - Evidence For Increased Proton Leak. *Journal of Neurochemistry* **70**: 2195-2202.

Brookes, P.S., Rolfe, D.F.S. and Brand, M.D. (1997) The Proton Permeability Of Liposomes Made From Mitochondrial Inner Membrane Phospholipids - Comparison With Isolated Mitochondria. *Journal of Membrane Biology* **155**: 167-174.

Brown, G.C. (1992) The leaks and slips of bioenergetic membrane. *FASEB J* **6**: 2961-2965.

Brown, G.C. (1994) Control analysis applied to the whole body: Control by body organs over plasma concentrations and organ fluxes of substances in the blood. *Biochemical Journal* **297**: 115-122.

Brown, G.C. and Brand, M.D. (1986) Changes in the permeability to protons and other cations at high proton motive force in rat liver mitochondria. *Biochemical Journal* **234**: 75-81.

Brown, G.C., Hafner, R.P. and Brand, M.D. (1990a) A 'top-down' approach to the determination of control coefficients in metabolic control theory. *European Journal of Biochemistry* **188**: 321-325.

Brown, G.C., Lakin-Thomas, P.L. and Brand, M.D. (1990b) Control of respiration and oxidative phosphorylation in isolated rat liver cells. *European Journal of Biochemistry* **192**: 355-362.

Chen, R.F. (1967) Removal of fatty acids from serum albumin by charcoal treatment. *Journal of Biological Chemistry* **242**: 173-181.

Davis, R.J., Brand, M.D. and Martin, B.R. (1981) The effect of insulin on plasma-membrane and mitochondrial-membrane potentials in isolated fat-cells. *Biochemical Journal* **196**: 133-47.

DeBry, R.W. and Seldin, M.F. (1996) Human/mouse homology relationship relationships. *Genomics* **33**: 337-351.

Desautels, M. (1980) Rat brown adipose tissue mitochondria and nonshivering thermogenesis. Ph.D. Thesis: University of Ottawa.

Desautels, M., Zaror-Behrens, G. and Himms-Hagen, J. (1978) Increased purine nucleotide binding, altered polypeptide composition, and thermogenesis in brown adipose tissue mitochondria of cold-acclimated rats. *Canadian Journal of Biochemistry* **56**: 378-383.

Di Monte, D., Sandy, M., DeLanney, L., Jewell, S., Chan, P., Irwin, I. and Langston, J. (1993) Age-dependent changes in mitochondrial enery production in striatum and cerebellum of the monkey brain. *Neurodegeneration* **2**: 93-99.

Edwards, H.H., Yeh, Y.-Y., Tarnowski, B.I. and Schonbaum, G.R. (1992) Acetonitrile as a substitute for ethanol/propylene oxide in tissue processing for transmission electron microscopy: Comparison of fine structure and lipid solubility in mouse liver, kidney and intestine. *Microscopy Research and Technique* **21**: 39-50.

Else, P.L. and Hulbert, A.J. (1985) Mammals: an allometric study of metabolism at tissue and mitochondrial level. *American Journal of Physiology* **248**: R415-R421.

Enerbäck, S., Jacobsson, A., Simpson, E.M., Guerra, C., Yamashita, H., Harper, M.E. and Kozak, L.P. (1997) Mice Lacking Mitochondrial Uncoupling Protein Are Not Obese. *Nature* **387**: 90-94.

Fell, D. (1992) Metabolic control analysis: a survey of its theoretical and experimental development. *Biochemical Journal* **286**: 313-330.

Field, J., Belding, H. and Martin, A. (1939a) Evaluation of wet and dry weight bases for expression of respiratory rate in vitro. *Proceedings of the Society for Experimental Biology and Medicine* **40**: 565-568.

Field, J., Belding, H. and Martin, A. (1939b) An analysis of the relation between basal metabolism and summated tissue respiration in the rat. *Journal of Cellular and Comparitive Physiology* **14**: 143-155.

Fleury, C., Neverova, M., Collins, S., Raimbault, S., Champigny, O., Levi-Meyrueis, C., Bouillard, F., Seldin, M.F., Surwit, R.S., Ricquier, D. and Warden, C.H. (1997) Uncoupling protein-2: a novel gene linked to obesity and hyperinsulinemia. *Nature Genetics* **15**: 269-272.

Freshney, I.R. (1987) *Culture of Animal Cells: A Manual of Basic Technique*. New York: Alan R. Liss, Inc.

Garruti, G. andRicquier, D. (1992) Analysis of uncoupling protein and its mRNA in adipose tissue deposits of adult humans. *International Journal of Obesity & Related Metabolic Disorders* **16**: 383-390.

Gimeno, R.E., Dembski, M., Weng, X., Deng, N., Shyjan, A.W., Gimeno, C.J., Iris, F., Ellis, S.J., Woolf, E.A. and Tartaglia, L.A. (1997) Cloning and characterization of an uncoupling protein homolog: a potential molecular mediator of human thermogenesis. *Diabetes* **46**: 900-906.

Gornall, A.G., Bardawil, C.J. and David, M.M.. (1949) Determination of serum proteins by means of the Biuret reaction. *Journal of Biological Chemistry* **177**: 751-766.

Hafner, R., Brown, GC, and Brand, MD. (1990a) Analysis of the control of respiration rate, phosphorylation rate, proton leak rate and protonmotive force in isolated mitochondria using the 'top-down' approach of metabolic control theory. *European Journal of Biochemistry* **188**: 313-319.

Hafner, R.P., Brown, G.C. and Brand, M.D. (1990b) Thyroid hormone control of state 3 respiration in isolated rat liver mitochondria. *Biochemical Journal* **265**: 731-734.

Hafner, R.P., Nobes, C.D., McGown, A.D. and Brand, M.D. (1988) Altered relationship between protonmotive force and respiration rate in non-phosphorylating liver mitochondria isolated from rats of different thyroid hormone status. *European Journal of Biochemistry* **178**: 511-518.

Hagen, T.M., Yowe, D.L., Bartholomew, J.C., Wehr, C.M., Do, K.L., Park, J.-Y. and Ames, B.N. (1997) Mitochondrial decay in hepatocytes from old rats: Membrane potential declines, heterogeneity and oxidants increase. *Proceedings of the National Academy of Science* **94**: 3064-3069.

Halliwell, B. and Gutteridge, J. (1989) *Free Radicals in Biology and Medicine*. Oxford: Clarendon.

Hansford, R. (1983) Bioenergetics in aging. *Biochimica et Biophysica Acta.* **726**: 41-80.

Harman, D. (1956) Aging: A theory based on free radical and radiation chemistry. *Journal of Gerontology* **11**: 298-300.

Harper, M.-E. and Brand, M.D. (1993) The quantitative contributions of mitochondrial proton leak and ATP turnover reactions to the changed respiration rates of hepatocytes from rats of different thyroid hormone status. *Journal of Biological Chemistry* **268**: 14850-14860.

Harper, M.-E. and Brand, M.D. (1994) Hyperthyroidism stimulates mitochondrial proton leak and ATP turnover in rat hepatocytes but does not change the overall kinetics of substrate oxidation reactions. *Canadian Journal of Physiology and Pharmacology* **72**: 899-908.

Harper, M.-E. and Brand, M.D. (1995) Use of top-down elasticity analysis to identify sites of thyroid hormone-induced thermogenesis. *Proceeding of the Society for Experimental Biology and Medicine* **208**: 228-237.

Heaton, G.M., Wagenvoord, R.J., Kemp, A. and Nicholls, D.G. (1978) Brown adipose tissue mitochondria: photoafinity labelling of the regulatory site of energy dissipation. *European Journal of Biochemistry* **82**: 515-521.

Heinrich, R. and Rapoport, T. (1973) A linear steady state treatment of enzymatic chains. General properties, control, and effector strength. *European Journal of Biochemistry* **42**: 97-105.

Himms-Hagen, J. (1990) Brown adipose tissue thermogenesis: Role in thermoregulation, energy regulation and obesity. *Thermoregulation: Physiology and Biochemistry.* New York: Pergamon Press Inc.

Himms-Hagen, J. 1992 Brown Adipose Tissue Metabolism. In *Obesity* (ed. Bjorntorp P. and Brodoff B.N.), pp. 15-34. Philadelphia: Lippincott.

Hinkle, P.C., Kumar, M.A., Resetar, A. and Harris, D.L. (1991) Mechanistic stoichiometry of mitochondrial oxidative phosphorylation. *Biochemistry* **30**: 3576-3582.

Hoch, F. (1988) Lipids and thyroid hormones. *Progress in Lipid Research* **27**: 199-270.

Hoch, F.L. (1992) Cardiolipins and biomembrane function. *Biochimica et Biophysica Acta* **1113**: 71-133.

Hogan, S. and Himms-Hagen, J. (1980) Abnormal brown adipose tissue in obese (ob/ob) mice: response to acclimation to cold. *American Journal of Physiology* **239**: E301 -E309.

Kacser, H. and Burns, J. (1973) The control of flux. *Symposium of the Society for Experimental Biology* **32**: 65-104.

Kacser, H. andPorteous, J.W. (1987) Control of metabolism: What do we have to measure? *TIBS* **12**: 5-13.

Kamo, N., Muratsugu, M, Hongoh, R, and Kobatake,Y. (1979) Membrane potential of mitochondria measured with an electrode sensitive to tetraphenyl phosphonium and relationship between proton electrochemical potential and phosphorylation potential in steady state. *Journal of Membrane Biology* **49**: 105-121.

Kissebah, A., Freedman, D. and Peiris, A. (1989) Health risks of obesity. *Medical Clinics of North America* **73**: 111-138.

Kleyn, P.W., Fan, W., Kovats, S.G., Lee, J.J., Pulido, J.C., Wu, Y., Berkemeier, L.R., Misumi, D.J., Holmgren, L., Charlat, O., Woolf, E.A., Tayber, O., Brody, T., Shu, P., Hawkins, F., Kennedy, B., Baldini, L., Ebeling, C., Alperin, G.E., Deeds, J., Lakey, N.D., Culpepper, J., Chen, H., Glucksmann-Kuis, M.A., Carlson, G.A., Duyk, G.M. and Moore, K.J. (1996) Identification and characterization of the mouse obesity gene tubby: a member of a novel gene family. *Cell* **85**: 281-290.

Krebs, H.A. (1950) Body size and tissue respiration. *Biochimica et Biophysica Acta* **4**: 249-269.

Krishnamoorthy, G. and Hinkle, P.C. (1984) Non-ohmic proton conductance of mitochondria and liposomes. *Biochemistry* **23**: 1640-45.

Laganiere, S. and Yu, B. (1993) Modulation of membrane phospholipid fatty acid composition by age and food restriction. *Gerontology* **39**: 7-18.

LaNoue, K.F., Strzelecki, T., Strzelecka, D. and Koch, C. (1986) Regulation of the uncoupling protein in brown adipose tissue. *Journal of Biological Chemistry* **261**: 298-305.

Larrouy, D., Laharrague, P., Carrera, G., Viguerie-Bascands, N., Levi-Meyrueis, C., Fleury, C., Pecqueur, C., Nibbellink, M., Andre, M., Casteilla, L. andRicquier, D. (1997) Kuppfer cells are a dominant site of uncoupling protein 2 expression in rat liver. *Biochemical and Biophysical Research Communications* **235**: 760-764.

Lin, C.S. and Klingenberg, M. (1982) Characteristics of the isolated purine nucleotide binding protein from brown fat mitochondria. *Biochemistry* **21**: 2950-6.

Locke, R.M., Rial, E., Scott, I.D. and Nicholls, D.G. (1982) Fatty acids as acute regulators of the proton conductance of hamster brown-fat mitochondria. *European Journal of Biochemistry* **129**: 373-380.

Loud, A.V. (1968) A quantitative stereological description of the ultrastructure of normal rat liver parenchymal cells. *Journal of Cell Biology* **37**: 27-46.

Lowell, B.B., V, S.S., Hamann, A., Lawitts, J.A., Himms-Hagen, J., Boyer, B.B., Kozak, L.P. and Flier, J.S. (1993) Development of obesity in transgenic mice after genetic ablation of brown adipose tissue [see comments]. *Nature* **366**: 740-742.

Mecocci, P., MacGarvey, U., Kaufman, A., Koontz, D., Shoffner, J., Wallace, D. and Beal, M. (1993) Oxidative damage to mitochondrial DNA shows marked age-dependent increases in human brain. *Annals of Neurology* **34**: 609-616.

Melnyk, A., Harper, M.-E. and Himms-Hagen, J. (1997) Raising at thermoneutrality prevents obesity and hyperphagia in BAT-ablated transgenic mice. *American Journal of Physiology* **272**: R1088-1093.

Mitchell, P. and Moyle, J. (1967) Respiration-driven proton translocation in rat liver mitochondria. *Biochemical Journal* **105**: 1147-1162.

Nicholls, D. (1974) The influence of respiration and ATP hydrolysis on the proton-electrochemical gradient across the inner membrane of rat-liver mitochondria as determined by ion distribution. *European Journal of Biochemistry* **50**: 305-315.

Nicholls, D.G. (1977) Cellular mechanisms in brown fat thermogenesis mitochondria. *Experientia* **33**: 1130-1.

Nicholls, D.G. and Locke, R.M. (1984) Thermogenic mechanisms in brown fat. *Physiological Reviews* **64**: 1-64.

Nobes, C.D. and Brand, M.D. (1989) A quantitative assessment of the use of $^{36}Cl^-$-distribution to measure plasma membrane potential in isolated hepatocytes. *Biochimica et Biophysica Acta* **987**: 115-123.

Nobes, C.D., Brown, G.C., Olive, P.N. andBrand, M.D. (1990a) Non-ohmic proton conductance of the mitochondrial inner membrane in hepatocytes. *Journal of Biological Chemistry* **265**: 12903-12909.

Nobes, C.D., Hay, W.W., Jr. and Brand, M.D. (1990b) The mechanism of stimulation of respiration by fatty acids in isolated hepatocytes. *Journal of Biological Chemistry* **265**: 12910-12915.

Pietrobon, D., Azzone, G.F. andWalz, D. (1981) Effect of funiculosin and antimycin A on the redox-driven H^+-pumps in mitochondria. *European Journal of Biochemistry* **2**: 389-94.

Pi-Sunyer, X. (1993) Medical hazards of obesity. *Annals of Internal Medicine* : 657-660.

Porter, R.K. and Brand, M.D. (1993) Body mass dependence of H^+leak in mitochondria and its relevance to metabolic rate. *Nature* **362**: 628-630.

Rial, E. and Nicholls, D.G. (1983) The regulation of the proton conductance of brown fat mitochondria. Identification of functional and non-functional nucleotide-binding sites. *FEBS Letters* **161**: 284-288.

Rial, E., Poustie, A. and Nicholls, D.G. (1983) Brown-adipose-tissue mitochondria: the regulation of the 32000-Mr uncoupling protein by fatty acids and purine nucleotides. *European Journal of Biochemistry* **137**: 197-203.

Richter, C., Park, J. and Ames, B. (1988) Normal oxidative damage to mitochondrial and nuclear DNA is extensive. *Proceedings of the National Academy of Science* **85**: 6465-6467.

Rolfe, D.F.S. and Brand, M.D. (1996) Contribution Of Mitochondrial Proton Leak to Skeletal Muscle Respiration and to Standard Metabolic Rate. *American Journal of Physiology* **271**: C1380-C1389.

Rolfe, D.F.S. and Brand, M.D. (1997) The physiological significance of mitochondrial proton leak in animal cells and tissues [Review]. *Bioscience Reports* **17**: 9-16.

Rosenbaum, M., Leibel, R. and Hirsch, J. (1997) Obesity. *New England Journal of Medicine* **337**: 396-407.

Shigenaga, M., Hagen, T. and Ames, B. (1994) Oxidative damage and mitochondrial decay in aging. *Proceedings of the National Academy of Science* **91**: 10771-10778.

Skulachev, V.P. (1996) Role of uncoupled and non-coupled oxidations in maintenance of safely low levels of oxygen and its one-electron reductants. *Quarterly Reviews of Biophysics* **29**: 169-202.

Sohal, R.S. and Weindruch, R. (1996) Oxidative Stress, Caloric Restriction, and Aging. *Science* **273**: 59-63.

Stadtman, E. (1992) Protein oxidation and aging. *Science* **257**: 1220-1224.

Taylor, B.A. and Phillips, S.J. (1996) Detection of obesity quantitative trait loci on mouse chromosome 1 and 7 by selective DNA pooling. *Genomics* **34**: 389-398.

Torii, K., Sugiyama, S., Takagi, K., Satake, T. andOzawa, T. (1992) Age-related decrease in respiratory muscle mitochondrial function in rats. *American Journal of Respiratory Cell and Molecular Biology* **6**: 88-92.

Tung, R. (1997) Obesity as a disease. *British Medical Journal* **53**: 307-321.

Vidal-Puig, A., Solanes, G., Grujic, D., Flier, J.S. and Lowell, B.B. (1997) UCP3: an uncoupling protein homologue expressed preferentially and abundantly in skeletal muscle and brown adipose tissue. *Biochemical and Biophysical Research Communications* : **235**:79-82.

Weibel, E. (1969) Stereological principles for morphology in electron microscopic cytology. *Int. J. Rev. Cytol.* **26**: 235-302.

Weindruch, R. and Sohal, R.S. (1997) Caloric intake and aging. *New England Journal of Medicine* **337**: 986-994.

Wilson, P.D. and Franks, L.M. (1975) The effect of age on mitochondrial ultrastructure and enzymes. *Advances in Experimental Biology and Medicine* **53**: 171-183.

Yu, B., Suescun, E. and Yang, S. (1992) Effect of age related lipid peroxidation on membrane fluidity and phospholipase A2: modulation by dietary restriction. *Mech. Ageing and Developmrent* **65**: 17-33.

Yu, B.P. (1996) Aging and oxidative stress- modulation by dietary restriction [Review]. *Free Radical Biology & Medicine* **21**: 651-668.

Curriculum Vitae

Shadi Monemdjou
Department of Biochemistry, Microbiology and Immunology
University of Ottawa
Health Sciences Building
451 Smyth Road
Ottawa, Ontario
K1H 8M5
Tel: (613) 562-5800 x8230
(613) 565-7042 (H)
Fax: (613) 562-5440
email: shadim@uottawa.ca

DATE OF BIRTH: December 10, 1973
CITIZENSHIP: Canadian

EDUCATION

M.Sc.	Department of Biochemistry, Microbiology and Immunology University of Ottawa December 1998
B.Sc. (Hon.)	Department of Biochemistry University of Ottawa, 1996
Ontario Secondary School Diploma	Lisgar Collegiate Institute Ottawa, Ontario, 1992

ACADEMIC AWARDS

1999-2001	University of Ottawa Ph.D. Entrance Scholarship
1998	North American Association for the Study of Obesity: Young Investigator of the Year Award
1998	North American Association for the Study of Obesity: Travel Grant ($1500)
1998	Eva Princz Memorial Fund Travel Grant ($500)
1997	North American Association for the Study of Obesity: Young Investigator Award Finalist ($1000)
1992	Ontario Scholar, Lisgar Collegiate Institute

SOCIETIES

- North American Association for the Study of Obesity (NAASO)
- The Society of Experimental Biology and Medicine
- The Biochemical Society (Britain)

VOLUNTEER ACADEMIC SERVICE

1997-present	Vice-President of the Biochemistry Graduate Student's Association
1997	Let's Talk Science Leader

WORK EXPERIENCE

1996	**Fourth Year Honours Student** in the lab of Dr. Mary-Ellen Harper in the Department of Biochemstry at the University of Ottawa. The title of my thesis was *"Metabolic control and regulation of oxidative phosphorylation in hepatocytes of UCP-DTA mice".*
1996-1998	**Graduate Student** in the M.Sc. program in the Department of Biochemistry, Microbiology and Immunology at the University of Ottawa under the supervision of Dr. Mary-Ellen Harper. The title of my thesis was *"Metabolic Control and Regulation of Mitochondrial Proton Leak: Effects of UCP1 Deficiency and Aging in Mice"*
1996-present	**Laboratory Demonstrator** for second and third year undergraduate biochemistry labs at the University of Ottawa. The courses were: Introduction to Biochemistry (BCH 2936) and Physical and Chemical Methods Applied to Biochemistry (BCH 3140)

PUBLICATIONS

PAPERS:

Harper M-E., Monemdjou S., Weindruch R, and Ramsey J.J. (1998) Age-related increase in mitochondrial proton leak and decrease in ATP turnover reactions in hepatocytes of mice. *American Journal of Physiology.* 275(2): E197-E206 August 1998.

Monemdjou S., Kozak L.P., and Harper M-E. (1998) Mitochondrial proton leak in brown adipose tissue mitochondria of UCP1 knockout mice is GDP-insensitive. Submitted to the *American Journal of Physiology;* October 15, 1998

Lal S.B., Ramsey J.J., Monemdjou S., Weindruch R.W., and Harper M-E. (1998) Evidence that caloric restriction lowers mitochondrial proton leak from old rats. Submitted to *Archives of Biochemistry and Biophysics*; September 11, 1998.

ABSTRACTS:

Monemdjou S., Kozak L.P, and Harper M-E. (1998) Altered mitochondrial proton leak in skeletal muscle mitochondria of UCP1 knockout mice. 8th International Congress on Obesity: Paris, France; August 1998.

Harper M-E., Monemdjou S., Gagne M, Steffey M.E., VanLeeuwen D.H, and MacKenzie R.G. (1998) Bromopalmitate stimulation of a state 4 respiration in yeast mitochondria expressing rat UCP1 is GDP sensitive while stimulation of human $UCP3_L$ is not. 8th International Congress on Obesity: Paris, France; August 1998.

Monemdjou S., Kozak L.P., and Harper M-E. (1997) Mitochondrial proton leak in brown adipose tissue (BAT) mitochondria of UCP1 knockout mice is GDP-insensitive. *Obesity Research* Vol. 5: Supplement 1. November 1997. NAASO confrerence: Cancun, Mexico.

Monemdjou S., Camet P., West D.B., and Harper M-E. (1997) Lower resting oxygen consumption and greater metabolic efficiency in AKR/J than in SWR/J mice. 16th International Congress of Nutrition: Montreal, Que; July 1997

Harper M-E., Monemdjou S., Weindruch R., Ramsey J.J. (1997) Age-related increase in mitochondrial proton leak and decrease in ATP turnover reactions in hepatocytes of mice. 16th International Congress of Nutrition: Montreal, Que; July 1997

Monemdjou S., West D.B., and Harper M-E. (1996) Lower resting oxygen consumption and temperature in AKR/J than in SWR/J mice.
FASEB J. 7:A595 Experimental Biology: New Orleans, LA: April 1996

Harper M-E., Monemdjou S., Weindruch R., and Ramsey J.J. (1996) Increased mitochondrial proton leak in hepatocytes from old C57BL/J mice.
FASEB J. 7:A176 Experimental Biology: New Orleans, LA: April 1996

IMAGE EVALUATION TEST TARGET (QA-3)

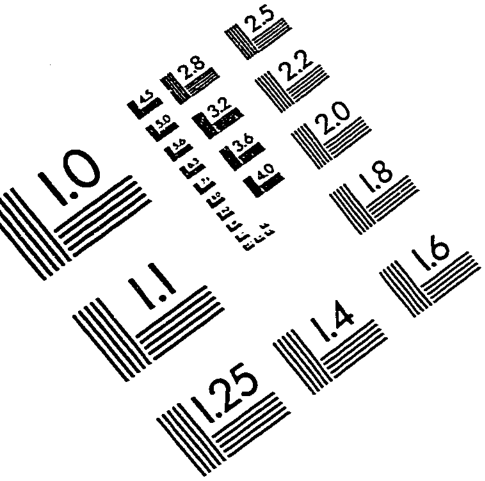

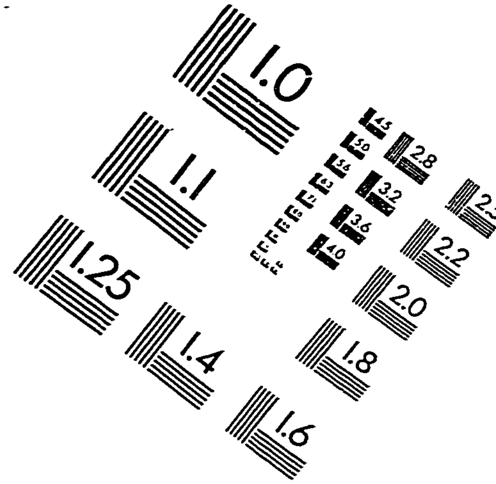

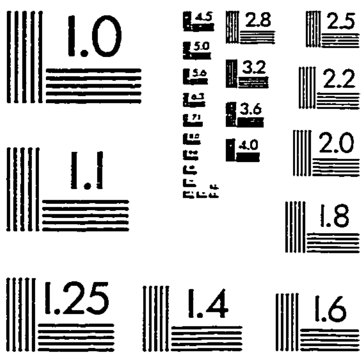

150mm

6"

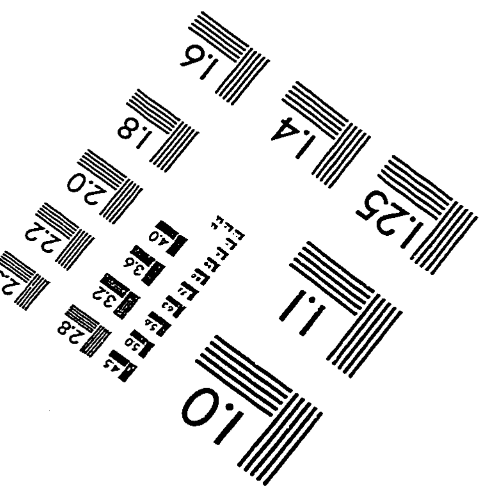

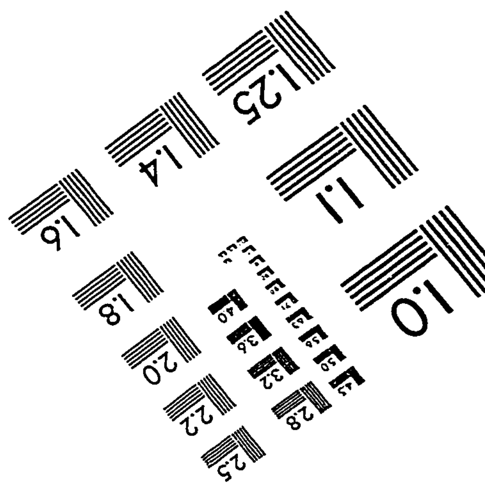

APPLIED IMAGE . Inc
1653 East Main Street
Rochester, NY 14609 USA
Phone: 716/482-0300
Fax: 716/288-5989